40510

National Library of Canada | Bibliothèque nationale du Canada

CANADIAN THESES ON MICROFICHE | THÈSES CANADIENNES SUR MICROFICHE

NAME OF AUTHOR/*NOM DE L'AUTEUR* JOSEPH SHEK-HUNG TANG

TITLE OF THESIS/*TITRE DE LA THÈSE* Ozonation of Cyanide and Ferricyanide

UNIVERSITY/*UNIVERSITÉ* Alberta

DEGREE FOR WHICH THESIS WAS PRESENTED/ *GRADE POUR LEQUEL CETTE THÈSE FUT PRÉSENTÉE* M.Sc.

YEAR THIS DEGREE CONFERRED/*ANNÉE D'OBTENTION DE CE GRADE* 1979

NAME OF SUPERVISOR/*NOM DU DIRECTEUR DE THÈSE* Dr. F. D. Otto

Permission is hereby granted to the NATIONAL LIBRARY OF CANADA to microfilm this thesis and to lend or sell copies of the film.

The author reserves other publication rights, and neither the thesis nor extensive extracts from it may be printed or otherwise reproduced without the author's written permission.

L'autorisation est, par la présente, accordée à la BIBLIOTHÈQUE NATIONALE DU CANADA de microfilmer cette thèse et de prêter ou de vendre des exemplaires du film.

L'auteur se réserve les autres droits de publication; ni la thèse ni de longs extraits de celle-ci ne doivent être imprimés ou autrement reproduits sans l'autorisation écrite de l'auteur.

DATED/*DATÉ* 11 Dec 1978 SIGNED/*SIGNÉ* [signature]

PERMANENT ADDRESS/*RÉSIDENCE FIXÉ* c/o Esso Resources Can. Ltd.
339 50 Ave. S.E.
Calgary Alta.

NL-91 (3-74)

National Library of Canada

Cataloguing Branch
Canadian Theses Division

Ottawa, Canada
K1A 0N4

Bibliothèque nationale du Canada

Direction du catalogage
Division des thèses canadiennes

NOTICE

The quality of this microfiche is heavily dependent upon the quality of the original thesis submitted for microfilming. Every effort has been made to ensure the highest quality of reproduction possible.

If pages are missing, contact the university which granted the degree.

Some pages may have indistinct print especially if the original pages were typed with a poor typewriter ribbon or if the university sent us a poor photocopy.

Previously copyrighted materials (journal articles, published tests, etc.) are not filmed.

Reproduction in full or in part of this film is governed by the Canadian Copyright Act, R.S.C. 1970, c. C-30. Please read the authorization forms which accompany this thesis.

THIS DISSERTATION
HAS BEEN MICROFILMED
EXACTLY AS RECEIVED

AVIS

La qualité de cette microfiche dépend grandement de la qualité de la thèse soumise au microfilmage. Nous avons tout fait pour assurer une qualité supérieure de reproduction.

S'il manque des pages, veuillez communiquer avec l'université qui a conféré le grade.

La qualité d'impression de certaines pages peut laisser à désirer, surtout si les pages originales ont été dactylographiées à l'aide d'un ruban usé ou si l'université nous a fait parvenir une photocopie de mauvaise qualité.

Les documents qui font déjà l'objet d'un droit d'auteur (articles de revue, examens publiés, etc.) ne sont pas microfilmés.

La reproduction, même partielle, de ce microfilm est soumise à la Loi canadienne sur le droit d'auteur, SRC 1970, c. C-30. Veuillez prendre connaissance des formules d'autorisation qui accompagnent cette thèse.

LA THÈSE A ÉTÉ
MICROFILMÉE TELLE QUE
NOUS L'AVONS REÇUE

THE UNIVERSITY OF ALBERTA

OZONATION OF CYANIDE AND FERRICYANIDE

BY

(C) JOSEPH SHEK-HUNG TANG

A THESIS

SUBMITTED TO THE FACULTY OF GRADUATE STUDIES AND RESEARCH IN

PARTIAL FULFILMENT OF THE REQUIREMENTS FOR THE DEGREE OF

MASTER OF SCIENCE

DEPARTMENT OF CHEMICAL ENGINEERING

EDMONTON, ALBERTA

SPRING 1979

THE UNIVERSITY OF ALBERTA

FACULTY OF GRADUATE STUDIES AND RESEARCH

The undersigned certify that they have read, and recommend to the Faculty of Graduate Studies and Research, for acceptance, a thesis entitled OZONATION OF CYANIDE AND FERRICYANIDE

submitted by JOSEPH SHEK-HUNG TANG

in partial fulfilment of the requirements for the degree of Master of Science.

F.D.Otto, Supervisor

S.E.Wanke

B.G.Kratochvil

D.W.Smith

Date November 10,1978

ABSTRACT

A continuous flow well-stirred tank photochemical reactor of known surface area was used to obtain measurements of the rate constants for the ozonation of free cyanide at various UV intensities and 22°C.

The ozonation of free cyanide, with concentrations ranging from 1.14×10^{-3} M to 7.69×10^{-3} M, was carried out at pH 12 with and without UV. The reaction scheme was regarded as consisting of the main cyanide oxidation reaction, a parallel ozone decomposition reaction, and a consecutive cyanate oxidation reaction. The rate constant and stoichiometry of the cyanate reaction were assumed from Balyanskii's work, while the ozone decomposition rate constant was predicted by Stumm's and Czapski's correlations interchangeably. A fast reaction regime model was used to decouple the mass transfer from the overall reaction. The rate constant for cyanide was found to be independent of UV intensity and had an average value of 19086 $M^{-1} s^{-1}$ with an uncertainty of 18%.

A transition from fast to instantaneous reaction regime model was also applied to the free cyanide ozonation reaction, and the value of the rate constant obtained was higher than that of the fast reaction model by 5%. The gas phase resistance only accounted for 2% of the total resistance.

The ozonation of ferricyanide, with concentrations ranging from 1.84×10^{-4} M to 3.68×10^{-2} M, was studied at four different UV intensities and pH of 7 and 12. The rate constant was obtained by characterizing the reaction to be in a transition from slow to fast reaction regime using either a flat or quadratic cyanate concentration profile. A reaction scheme similar to that of the free cyanide ozonation was assumed. The rate constant for the ferricyanide ozonation reaction depended on the UV intensity when the cyanide content was lower than 1.5×10^{-3} M or 40 ppm above which a value of $1100\ M^{-1}\ s^{-1}$ was obtained independent of UV intensity. The rate constant at pH 12, where the ozone decomposition accounted for 90% of the total ozone consumed, agreed with that at pH 7 where the ozone decomposition was negligible. The agreement at different pH's supports the model proposed.

The dependence of the rate constant, K, on UV intensity and ferricyanide concentration was interpreted by proposing a molecular mechanism involving the formation of an ozonide intermediate. Two other reported mechanisms, i.e. free radical and ferricyanide dissociation mechanisms, were also considered. Even though these two mechanisms do not comply with the behavior of K observed, the possibility of the presence of these mechanisms cannot be excluded. The ozonation reaction proceeds most likely through a combination of the above three mechanisms. Further work to elucidate the mechanism and reaction kinetics of ozonation reactions is required.

ACKNOWLEDGEMENT

The author would like to express his appreciation to Dr.F.D.Otto for his guidance and encouragement throughout this project.

Financial assistance from the National Research Council of Canada and the University of Alberta is gratefully acknowledged.

TABLE OF CONTENTS

		Page
List of Tables		
List of Figures		
Chapter 1	INTRODUCTION	1
CHAPTER 2	LITERATURE REVIEW	7
2.1	Chemistry of Ozone, Cyanide and Ferricyanide	7
2.1.1	Ozone Chemistry	7
2.1.2	Cyanide and Ferricyanide Chemistry	11
2.2	Physical Properties of Ozone	13
2.2.1	Solubility of Ozone in Aqueous Media	13
2.2.2	Diffusivity	13
2.3	Ozone/Cyanide Reaction	14
CHAPTER 3	THEORY	18
3.1	Background for Mass Transfer Modelling	18
3.2	Modelling of Ozonation Reactions	28
3.2.1	Stoichiometry of the Ozonation Reactions	28
3.2.2	Reaction Scheme - O_3/CN^- Reaction	30
3.2.3	Reaction Scheme - UV/O_3/Ferricyanide Reaction	31
3.3	Modelling of the $CN^-/O_3/UV$ Reaction	34
3.3.1	Transition from Slow to Fast Reaction Regime - Film Model	34

Page

CHALTER 3 (cont'd)

3.3.2 Transition Regime with C_{Ao} Equal to Zero - Film Model 39

3.3.3 Fast Reaction Regime - Film Model 39

3.3.4 Transition from Fast to Instantaneous Reaction Regime - Film Model 40

3.4 Modelling of the Ferricyanide/O_3/UV Reaction 43

3.4.1 Flat CNO Concentration Profile - Film Model 43

3.4.2 Quadratic CNO Concentration Profile - Film Model 43

3.4.3 Flat CNO Concentration Profile - Penetration Model 49

CHAPTER 4 EXPERIMENTAL 51

4.1 Equipment Description 51

4.1.1 Reactor and UV Lamp Assembly 51

4.1.2 General Description of the Set-up and Flow Diagram 54

4.1.3 Safety Measures 57

4.2 Reactor Characterization 58

4.2.1 Mixing Pattern 58

4.2.2 Physical Mass Transfer 61

4.2.3 Characterization of UV Intensity 66

4.3 Analytical Procedures 69

4.3.1 Ozone Analysis 69

4.3.2 Analytical Method for Free Cyanide Determination 70

4.3.3 Ferricyanide Analysis 72

i) Reagents 74

Page

CHAPTER 4 (cont'd)

ii) Apparatus 74

iii) Evaluation of Method 77

4.4 Experimental Procedure - CN^-/O_3/UV Reaction 81

4.5 Experimental Procedure - Ferricyanide/O_3/UV/Reaction 82

CHAPTER 5 DATA TREATMENT 83

5.1 Summarization of the Equations to be Solved for the Rate Constant 83

5.2 CN/O_3/UV Reaction 87

5.2.1 Fast Reaction Regime 87

5.2.2 Transition from Fast to Instantaneous Reaction Regime 91

5.3 Ferricyanide/O_3/UV Reaction 92

CHAPTER 6 RESULT AND DISCUSSION 95

6.1 CN/O_3/UV Reaction 95

6.2 Ferricyanide/O_3/UV Reaction 112

6.3 Proposed Mechanism for the Ferricyanide/O_3/UV Reaction 135

6.4 Other Possible Mechanisms 138

6.4.1 Free Radical Mechanism 138

6.4.2 Mechanism Involving Ferricyanide Dissociation 140

6.5 Conclusions 141

		Page
CHAPTER 7	FUTURE WORK	143
NOMENCLATURE		147
REFERENCES		151
APPENDICES		
1	Mueller's Method	156
2	Detailed Operating Procedure	159
3	Mixed Pattern	166
4	Detailed Physical Mass Transfer Measurement	175
5	Detailed UV Characterization Procedure	185
6	Detailed Analyses of the Ozonation Reactions	196
7	Listing of Program THES	209

LIST OF FIGURES

Figure		Page
1	QVF photochemical reactor for the O_3/Ferricyanide/UV reaction	52
2	Schematic representation of the set-up for the O_3/Ferricyanide/UV reaction	55
3	Plots of log K_0S by both O_3-H_2O and CO_2-H_2O methods vs log rpm at 22°C	63
4	Apparatus for cyanide open distillation	75
5	Plot of cyanide content measured vs cyanide content added in the determination of ferricyanide at 22°C	80
6	Plot of K_f vs cyanide concentration at 22°C and 108 rpm	104
7	Plot of the measured ozone consumption ratio S_0 vs the calculated ozone consumption ratio S_1	110
8	Plot of K from film model, flat CNO profile vs cyanide content, CN, at 22°C, pH 7, 108 rpm and various UV intensities	122
9	Plot of KP from penetration model, flat CNO profile vs cyanide content, CN, at 22°C, pH 7, 108 rpm and various UV intensities	123
10	Plot of KQ from film model, quadratic CNO profile vs cyanide content, CN, at 22°C, pH 7, 108 rpm and various UV intensities	124
11	Plot of K vs UV intensity at 22°C, pH 7, 108 rpm and various cyanide contents	126
12	Plot of K, KQ vs cyanide content, CN, at 100% UV, 22°C, pH 12 and 108 rpm	127
13	Plot of calculated cyanate concentration CNO vs cyanide content CN for ferricyanide at pH 7 and 12, 100% UV; and for free cyanide at pH 12, flow rates of 0.4944 and 0.765 ml/sec	129
14,15	Plot of fraction of ozone decomposed FRD vs CN for ferricyanide at pH 7 and 12, 100% UV and for free cyanide at pH 12, flow rates of 0.4944 and 0.765 ml/sec	131-132

Figure		Page
16	Plot of fraction of ozone reacted with cyanate vs CN for ferricyanide at pH 7 and 12, 100% UV and for free CN^- at pH 12, flow rates of 0.4944 and 0.765 ml/sec	134
A1	Typical recorder ouput; pH vs time at 85 rpm	170
A2 - A5	Plots of $\log(C_f-C/C_f-C_o)$ vs time at the stirring rates of 102, 85, 59.5, 0 rpm respectively	171-174
A6	Calibration curve by plotting absorbance against the ferrous ion concentration at 22°C	195

LIST OF TABLES

Table		Page
1	Comparison of $\bar{t}_R$ and t_L from graphical method and direct calculation at different stirring rates	60
2	Comparison of K_0 of ozone measured by O_3-H_2O and CO_2-H_2O systems	64
3	Characterization of UV intensities by ferri-oxalate actinometer at 21°C	68
4	Characterization of UV intensities by Blak-Ray UV intensity meter	68
5	Percentage of cyanide recovery at various levels of ferricyanide by the open distillation method	79
6	Directly measurable experimental variables for the CN^-/O_3/UV reaction at a flow rate of 0.765 ml/sec, ozonator setting of 100%, pH 12 and temperature 21°C	96
7	Directly measurable experimental variables for the CN^-/O_3/UV reaction at a flow rate of 1.094 ml/sec, ozonator setting of 75%, pH 12 and temperature 21°C	97
8	Comparison of rate constants K_f and mass transfer coefficients K_L obtained by four different methods (A to D) for the cyanide concentrations listed in Table 6	99
9	Comparison of rate constants K_f and mass transfer coefficients K_L obtained by four different methods (A to D) for the cyanide concentrations listed in Table 7	102
10	Comparison of K_f for the CN^-/O_3/UV reaction calculated by assuming the transition from fast to instantaneous reaction regime and fast reaction regime	108
11	Directly measurable experimental variables for the ferricyanide/O_3/UV reaction at a flow rate of 0.4944 ml/sec, pH 7 and temperature 21°C	115

Table		Page
12	Directly measurable experimental variable for the ferricyanide/O_3/UV reaction at a flow rate of 0.5525 ml/sec, pH 12 and temperature 21°C	117
13	Comparison of rate constants K, KQ, KP from three different models for the ferricyanide concentrations listed in Table 11	119
14	Comparison of rate constants K, KQ, KP from three different models for the ferricyanide concentrations listed in Table 12	121
A1	Quantum yield of Fe^{2+} in the $K_3Fe(C_2O_4)_3$ chemical actinometer at 22°C	188
A2	Energy distribution in low and medium-pressure mercury arcs	188
A3	Absorbances of the standard Fe^{2+} solutions for the calibration of Spectronic 20 spectrometer	194
A4	Detailed analysis of the CN^-/O_3/UV reaction for the cyanide concentrations and experimental conditions listed in Table 6.	197
A5	Detailed analysis of the CN^-/O_3/UV reaction for the cyanide concentrations and experimental conditions listed in Table 7	200
A6	Detailed analysis of the ferricyanide/O_3/UV reaction for the ferricyanide concentrations and experimental conditions listed in Table 11	201
A7	Detailed analysis of the ferricyanide/O_3/UV reaction for the ferricyanide concentrations and experimental conditions listed in Table 12	208

CHAPTER 1

INTRODUCTION

Cyanide is one of the most poisonous chemicals known by man. Wuhrmann[1] discovered in 1948 that the toxicity of cyanide comes chiefly from the molecular species HCN, but not the ion CN^-. Generally speaking, the toxicity increases with temperature and the age of the victim and decreases with the oxygen content in the air and the pH. As reported by Doudorff[2] and Mckee[3], cyanide causes osmoregulatory and excretory failures, internal hemorrhages as well as the inhibition of the functioning of oxidase responsible for transferring oxygen from the blood to the tissues. Exposure to air containing a high concentration of HCN (10 ppm by volume) causes the symptoms of acute cyanide poisoning to appear almost instantaneously, namely, giddiness, headache, unconsciousness, convulsion and finally cessation of respiration as a result of the paralysis of the respiratory center located in the brain[4]. An exposure time longer than one hour may cause serious health damage and even death. At concentrations higher than 200 ppm, fatality happens almost immediately. With rainbow trout as a test species, the 48 hour LC_{50} for cyanide (the concentration of cyanide that kills half of the test organisms in 48 hours) is 0.07 mg/L. This serves as a guide-line for cyanide discharge. The Ohio River Valley Sanitation

Commission, U.S.A. recommended the permissible level of cyanide in receiving waters (1960) to be 0.025 mg/L, and a discharge level of 0.1 mg/L; the same standard had been adopted by Canada[5].

The use of cyanide for industrial processing is not extensive in Alberta[5]. However, on a national scale, it is by no means negligible. Cyanide waste streams result from industries such as gold and silver mining, electroplating, photographic processing, coke furnaces and synthetics manufacturing. The major source of waste cyanide is the electroplating industry[6,7] in which a cyanide bath is used to hold ions such as Zn^{+2} and Cd^{+2} in solution as well as to give a uniform and lustrous metallic coating on the surface of the object to be plated. "Drag over" of the plating solution containing cyanide and metal cyanide complexes (e.g. $Zn(CN)_4^{-2}$, $Cd(CN)_4^{-2}$) contaminates the rinsing baths. The cyanide in the rinse water ranges from 10 mg/L to 700 mg/L[6]. For a typical medium size plant, the waste contains an average cyanide content of 33 mg/L at a discharge rate of 200,000 gallons per month. Another major source for waste cyanide is the gold mining industry in which cyanide is used to extract the precious metal from the ore. The gold mine operated in Yellow Knife, North West Territories, discharges 200,000 ~ 300,000 gallons of barren liquid per day containing 30 ~ 50 mg/L of cyanide. This cyanide has a major impact on the environment and, in order

to comply with the government's environmental protection regulations, the cyanide level has to be lowered to 0.1 mg/L before the effluent can be discharged.

The major industrial sources of ferricyanide are blast furnaces in steel plants, photographic processes and the inadvertent mixing of streams containing ferric ion and cyanide. Fe(II) and Fe(III) can both react with cyanide to form extremely stable complexes ferrocyanide and ferricyanide, with the instability constants of 10^{-35} and 10^{-42} [8] respectively. The complexes are so stable that the tests for cyanide and iron are both negative in aqueous solution. The complexes are not only thermodynamically stable but also inert in a kinetic sense as reflected by the slow ligand isotope exchange rate ($t_{\frac{1}{2}}$ = 52 hrs at pH = 3.5).[9] Nevertheless, ferricyanide and ferrocyanide may undergo photo-decomposition under sunlight to liberate the poisonous compound HCN. In order to keep the free cyanide level below the 0.1 mg/L limit, the allowable ferricyanide discharge concentration has to be lower than 1.5 mg/L.

The current popular cyanide treatment methods include acidification[10], ion exchange[11], biological oxidation[12], electrolytic oxidation[13,14], carbon adsorption[15], alkali chlorination[16,17] and ozonation. Among these methods, only the last two receive widespread attention[18,19,20].

As a comparison of alkali chlorination and ozonation[20], chemical oxidation by chlorination requires a high concentration of chlorine to drive the reaction towards

completeness owing to the lower potential for chlorine ($E = 1.36$ v for Cl_2, and 2.07 v for ozone). The residual chlorine built up in the effluent has to be dechlorinated while the residual ozone at 2 ppm level can quickly decompose by itself into a harmless product, O_2; and also there is no formation of the undesirable final products like the chlorinated compounds in chlorination. Furthermore, ozone may be generated only as needed so that there is no transportation or storage problem. On the other hand, the basic chlorinator is less expensive than the ozonation equipment, but requires extensive support equipment. With the advent of modern effective ozone generators, the total equipment cost tends to be equalized, and the more economical operation of ozone equipment will more than compensate for any equipment cost advantage remaining to chlorine. The trend of ozonation replacing chlorination can be foreseen.

While the reaction between ozone and free cyanide as well as other metal cyanide complexes is quite spontaneous, the reaction between ozone and ferricyanide is slow particularly at low ferricyanide concentration. For example, ozonating for 75 minutes causes negligible decomposition of ferricyanide at the 57 ppm level[21]. Ferricyanide is classified as a "highly refractory compound" in waste water treatment technology, and has a Refractory Index RFI of 270[22] (cf. 0.41 for free cyanide, a slightly refractory compound). RFI is a measure of the difficulty of oxidation

of a species, and is defined as

$$RFI = \frac{B^{O}(mg/L)\ t_{\frac{1}{2}}(hrs)}{A^{O}(mg/L)}$$

$$B^{O} = \frac{\dot{m}_{B}(mg/min)\ t_{\frac{1}{2}}(min)}{V(L)}$$

where B^{O} is the cumulative ozone pumped into the solution from $t = 0$ to $t = t_{\frac{1}{2}}$ per liter of the solution, $t_{\frac{1}{2}}$ is the time required for 50% conversion of the reactant component, A_{o} is the initial amount of the reactant component, $\dot{m}_{B}$ is the ozone mass feed rate to the reactor, and V is the solution volume in the reactor.

While the rate of oxidation of ferricyanide can be enhanced by elevated temperature and high ozone concentration, neither of these appears to be as effective as UV irradiation[23,24,20]. The UV intensity is an important factor and should be optimized. The ozone treatment of ferricyanide has been proven to be technically and economically feasible for industrial purposes.

A literature review of the O_3/CN^- reaction shows that the reaction rate is limited by the ozone mass transfer from the gas to the liquid phase. Presently, the great excess of data lumps the mass transfer and the internal reaction processes into one overall effective "rate constant". This makes the interpretation of data almost impossible. These "rate constants" are valid for a particular contactor and at certain narrow gas flow rate and

concentration ranges. They are obviously not suitable for design purposes. The mass transfer characteristics, reaction kinetics and mechanism of the UV-Ozone-Ferricyanide reaction still remain untouched. It is the main purpose of this research project to further explore the CN^- and $Fe(CN)_6^{-3}$ / O_3/UV reaction systems, and hopefully, from the experimental measurements, to determine kinetic rate constants that are entirely separated from hydrodynamic influences. The ozonation reactions are conducted in a continuous flow, well stirred reactor with known interfacial area and mass transfer characteristics, and the theory of simultaneous absorption and chemical reaction is applied to determine the parameters that characterize the chemical kinetic processes.

CHAPTER 2

LITERATURE REVIEW

2.1 Chemistry of Ozone, Cyanide and Ferricyanide

2.1.1 Ozone Chemistry

Ozone is usually prepared by the action of a static electric discharge upon O_2 or air and concentrations up to 10% O_3 are obtainable[25]. Different sizes of ozone generators are available commercially from companies (such as The Welsbach Corp. and PCI Ozone Corp.[26]) ranging from laboratory scale (3-48 gO_3/day) to industrial scale (50~1000 lbO_3/day).

The chemical reactivity of ozone as a hostile component of the environment is widely recognized. Ozone is characterized as a very toxic compound and has a characteristic odor readily detected even at low concentration. Ozone can be regarded as an allotropic form of oxygen. Because of its oxidizing power, it tends to be reduced to the more stable O_2 form either by reaction with other reducing agents or by self-decomposition. One proposed mechanism for ozone oxidation involves the formation of the active oxygen atom[27] (singlet oxygen) as an intermediate,

$$O_3 \overset{h\nu}{\rightleftharpoons} O_2 + O$$

and this singlet oxygen is believed to be the key component

responsible for smog formation in the atmosphere. The rate of singlet oxygen production is increased by UV irradiation as indicated by the strong absorption band in the UV region (2000~3000°A, Hartley band[28]).

Being a powerful oxidant with a standard half-cell potential of 2.07 v,

$$O_3 + 2H^+ + 2e \rightleftarrows O_2 + H_2O \qquad 2.07\ v$$

ozone has an oxidizing power similar to that of the peroxodisulfate ion and larger than those of permanganate, chromate and hydrogen peroxide. Because of its high potential, ozone will oxidize most of the metals and nonmetals to their highest oxidation state by the 'transferring' of an oxygen atom through a free radical mechanism. The active oxygen atom in ozone can also be transferred to the substance to be oxidized through an ozonide intermediate. Ozone reacts with alkene to give an ozonide[29] which consists of a 5 member ring, and this ozonide can rearrange rapidly to give another different 5 member ring compound

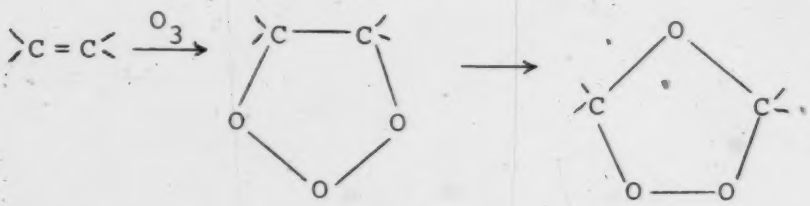

which is quite stable at low temperature but becomes explosive at high temperature. This ozonide can decompose into aldehyde, ketone or carboxylic acid by hydrolysis in

the presence of a reducing agent, e.g. Zn, or it may undergo hydrogenation by H_2 with Pd as catalyst.

The decomposition reaction

$$O_3 \overset{K_D}{\rightleftharpoons} \frac{3}{2} O_2$$

is very exothermic ($\Delta H = -142$ Kcal/mole)[30], and is catalyzed by catalysts such as platinum, nickel and oxides. In the absence of catalyst, the decomposition reaction was found to be first order with respect to ozone. The reaction rate, r mole/ℓ-s, can be expressed as [31,32]

$$r = - K_D [O_3]$$

where K_D is the rate constant at a certain temperature and pH. The effect of pH on the decomposition rate is still controversial. While some workers found the decomposition rate to be lower in an alkaline medium[30,33], Shambaugh and Melnyk[31] held an opposite opinion. They claim that Stumm's correlation can be used to estimate K_D in the pH range from 7.6 to 10.4

$$K_D = k[OH^-]^{0.75} \quad sec^{-1} \quad \text{at } 20°C \qquad (1)$$

and $k = 242$ if $[OH^-]$ is expressed in the unit of molar concentration. At the same time, Czapski[32] correlated K_D and pH in a somewhat different manner

$$K_D = 700[OH^-] \quad sec^{-1} \quad \text{at } 25°C \qquad (2)$$

$$10 < pH < 13 .$$

The dependence of ozone decomposition rate constant on pH can be explained by the mechanism proposed by Alder and Hill[34]

$$O_3 + H_2O \xrightarrow{K_1} HO_3^+ + OH^-$$

$$HO_3^+ + OH^- \underset{K_3}{\overset{K_2}{\rightleftharpoons}} 2HO_2$$

$$O_3 + HO_2 \xrightarrow{K_4} HO + 2O_2$$

$$HO + HO_2 \xrightarrow{K_5} H_2O + O_2 \quad .\ .\ .$$

The change in ozone concentration can be expressed by the following reaction rate equation

$$\frac{r_{O_3}}{dt} = -3 K_3 K_1 [HO_3^+]^{\frac{1}{2}} [OH^-]^{\frac{1}{2}} [O_3]^{\frac{1}{2}} .$$

Both correlations indicate the positive effect of hydroxyl ion concentration on the decomposition rate, and yield similar K_D values at the same pH. The fact that the decomposition of ozone becomes significant at higher pH imposes a limit on the use of ozone as an oxidant in the chemical treatment of waste water at high pH. For instance, Stumm and Czapski predict a K_D of 7.65 and 7 respectively at pH 12, which means that half of the ozone will be destroyed by decomposition in 0.1 sec (half life); thus a large percentage of ozone will be wasted by decomposition especially when the reaction between ozone and the pollutants is slow, as in the case of ferricyanide-O_3 reaction.

Owing to its high reactivity, the popularity of ozone is only second to that of chlorine in water treatment. Numerous articles have been published in that field [35,36]. In summary, the typical applications of ozone include the following:

a) Treatment of industrial waste water containing cyanide, phenol, sulfur compounds, surfactants and polymers;

b) Disinfection of process water and deionized water;

c) Algaecide for cooling towers;

d) Bleaching agent for textile and paper industries;

e) Odor control in water treatment plants and industrial plants;

f) Treatment of domestic waste water (tertiary treatment);

g) Disinfection of biologically treated waste water.

2.1.2 Cyanide and Ferricyanide Chemistry

Cyanide is one of the most poisonous chemicals known by man. Being a strong complexing agent, cyanide has the ability to form stable complexes with virtually every heavy metal in the transition metal block. In aqueous solution, it can undergo hydrolysis easily to give a volatile weak acid, HCN, which has a dissociation constant of 4.93×10^{-10} at 25°C [37].

Fe(II) and Fe(III) can both react with cyanide to form extremely stable complexes ferrocyanide and ferricyanide, with the instability constants of 10^{-35} and 10^{-42} [8]

respectively. The complexes are so stable that the tests for cyanide and iron are both negative in aqueous solution. The complexes are not only thermodynamically stable, but also inert in a kinetic sense as reflected by the slow isotope exchange rate ($t_{\frac{1}{2}}$ = 52 hrs at pH = 3.5) [9]. Both complexes may undergo photo-decomposition under sunlight to liberate the poisonous compound HCN. Devonshire and Weiss [38] found that UV irradiation of ferrocyanide and other anions leads to an unstable species with an absorption spectrum identical with the spectrum of the hydrated electron (~700 nm). The mechanism of the photo-chemical primary process in aqueous ferrocyanide solution is a predissociation of the ferrocyanide ion leading to the trapping of an electron at some distance from its parent center.

$$Fe(CN)_6^{-4} + h\nu \longrightarrow Fe(CN)_6^{-4*} \qquad \text{excited ion}$$

$$Fe(CN)_6^{-4*} \longrightarrow Fe(CN)_6^{-3} + e$$

$$e + \text{trap} \longrightarrow e_t \qquad \text{trapped electron}$$

e_t may react with any oxidants in aqueous solution, for instance, H_3O^+, dissolved oxygen etc. Ohno [39] investigated the other aspect of photo-chemical dissociation of ferrocyanide in aqueous solution by using a high pressure Mercury lamp (366 nm) to irradiate $10^{-3} - 10^{-2}$ M potassium ferrocyanide solution in a quartz vessel. The following reactions are observed:

$$Fe(CN)_6^{4-} + H_2O \overset{h\nu}{\rightleftharpoons} Fe(CN)_5(OH_2)^{3-} + CN^-$$

$$CN^- + H_2O \rightleftharpoons HCN + OH^-$$

The species $Fe(CN)_5OH_2^{3-}$ is identified by its UV absorption peak which ranges from 410 nm at pH 1.14 to 450 nm at pH = 6.5. Ferricyanide reacts with UV in a similar fashion[40], a dissociated product $Fe(CN)_5(OH)_2^{2-}$ is produced upon UV irradiation at the wavelengths of 254, 313, 405 nm.

2.2 Physical Properties of Ozone

2.2.1 Solubility of Ozone in Aqueous Media

The values of Henry's law constant are not consistent in the literature. A value of 67680 atm/mole/cc at 20°C is quoted from Perry's Handbook[41], whereas 79400 atm/mole/cc at 20°C is from Matrozov's publication[42]. The temperature coefficient of Henry's law constant $\Delta H/\Delta T$ is provided by Matrozov's work. The coefficient in the range from 20 to 25°C is found to be 2870 atm/mole/cc per °C by interpolation.

2.2.2 Diffusivity

The values of diffusivity of O_3 in water can be estimated from the Wilke and Chang correlation or obtained from experimental works. The values from various sources are as follows:

$D = 1.984 \times 10^{-5} cm^2/sec$ at 25°C from Wilke & Chang correlation

$D = 1.26 \times 10^{-5} cm^2/sec$ at 20°C from Metrozov [43] .

2.3 Ozone/Cyanide Reaction

The ozone and free cyanide reaction has been studied in a batch reactor with continuous O_3 flow by Sondak and Dodge [44,45], Khandelwal et al. [46], Balyanskii et al. [47], Kandzas et al. [48] as well as Matsuda et al. [49]. For the most part these studies are unsatisfactory because they fail to decouple the ozone mass transfer step from the internal reaction step. For the ozonation reaction expressed as $CN^- + O_3(g) \xrightarrow{K'} O_2(\ell) + CNO^-$, the rate law can be written as

$$\frac{r_{CN}}{dt} = - K'[CN]^n$$

when the partial pressure of O_3 is constant. Sondak and Dodge found that the overall oxidation rate constant K' is almost independent of temperature, which implies a diffusion control mechanism. They reported that the reaction is 0^{th} order with respect to cyanide for cyanide concentrations greater than 4 ppm, and pseudo first order for concentrations between 2 to 4 ppm. In addition to the variation of reaction order, K' was found to depend on the gas flow rates, and the ozone and cyanide inlet concentrations in a very complicated way. In summary, Dodge and Sondak found

$n = 0$ $\quad [CN]_i > 4$ ppm

$n = 1$ $\quad 4$ ppm $> [CN]_i > 2$ ppm

$K' = f(Fg, [CN]_i, P_A)$

However, Khandelwal et al. found that n is equal to 1/3 over a large concentration range.

Balyanskii et al. investigated the CN^-/O_3 reaction in more detail at pH 11-12. The oxidation of cyanide ions by ozone was described by two consecutive reactions (unbalanced)

$$CN^-(\ell) + 1.3\,O_3(g) \xrightarrow{OH^-} CNO^- \qquad (a)$$

$$CNO^-(\ell) + 4.5\,O_3(g) \xrightarrow{OH^-} 0.7\,NO_3^- + 0.15\,N_2 + HCO_3^- \qquad (b)$$

Both processes are pseudo first order with respect to CN^- and CNO^- respectively. They report that the rate of cyanide oxidation is about 5.1 times higher than that for cyanate (CN^-, 0.634 min^{-1}, CNO^-, 0.124 min^{-1} at Fg = 0.34 L/min). From reaction (a) and (b), the ozone consumption is found to be far above the value predicted by simple stoichiometry. This may be due to the fact that the possibility of ozone decomposition has been overlooked.

Selm[46] also indicated that the ozonation of cyanide ion is very fast with no ozone existing in the solution until the cyanide is completely oxidized. The overall conversion of cyanide was determined by how fast the ozone can be transferred from the gas phase to the liquid phase.

Heist[50] suggested that ozone oxidation of cyanide involves an electrophilic reaction either initiated by a singlet oxygen or proceeded through an ozonide intermediate as mentioned in Section 2.2.1 Ozone Chemistry. It is still not clear whether the ozonation of cyanide proceeds through a free radical, the formation of ozonide or a combination of the two.

It has been mentioned in Section 2.1.2 Cyanide and Ferricyanide Chemistry that the reaction between ozone and ferricyanide is slow[21], and it can be enhanced by UV irradiation. Prengle et al.[20,23,24] studied the UV-Ozone-Ferricyanide reaction in both laboratory and pilot scale reactors. A batch reactor with a continuous flow of ozone was used to study the reaction characteristics, and the gas phase was well dispersed to enhance the ozone mass transfer. The concentration of cyanide was recorded at different time intervals and the effect of UV, temperature and concentration of ozone studied qualitatively by comparing the cyanide concentration vs time curves running at various conditions. However, basic kinetic parameters and the reaction mechanism cannot be obtained by this approach because no attempt is made to decouple the mass transfer from the reaction step. Generally speaking, Prengle et al. found that the reaction is favored by high UV intensity, high temperature and high ozone partial pressure.

A six stage continuous flow reactor system has been developed by the Houston Research Group[20], in which the concentration of ferricyanide can be reduced from 4000 ppm at the first stage down to 0.3 ppm at the sixth stage. UV irradiation (75 min) is only applied to the last stage where the ferricyanide concentration is below 20 ppm. There seems to be no apparent advantage to use UV at ferricyanide concentrations higher than 20 ppm.

CHAPTER 3

THEORY

3.1 Background for Mass Transfer Modelling[51,52,53]

Each gas/liquid two phase reaction involves the transfer of a component, A, from the gas phase to the liquid in which the reaction takes place and simultaneous transfer and reaction in the liquid phase. The liquid phase reaction may be a very complicated one consisting of a series of parallel and sequential reactions involving A and B, the liquid reactant, as well as a number of intermediates. The technique of studying a complicated gas-liquid system is to classify the system into a reaction regime and then reduce the system into a number of simpler elementary steps, from which useful kinetic information can be obtained by the application of models. The film model and the penetration model serve equally well for this purpose.

Consider a case where the gas component A transfers into the liquid and reacts with B irreversibly according to the following reactions

$$A(g) \rightleftharpoons A(\ell)$$

$$B(\ell) + A(\ell) \xrightarrow{K_{AB}} P \quad .$$

If the reaction is first order with respect to both A and B, the reaction rate can be expressed as

$$r_B = r_A = K_{AB} C_A C_B \quad . \tag{3}$$

By material balance on A and B, the following differential equations can be written

$$D_A \frac{\partial^2 C_A}{\partial X^2} = \frac{\partial C_A}{\partial t} + K_{AB} C_A C_B \quad . \tag{4}$$

↓ ↓ ↓

Diffusion accumulation reaction

$$D_B \frac{\partial^2 C_B}{\partial X^2} = \frac{\partial C_B}{\partial t} + K_{AB} C_A C_B \quad . \tag{5}$$

At steady state, the equations can be simplified as

$$D_A \frac{\partial^2 C_A}{\partial X^2} = K_{AB} C_A C_B \tag{6}$$

and

$$D_B \frac{\partial^2 C_B}{\partial X^2} = K_{AB} C_A C_B \quad . \tag{7}$$

In the film model, it is assumed that a fictitious stagnant film exists near the surface, outside which there is no concentration gradient. The thickness of the film δ is not directly measurable, it is even questionable whether such a film exists at all. Nevertheless, the thickness is related to a well defined physical quantity K_0, the mass transfer coefficient, by

$$K_0 = \frac{D_A}{\delta} \tag{8}$$

where

$$J = S K_0 (C_{AS} - C_{A0}) \quad . \tag{9}$$

The penetration model takes as its basis the replacement at intervals of elements of liquid at the surface by the liquid from the interior which has the local mean bulk composition. While the element of liquid is at the surface and is exposed to the gas, it absorbs as though it were quiescent and infinitely deep. The rate of absorption is a function of the time of exposure of the element (contact time θ), and can be obtained by solving the unsteady state partial differential equations for material balance (Equations (4), (5)). The physical mass transfer coefficient K_0 is directly related to the contact time θ, which depends solely on the hydrodynamic conditions:

$$K_0 = 2\sqrt{\frac{D_A}{\pi\theta}} \quad . \tag{10}$$

In case of mass transfer with chemical reaction, the transfer of A across the surface will be augmented owing to the additional driving force on the gas molecule. Thus for simultaneous mass transfer and chemical reaction

$$J' = S K_L (C_{AS} - C_{A0}) \quad . \tag{11}$$

K_L is always greater than K_0. The extent of the increase in mass transfer because of chemical reaction is expressed quantitatively by the ratio of K_L to K_0, known as the enhancement factor

$$E_n = \frac{K_L}{K_0} \geq 1 \quad . \tag{12}$$

Two more important parameters t_R, t_D which are borrowed conceptually from the penetration model have to be introduced in order to define the reaction regimes:

$$t_D = \frac{D_A}{K_0^2} \tag{13}$$

$$t_R = \frac{1}{K_{AB} C_B} \tag{14}$$

The diffusion time, t_D, is the average life of the surface element; in other words, the interval of time among successive mixing processes which makes the concentration within the liquid element uniform. The parameter, t_D, depends solely on the hydrodynamic condition. The reaction time, t_R, is the length of time required in order that the reaction may proceed to an appreciable extent. t_R is only affected by the kinetics of the reaction but not the hydrodynamic condition. The solution of the simultaneous ordinary differential equations, Equations (6) and (7), for the film model depends on the boundary conditions at the surface ($x = 0$) and the thickness of the film ($x = \delta$); the boundary conditions are, in turn, governed by the relative magnitude of t_R and t_D. Several regimes are defined for the sake of convenience and simplifying the solution procedure. Astarita[51] provides both the criteria for defining the regimes and the methods for determining the effect of the liquid phase reaction on K_L.

A slow reaction regime refers to the case where the reaction is slower than the mass transfer, i.e.

$$t_R >> t_D \quad . \tag{15}$$

The solution would probably (but not always) be saturated with A; the system is regarded as reaction controlled. Either using a mathematical approach by setting the appropriate boundary conditions or solely by physical argument, it can be shown that K_L is equal to K_0. If the reaction is in the kinetic sub-regime where $SK_0C_{AS} >> VK_{AB}C_{AS}C_{Bo}$

$$J' = r_A = r_B = VK_{AB}C_{AS}C_{Bo} = -V\frac{\partial C_A}{\partial t} \quad . \tag{16}$$

Since the reaction is unaffected by mass transfer and C_{AS} is well defined (P_A/H_A), the reaction can be studied by the conventional time-dependent batch reactor, thus the value of K_{AB} can be calculated from the slope of the log C_A vs t plot. For a CSTR, the mass balance will be

$$J' = F_L\Delta C_A = K_{AB}C_{AS}C_{Bo}V \quad . \tag{17}$$

In the case of slow mass transfer i.e. $t_R << t_D$ where the reaction is fast yet not fast enough to affect the concentration profile of B significantly, and if the reaction can be regarded as pseudo first order, the system is said to be in the fast reaction regime. The solution of Equations (6) and (7) is

$$K_L = \sqrt{D_A K_{AB} C_{Bo}} \quad . \tag{18}$$

A system sitting somewhere between the above two extremes is said to be in a transition regime, where $t_R \doteq t_D$. An analytical solution can be obtained from Equations (6) and (7) by the boundary conditions

$$x = 0 \qquad C_A = C_{AS} = P_A/H_A$$

$$x = \delta \qquad C_A = 0 \qquad (19)$$

The solution is

$$K_L = \frac{\sqrt{D_A K_{AB} C_{Bo}}}{\tanh\left(\sqrt{\frac{D_A K_{AB} C_{Bo}}{K_0}}\right)} \qquad (20)$$

This general solution can be reduced to the two extreme cases by taking the limits

$$\lim_{\substack{K_0 \to \infty \\ (t_R \to \infty)}} K_L = K_0 \qquad \text{slow reaction regime} \qquad (21)$$

$$\lim_{\substack{K_0 \to 0 \\ (t_D \to \infty)}} K_L = \sqrt{D_A K_{AB} C_{Bo}} \qquad \text{fast reaction regime} \qquad (18)$$

which is in perfect conformity with the solutions of the fast and slow reactions.

If the reaction is faster than that described by the fast reaction regime, the concentration of B will not be constant any more, and the assumption of pseudo first order reaction does not hold; the reaction is said to be in a transition from fast to instantaneous reaction regime.

The boundary conditions for the differential equations are

$$C_A = C_{AS} \qquad \text{at} \quad x = 0 \tag{22}$$

$$\frac{dC_B}{dx} = 0$$

$$C_A = 0 \qquad \text{at} \quad x = \delta$$

$$C_B = C_{Bo}$$

An analytical solution of this set of equations is not available, but van Krevelen and Hoftizer[52] (1948) computed an approximate solution and expressed the enhancement factor E as follows:

$$E = \frac{\sqrt{M\left(\frac{E_i - E}{E_i - 1}\right)}}{\tanh \sqrt{M\left(\frac{E_i - E}{E_i - 1}\right)}} \tag{23}$$

where

$$M = \frac{D_A K_{AB} C_{Bo}}{K_0^2} = \frac{t_D}{t_R}$$

$$E_i = \left(1 + \frac{D_B C_{Bo}}{q D_A C_{AS}}\right)$$

q is the stoichiometric factor for the reaction $A + qB \rightarrow P$; K_{AB} can be solved by trial and error.

Danckwerts suggested that if

$$\sqrt{M} > 10\, E_i$$

i.e. $$\sqrt{\frac{t_D}{t_R}} > 10\left(1 + \frac{D_B C_{B_o}}{q D_A C_{AS}}\right) \tag{24}$$

the reaction is in the instantaneous reaction regime, and the solution can be reduced to

$$E = E_i$$

$$\text{i.e.} \quad \frac{K_L}{K_0} = \left(1 + \frac{D_B C_{B_o}}{q D_A C_{AS}}\right) \quad . \tag{25}$$

Similar approach can be applied to the penetration model. In the transition regime, the second order reaction is again approximated by a pseudo first order one. The initial and boundary conditions are

$$\begin{aligned} &t = 0 \quad \text{all } x \quad C_A = C_{A0} \quad C_B = C_{B_o} \\ &t > 0 \quad x = 0 \quad C_A = C_{AS} \quad C_B = C_{B_o} \\ &\qquad x \to \infty \quad C_A \neq \pm\infty \quad C_B = C_{B_o} \end{aligned} \tag{26}$$

then Equation (4) can be solved readily. The flux J' is found to be[51,52]:

$$J' = -D_A \left(\frac{\partial C_A}{\partial x}\right)_{x=0} = C_{AS}\sqrt{K_{AB} C_{B_o} D_A}\left\{\operatorname{erf}\sqrt{K_{AB} C_{B_o}\, t} + \frac{\exp(-K_{AB} C_{B_o} t)}{\sqrt{K_{AB} C_{B_o}\, t\pi}}\right\} \tag{27}$$

where

$$\operatorname{erf} x = \frac{2}{\sqrt{\pi}} \int_0^x \exp(-x^2)\, dx \quad .$$

Taking the average J' over a period of time from t = 0 to t = θ, the life time of an element, then it can be written as:

$$\bar{J}' = \frac{1}{\theta}\int_0^{\theta} J'\,dt = C_{AS}\underbrace{\sqrt{K_{AB}C_{Bo}D_A}\left\{\operatorname{erf}\sqrt{K_{AB}C_{Bo}\theta}\left[1+\frac{1}{2K_{AB}C_{Bo}\theta}\right]+\frac{\exp(-K_{AB}C_{Bo}\theta)}{\sqrt{\pi K_{AB}C_{Bo}\theta}}\right\}}_{K_L}$$

$$= C_{AS}K_L \quad . \tag{28}$$

The limiting cases are:

$$\lim_{\substack{K_0\to\infty \\ (t_R\to\infty)}} K_L = K_0 \qquad (21) \quad \text{slow reaction regime}$$

$$\lim_{\substack{K_0\to 0 \\ (t_D\to\infty)}} K_L = \sqrt{D_A K_{AB} C_{Bo}} \qquad (18) \quad \text{fast reaction regime.}$$

Despite the minor difference, the result is entirely compatible with that of the film model, especially in the limiting cases of slow and fast reaction regimes, where they are identical. Either one of the models can be applied satisfactorily to the O_3-ferricyanide-UV reaction under study.

The approximate solution for the transition from fast to instantaneous reaction regime is provided by Brian et al.(56)

$$E' = \frac{\sqrt{M'\left(\frac{E_i - E}{E_i - 1}\right)}}{\tanh\sqrt{M'\left(\frac{E_i - E}{E_i - 1}\right)}} \tag{29}$$

where

$$M' = \frac{\pi}{4} K_{AB}C_{Bo}\theta = \frac{t_R}{t_D}$$

$$E_i = \frac{C_{B_o}}{qC_{AS}} \sqrt{\frac{D_B}{D_A}} + \sqrt{\frac{D_A}{D_B}} \quad .$$

If $\sqrt{M} = 10\ E_i$

i.e. $$\sqrt{\frac{t_R}{t_D}} > 10 \sqrt{\frac{D_A}{D_B}} \left[1 + \frac{C_{B_o} D_B}{qC_{AS} D_A}\right]$$

then $E = E_i$

i.e. $$\frac{K_L}{K_0} = \sqrt{\frac{D_A}{D_B}} \left[1 + \frac{C_{B_o} D_B}{qC_{AS} D_A}\right] \quad . \tag{30}$$

Using a two resistances in series model, the overall mass transfer coefficient in liquid phase, K_{0L}, can be expressed as a series combination of the two resistances in the gas phase, K_g, and the liquid phase, K_L.

$$\frac{1}{K_{0L}} = \frac{1}{K_L} + \frac{RT}{K_g H} \tag{31}$$

where H has units of atm/mole/cc and K_g has units of cm/s

$$H = 67680 + 2870(T - 20) \quad .$$

$$\therefore \quad \frac{1}{K_{0L}} = \frac{1}{K_L} + \frac{RT}{K_g \{67680 + 2870(T - 20)\}} \quad . \tag{32}$$

If the gas phase transfer resistance is very small compared with that of the liquid phase, the above equation can be reduced to

$$K_{0L} = K_L \quad . \tag{33}$$

J. Rowley[85] measured the gas phase resistance for the same reactor under a similar operating condition, a value of 1.53 cm/sec was obtained for K_g, hence the term RT/K_gH would be equal to 2.15 cm/sec at 22°C.

If the reaction regime is well characterized, the basic parameters can be obtained by applying the appropriate solution for that regime.

3.2 Modelling of Ozonation Reaction

3.2.1 Stoichiometry of the Ozonation Reactions

It has been revealed in Chapter 2 Literature Review that the ozone consumption in Balyanskii's work is far above the value allowed by simple mass balance. This may be due to the fact that ozone decomposition is significant at high pH; the additional consumption of ozone by decomposition causes a higher apparent ozone/cyanide or cyanate ratio. Attributing the excess consumption of ozone to decomposition and completing the material balance in the following unbalanced overall reactions provided by Balyanskii[47]

$$CN^- + 1.3\,O_3^{\cdot} \longrightarrow CNO^- \qquad a)$$

$$CNO^- + 4.5\,O_3 \longrightarrow 0.7\,NO_3^- + 0.15\,N_2 + HCO_3^- \qquad b)$$

the second reaction can be expanded into 2 balanced parallel reactions c) and d), one of which is the cyanate oxidation reaction while the other is the decomposition reaction.

$$0.85\ H_2O + CNO^- + 3.25\ O_3 \longrightarrow 0.7\ NO_3^- + 0.15\ N_2 + HCO_3^- + 3.25\ O_2 + 0.7\ H^+ \quad c)$$

$$1.25\ O_3 \longrightarrow 1.875\ O_2 \quad d)$$

By summing up these two reactions, a balanced reaction b) (reaction e) can be obtained

$$0.85\ H_2O + CNO^- + 4.5\ O_3 \longrightarrow 0.7\ NO_3^- + 0.15\ N_2 + HCO_3^- + 5.125\ O_2 + 0.7H^+ \quad e)$$

The cyanate oxidation reaction itself is composed of two parallel reactions. Cyanate can be oxidized directly to N_2, or hydrolyzed in water to give NH_3, which is then oxidized by ozone to NO_3^-. The oxidation products depend on the residence time of cyanide in the reactor.

Based on this analysis it can be assumed that 1 mole of cyanate reacts with 3.25 moles of ozone after the correction for ozone decomposition has been made. Stoichiometric ratios of 3.25 for cyanate, 1 for cyanide and 1 for ozone self-decomposition are used for all subsequent calculation:

$$q_{CNO} = 3.25$$

$$q_{CN} = 1$$

$$q_{O_3} = 1 \quad .$$

3.2.2 Reaction Scheme - O_3/CN^- Reaction

The purpose of this research project is to model the CN^- and $Fe(CN)_6^{-3}/O_3/UV$ reaction systems and hopefully, from the experimental measurements, to be able to produce a more meaningful and interpretable value of K which is entirely separated from the hydrodynamic influences. In the modelling the whole 2 phase system has been broken into a number of simple consecutive and parallel elementary processes which can be handled proficiently by the models mentioned in the last section after the proper regime is defined.

Schematically, the system can be described as a mass transfer process in series with a family of elementary reactions

$$O_3(g) \xrightarrow[(f)]{K_L} O_3(\ell) \xrightarrow[K_f]{(g)\ CN^-} O_2 + CNO^-$$

$$(i)\downarrow K_D \qquad\qquad K_B \downarrow q_{CNO}O_3 \quad (c)$$

$$1\tfrac{1}{2}\ O_2 \qquad\qquad NO_3^-, N_2, HCO_3^- \ldots.$$

where (f) is the mass transfer process; reaction (g) is the free cyanide oxidation reaction, and K_f the rate constant; reaction (c) is the cyanate oxidation reaction, and K_B the rate constant; reaction (i) is the ozone decomposition reaction, and K_D the rate constant.

According to Balyanskii's work, reactions g, c, i can be written in a more detailed form

$$O_3 \xrightarrow{K_D} \frac{3}{2} O_2$$

$$CN^- + O_3 \xrightarrow{K_f} CNO^- + O_2$$

$$0.85\ H_2O + CNO^- + 3.25\ O_3 \xrightarrow{K_B} 0.7\ NO_3^- + 1.5\ N_2 + HCO_3^- + 3.25\ O_2 + 0.7\ H^+ \quad .$$

The reaction rates are assumed to obey simple rate laws.

$$\text{rate of ozone decomposed} = K_D[O_3]$$

$$\text{rate of cyanide oxidized} = K_f[O_3][CN^-]$$

$$\text{rate of cyanate oxidized} = K_B[O_3][CNO^-]$$

From Balyanskii's work, the ratio of K_f to K_B can be approximated by

$$\frac{K_f}{K_B} \doteq 5.1 \quad . \tag{34}$$

From Stumm's correlation[31]

$$K_D = 242\ [OH^-]^{0.75} \quad \text{at} \quad 20°C \quad . \tag{1}$$

3.2.3 Reaction Scheme - UV/O_3/Ferricyanide Reaction

In contrast to the chemistry of the $O_3/CN^-/UV$ reaction, the reaction system of $O_3/Fe(CN)_6^{-3}/UV$ is more complicated. There is little work done on the properties of cyano group in the ferricyanide molecule; only the cyanide ligand exchange rate has been studied so far[87,88] and the destruction of cyanide in the ferricyanide complex has not been attempted at all. The work shown below only

deals with the mass transfer characteristics and the rate of consumption of ozone. No attempt is made to elucidate the chemistry of the whole system; further research is warranted in this area.

Similar to the free cyanide case, the reaction scheme for ferricyanide can be postulated as

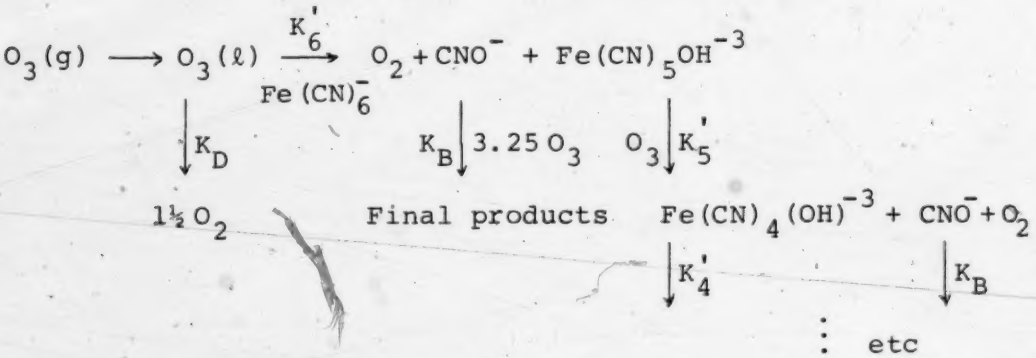

The only difference between the free cyanide and ferricyanide cases is the assumption of the additional consecutive oxidation of the ferricyanide molecule and its intermediate until all the cyanide groups in the complex are exhausted. $Fe(CN)_5OH^{-3}$, $Fe(CN)_4(OH)_2^{-3}$...$Fe(CN)(OH)_5^{-3}$ are the postulated reaction intermediates containing 5 to 1 cyanide groups, and K_5', K_4'...K_1' the corresponding rate constants. The rate of cyanide destruction can be written as:

$$R = [O_3]\{K_6'[Fe(CN)_6^{-3}] + K_5'[Fe(CN)_5(OH)^{-3}] + \ldots K_1'[Fe(CN)(OH)_5^{-3}]\} \quad (35)$$

The subscripts from 1 to 6 are to indicate that these cyanides are different chemically, and thus would have different reaction rates. In order to simplify the model, $K_1'...K_6'$ are lumped into a collective term K, which can be regarded as the effective rate constant, and then R can be rewritten as

$$R = K[O_3][CN] \tag{36}$$

where

$$[CN] \equiv \sum_{i=1}^{6} i\,[Fe(CN)_i(OH)_{6-i}^{-3}] \quad ,$$

the total cyanide content. The above expression holds for one of the following special cases:

i) All cyanides are identical so that they can react with ozone at the same rate. By taking into account the stoichiometric ratio, the following relationships between individual K_i' can be established:

$$K_6' : K_5' : K_4' : \ldots : K_1' = 6 : 5 : 4 : \ldots : 1$$

because the number of cyanides in $Fe(CN)_6^{-3}$ is 6, $Fe(CN)_5OH^{-3}$, 5 and $Fe(CN)_4(OH)_2^{-3}$, 4 etc. Then

$$\sum_{i=1}^{6} K_1'[Fe(CN)_i(OH)_{6-i}^{-3}] = \sum_{i=1}^{6} K_i'\, i[Fe(CN)_i(OH)_{6-i}^{-3}]$$

$$= K_1'[CN] \tag{37}$$

$$\therefore \quad K \equiv K_1' \tag{38}$$

ii) The subsequent oxidations of ferricyanide intermediates are fast comparing with the oxidation of ferricyanide, i.e.

$$K_1', K_2', K_3' \ldots K_5' >> K_6'$$

then

$$K = K_6' \quad . \tag{39}$$

In this case, the intermediates do not exist. Applying the approximation in Equation (36), the complex reaction scheme can be reduced readily into a simple one identical to that assumed for the ozonation of free cyanide except the different rate constant. Because of the approximation made in Equation (36) K would be a weak function of cyanide concentration.

3.3 Modelling of the CN^-/O_3/UV Reaction

3.3.1 Transition from Slow to Fast Reaction Regime - Film Model

The derivation here is to develop the formulation which holds for general cases from slow to fast reaction regimes with bulk ozone concentration not equal to zero. Referring to the reaction scheme shown in Section 3.2.2 Reaction Scheme - O_3/CN^- Reaction, the general material balances for CNO^-, CN^- and O_3 at steady state can be expressed by a set of ordinary differential equations:

$$D_A \frac{\partial^2 C_A}{\partial x^2} = K_f C_A C_B + 3.25\ K_B C_A C_C + K_D C_A \qquad (40)$$

$$D_B \frac{\partial^2 C_B}{\partial x^2} = K_f C_A C_B$$

$$D_C \frac{\partial^2 C_C}{\partial x^2} = -K_f C_A C_B + K_B C_A C_C$$

where C_A, C_B, C_C are the concentrations of ozone, cyanide and cyanate respectively. The equations might be solved by a tedious numerical analysis method. However, the equations can be simplified tremendously by making several bold yet valid assumptions. Providing the reaction to be in a fast or slow reaction regime, the cyanide concentration can be readily assumed to be constant from the interface to the bulk solution (i.e. a flat concentration profile), so the second order reaction of cyanide and ozone can be regarded as a pseudo first order one (Section 3.1 Background for Mass Transfer Modelling, Equation (5)). Since cyanide is in a much larger amount than ozone in solution, the flat cyanide concentration profile assumption should be valid as long as the reaction is not in the instantaneous reaction regime. The material balance of cyanide need not to be considered. To assume a flat profile for cyanate is not so easily justifiable as that for cyanide because the concentration of cyanate in the film has to be higher than that in the bulk solution.

However, cyanate is present only in a minute amount compared with cyanide for the residence time used in the experiments (cf. Mixing Pattern section) and since the reaction rate of cyanate is only 1/5 of that of cyanide, the error associated with the over-simplification will not affect the result to any significant extent. The validity of this assumption will be discussed in Section 6.1 CN/O_3/UV Reaction. The above 3 differential equations can then be reduced into one

$$D_A \frac{\partial^2 C_A}{\partial x^2} = K_f C_A C_{Bo} + 3.25\ K_B C_A C_{Co} + K_D C_A \qquad (41)$$

with the boundary conditions:

$$x = 0 \qquad C_A = C_{As}$$

$$x = \delta \qquad C_A = C_{Ao}$$

where C_{Ao}, C_{Bo}, C_{Co} are the bulk concentrations of ozone, cyanide and cyanate respectively.

The solution of the differential equation is[51]

$$C_A = \frac{C_{Ao} \sinh(a_1 x) + C_{As} \sinh[a_1(\delta - x)]}{\sinh(a_1 \delta)} \qquad (42)$$

where

$$a_1 = \sqrt{\frac{K_1}{D_A}}$$

$$K_1 = K_f C_{Bo} + 3.25\ K_B C_{Co} + K_D$$

$$\delta = \frac{D_A}{K_0}$$

a) Mass Balance of Ozone in the Film

The amount of ozone reacted in the film r_1 is

r_1 = O_3 coming in - O_3 going out

$$= D_A S\left(\frac{\partial C_A}{\partial x}\right)_{x=\delta} - D_A S\left(\frac{\partial C_A}{\partial x}\right)_{x=0} \quad . \tag{43}$$

From Equation (42):

$$\left(\frac{\partial C_A}{\partial x}\right)_{x=\delta} = a_1\left(\frac{C_{Ao}\cosh(a_1\delta) - C_{As}}{\sinh(a_1\delta)}\right) \tag{44}$$

$$\left(\frac{\partial C_A}{\partial x}\right)_{x=0} = a_1\left(\frac{C_{Ao} - C_{As}\cosh(a_1\delta)}{\sinh(a_1\delta)}\right) \tag{45}$$

$$\therefore \quad r_1 = \frac{D_A S a_1}{\sinh(a_1\delta)}\,[\cosh(a_1\delta) - 1]\,[C_{As} + C_{Ao}] \quad . \tag{46}$$

The amount of ozone reacted in the bulk phase r_2 is:

$$r_2 = K_1 C_{Ao} V \quad .$$

The total amount of ozone reacted, RT, is:

$$RT = r_1 + r_2 = \frac{D_A S a_1}{\sinh(a_1\delta)}[\cosh(a_1\delta) - 1]\,[C_{As} + C_{Ao}] + K_1 C_{Ao} V \tag{47}$$

b) Mass Balance of Ozone at the Interface

The flux $J' = -SD_A\left(\frac{dC_A}{dx}\right)_{x=0}$ = total ozone reacted + ozone flowing out in the liquid phase.

$$\therefore \quad \frac{SD_A a_1 [C_{As}\cosh(a_1\delta) - C_{Ao}]}{\sinh(a_1\delta)} = RT + F_L C_{Ao} \quad . \tag{48}$$

c) Bulk Concentration of Cyanate: C_{Co}

Working on the cyanide material balance in a CSTR, it can be shown that

$$F_L[C_{Bi} - C_{Bo}] = [\frac{\partial C_{Bo}}{\partial t} + K_f C_{Bo} C_A'] V \qquad (49)$$

where C_{Bi} is the inlet cyanide concentration and C_A' the effective ozone concentration averaging over the film and the bulk. At steady state $\partial C_{Bo}/\partial t = 0$,

$$F_L[C_{Bi} - C_{Bo}] = K_f C_{Bo} C_A' V \qquad (50)$$

Similarly, the balance on cyanate gives

$$F_L[- C_{Co}] = K_B C_A' C_{Co} V - K_f C_{Bo} C_A' V \qquad (51)$$

Solving C_{Co} from Equations (50) and (51)

$$C_{Co} = \frac{1}{\frac{K_B}{K_f C_{Bo}} + \frac{1}{C_{Bi} - C_{Bo}}} \qquad (52)$$

d) Evaluation of RT, the Total Ozone Reacted

The ozone consumption can be calculated from several possible ways:

i) RT is related to R by the rate constants

$$\frac{RT}{R} = \frac{K_D C_A' + K_f C_{Bo} C_A' + 3.25\ K_B C_{Co} C_A'}{K_f C_{Bo} C_A'} \qquad (53)$$

where C_A' is the effective ozone concentration in the solution

$$R = F_L(C_{Bi} - C_{Bo}) \tag{54}$$

$$\therefore \quad RT = \left[\frac{K_D + K_f C_{Bo} + 3.25\ K_B C_{Co}}{K_f C_{Bo}}\right] F_L(C_{Bi} - C_{Bo}) \quad . \tag{55}$$

ii) RT is directly measured from the gas phase ozone mass balance,

$$RT = R0 \quad . \tag{56}$$

3.3.2 Transition Regime with C_{Ao} Equal to Zero - Film Model

Equations (47), (48) can be tremendously simplified by setting C_{Ao} equal to zero; then a standard solution of the form

$$K_L = \frac{\sqrt{D_A K_1}}{\tanh(a_1 \delta)} = \frac{RT}{SC_{As}} \tag{57}$$

can be obtained from the literature[51]. Equations (47) and (48) in Section 3.3.1 are replaced by Equation (57) with the definition of a_1, K_1, δ remaining unchanged; then the only unknown is K_f which can be solved by Mueller's method[54,55] (Appendix 1). The concentration of ozone drops fairly rapidly as the reaction proceeds from the slow reaction regime to transition regime.

3.3.3 Fast Reaction Regime

The system is simplified a step further by the assumption of fast reaction regime. The reaction is in a fast reaction regime if $t_R << t_D$, and for this case

$$K_L = \sqrt{D_A K_1} = \frac{RT}{SC_{As}} \quad . \qquad (58)$$

Similarly, replacing Equations (47) and (48) by (58), K_f can be solved.

3.3.4 Transition from Fast to Instantaneous Reaction Regime

For the reaction to be in the fast reaction regime, the following criterion should be fulfilled:

$$\sqrt{\frac{t_D}{t_R}} \leq \frac{1}{2}\left(1 + \frac{D_B C_{Bo}}{qD_A C_{As}}\right) \quad .$$

If not, the reaction would be in the transition or even the instantaneous reaction regime. In the transition from fast to instantaneous reaction regime, an approximate solution is available from Danckwerts[52] for the following differential equations:

$$D_A \frac{d^2C_A}{dx^2} - K_f C_A C_B = 0 \qquad (6)$$

$$D_B \frac{d^2C_B}{dx^2} - q_{AB} K_f C_A C_B = 0 \qquad (7)$$

$$x = 0 \;, \quad \frac{dC_B}{dx} = 0 \;, \quad C_A = C_{As} \qquad (22)$$

$$x = \delta \quad C_A = 0 \;, \quad C_B = C_{Bo} \quad .$$

(cf. Section 3.1 Background for Mass Transfer Modelling, Equation (23)).

In case of free cyanide, the differential equations for the reaction scheme developed previously can be written as

$$D_A \frac{d^2C_A}{dx^2} - K_f C_A C_B - K_D C_A - K_B C_A C_C = 0 \qquad (59)$$

$$D_B \frac{d^2C_B}{dx^2} - q_{AB} K_f C_A C_B = 0 \quad . \qquad (60)$$

A transformation technique is used to convert these equations into a simpler form

$$C_A^* \equiv C_1 C_A \qquad (61)$$

$$C_B^* \equiv C_B + C_2 \qquad (62)$$

where C_1 and C_2 are arbitrary constants, and

$$D_A \frac{d^2C_B^*}{dx^2} - K_f C_A^* C_B^* = 0 \qquad (63)$$

$$D_B \frac{d^2C_B^*}{dx^2} - q_{AB} K_f C_A^* C_B^* = 0 \qquad (64)$$

$$\therefore \quad C_2 = \frac{K_D}{K_f} + \frac{K_B}{K_f} C_C \quad . \qquad (65)$$

From Equation (60)

$$C_1 C_A (C_B + C_2) = C_A C_B \qquad (66)$$

$$\therefore \quad C_1 = \frac{C_B}{C_B + C_2} \quad . \qquad (67)$$

Strictly speaking, C_1 is not a constant because it is a function of C_B which varies in the film. However, C_1 can be assumed to be constant if the reaction is in the transition regime where the concentration of B (cyanide) at the film is nearly the same as that at the surface. Also, a flat cyanate concentration profile is assumed. The solution for the transformed equations is

$$E_N = \sqrt{M\left(\frac{E_i - E_N}{E_i - 1}\right)} \Big/ \tanh\sqrt{M\left(\frac{E_i - E_N}{E_i - 1}\right)} \qquad (68)$$

where

$$E_N = K_L/K_0$$

$$E_i = \left(1 + \frac{D_B C^*_{Bo}}{q_{AB} D_A C^*_{As}}\right) = \left(1 + \frac{C^*_{Bo}}{C^*_{As}}\right)$$

$$M = \frac{D_A K_f C^*_{Bo}}{K_0^2}$$

$$C^*_{Bo} = C_{Bo} + \frac{K_D}{K_f} + \frac{K_B}{K_f} C_{Co}$$

$$C^*_{As} = \frac{C_{Bo} C_{As}}{C_{Bo} + \frac{K_D}{K_f} + \frac{K_B}{K_f} \times C_{Co}}$$

It has been indicated by J. Rowley[85] that $D_B \doteq D_A$; and the stoichiometric ratio of ozone to cyanide, q_{AB}, is known to be 1 for free cyanide.

3.4 Modelling of the Ferricyanide/O_3/UV Reaction

3.4.1 Flat CNO Concentration Profile

The approach is essentially the same as that of the free cyanide, so the derivation developed earlier (3.3 Modelling of the CN^-/O_3/UV Reaction) for free cyanide can also be applied to ferricyanide with only minor modifications. K_f in free cyanide case is replaced by its counterpart K, the rate constant of the ozone/ferricyanide/UV reaction, and K_B, the rate constant of ozone/cyanate reaction, is assumed to be 1/5.1 of K_f determined from cyanide decomposition measurements. From Equation (1), K_D has the value of 8.5×10^{-4} sec^{-1} at pH = 7 and 700[OH] at pH 12 as calculated from the Czapski correlation. C_B in the equations stands for the total cyanide content in the solution, and the bulk concentration of ozone, C_{Ao}, is equal to zero. Since the reaction between ozone and ferricyanide is rather slow, the transition from slow to fast reaction regime is tried (cf. 3.3.2 Transition Regime with C_{Ao} Equal to Zero - Film Model).

3.4.2 Quadratic CNO Concentration Profile - Film Model

While the assumption of flat CN concentration profile holds for both cases, the approximation of constant CNO concentration is questionable in the case of ferricyanide because the reaction between ozone and ferricyanide is considerably so much slower such that cyanate plays a more

significant role in determining the overall ozone mass transfer; even a slight difference in cyanate concentration profiles may change the value of K completely. In order to improve the proposed model, the possibility of non-flat CNO profiles has to be explored.

Considering the mass balances of ozone and cyanate, the following ordinary differential equations can be written:

$$D_A \frac{\partial^2 C_A}{\partial x^2} = KC_A C_{Bo} + 3.25\, K_B C_A C_C + K_D C_A \qquad (69)$$

$$D_C \frac{\partial^2 C_C}{\partial x^2} = -KC_A C_{Bo} + K_B C_A C_C \qquad (70)$$

The mass balance of cyanide need not to be considered because it is in excess compared with ozone. There are a number of routes to solve these equations, for instance, numerical analysis[56,57,58] and collocation technique. The latter does not require as much computer effort and can give a result as good as the first one. In addition to its simplicity, the collocation technique can also furnish a better physical picture.

In the collocation technique, a quadratic CNO concentration profile is assumed. The three parameters involved i.e. b_1, b_2, b_3 in Equation (71) can be solved easily by imposing the boundary conditions onto the equation

$$\frac{C_C}{C_{Co}} = b_1 + b_2 \frac{x}{\delta} + b_3 \frac{x^2}{\delta^2} \qquad (71)$$

where b_1, b_2, b_3 are the dimensionless parameters, and C_{Co} the bulk concentration of CNO^-. The boundary conditions are:

i) $x = \delta$ $\qquad C_C = C_{Co}$ $\qquad (72)$

ii) $x = \delta$ $\qquad -S D_C \left.\frac{dC_C}{dx}\right|_{x=\delta} = F_L C_{Co}$. $\qquad (73)$

The amount of cyanate diffusing out of the film into the bulk phase per unit time is equal to the flow rate of cyanate going out of the reactor.

iii) $x = 0$ $\qquad \left.\frac{dC_C}{dx}\right|_{x=0} = 0$ $\qquad C_C = C_{Cs}$ $\qquad (74)$

where C_{Cs} is the surface cyanate concentration. The boundary conditions and the concentration profile can be represented schematically in the following diagram.

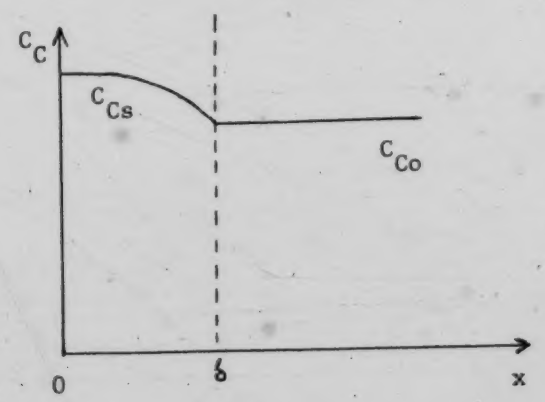

From the above boundary conditions, the following equations can be obtained:

i) At $x = \delta$, $C_C = C_{Co}$

$$b_1 + b_2 + b_3 = 1 \quad . \tag{75}$$

ii) $F_L C_{Co} = - C_{Co} D_C S \left(\frac{b_2}{\delta} + \frac{2b_3}{\delta}\right)$

$$- \frac{F_L \delta}{D_C S} = b_2 + 2b_3 \quad . \tag{76}$$

iii) At $x = 0$, $dC_C/dx = 0$

$$b_2 = 0 \quad . \tag{77}$$

Solving Equations (38), (39), (40),

$$\left.\begin{aligned} b_1 &= 1 + \frac{F_L \delta}{2D_C S} \\ b_2 &= 0 \\ b_3 &= - \frac{F_L \delta}{2D_C S} \end{aligned}\right\} \tag{78}$$

$$\therefore \quad \frac{C_C}{C_{Co}} = 1 + \frac{F_L \delta}{2D_C S} - \frac{F_L \delta}{2D_C S} \frac{x^2}{\delta^2} \tag{79}$$

$$C_{Cs} = \left(1 + \frac{F_L \delta}{2D_C S}\right) C_{Co} \doteq \left(1 + \frac{F_L}{2K_0 S}\right) C_{Co} > C_{Co} \quad .$$

This is obvious because the cyanate concentration in the film from which cyanate is generated has to be higher than that in the bulk solution. Using the typical values of F_L, K_0, S in the experiments, C_{Cs} can be related to C_{Co}

by

$$C_{Cs} \doteq 2.34\ C_{Co} \quad . \tag{80}$$

C_{Co} can be obtained from the cyanide concentration by Equation (52) and it is only a function of K.

A single ordinary differential equation containing C_C, C_A and x as variables can be got by combining two differential equations in Equation (69)

$$D_A \frac{d^2C_A}{dx^2} - 3.25\ D_C \frac{d^2C_C}{dx^2} = 4.25\ KC_{Bo}C_A + K_DC_A \quad .$$

Substituting Equation (79) into the above equation, then

$$D_A \frac{d^2C_A}{dx^2} - (4.25\ KC_{Bo} + K_D)\ C_A = -\ 3.25\ \frac{F_L}{S\delta}\ C_{Co} \quad . \tag{81}$$

The only variable is C_A, so Equation (81) is simply a second order homogeneous ordinary differential equation of which solution can be obtained readily.

$$\begin{aligned} C_A &= C_A(\text{complimentary}) + C_A(\text{particular}) \\ &= C_1'\exp(\sqrt{b_4}\,x) + C_2'\exp(-\sqrt{b_4}\,x) + b_5/b_4 \\ &= C_1\sinh(\sqrt{b_4}\,x) + C_2\cosh(\sqrt{b_4}\,x) + b_5/b_4 \end{aligned} \tag{82}$$

C_1', C_2' or C_1, C_2 are the integration constants to be specified by boundary conditions, b_5 and b_4 are constants defined as

$$\left.\begin{aligned} b_4 &\equiv \frac{4.25\ KC_{Bo} + K_D}{D_A} \\ b_5 &\equiv 3.25\ \frac{F_L}{D_A S\delta}\ C_{Co} \end{aligned}\right\} \qquad (83)$$

The boundary conditions for ozone are

$$x = 0 \qquad C_A = C_{As}$$

$$x = \delta \qquad C_A = C_{Ao} = 0 \quad .$$

Substituting these conditions into Equation (82)

$$C_{As} = C_2 + b_5/b_4$$

$$0 = C_1 \sinh(\sqrt{b_4}\,\delta) + C_2 \cosh(\sqrt{b_4}\,\delta) + b_5/b_4 \quad .$$

Solving C_1, C_2 from the two equations, and substituting the values into Equation (82),

$$C_A = \left[\frac{C_{As} - b_5/b_4}{\sinh(\sqrt{b_4}\,\delta)}\right] \sinh[\sqrt{b_4}(\delta - x)] + \frac{b_5/b_4}{\sinh(\sqrt{b_4}\,\delta)}$$

$$\times\ [\sinh(\sqrt{b_4}\,\delta) - \sinh(\sqrt{b_4}\,x)] \qquad (84)$$

$$K_L = -\left(\frac{1}{C_{As}}\right)\left(\frac{dC_A}{dx}\right)_{x=0} = \frac{D_A\sqrt{b_4}}{C_{As}\sinh(\sqrt{b_4}\,\delta)} \left\{\frac{b_5}{b_4} + \left[C_{As} - \frac{b_5}{b_4}\right]\cosh(\sqrt{b_4}\,\delta)\right\} \qquad (85)$$

$$K_L = \frac{RT}{SC_{As}} \quad . \qquad (86)$$

The assumption of zero bulk ozone concentration is always valid as long as the reaction is in the transition regime. In fact, ozone bulk concentration drops fairly rapidly as the reaction proceeds from the slow reaction to the transition regime as indicated by the value of C_{Ao} calculated in 3.3.1 Transition from Slow to Fast Reaction Regime (not listed in the thesis). Equation (87) is a combination of Equations (85) and (86)

$$RT = \frac{SD_A\sqrt{b_4}}{\sinh(\sqrt{b_4}\delta)} \left\{\frac{b_5}{b_4}\left[C_S - \frac{b_5}{b_4}\right]\cosh(\sqrt{b_4}\delta)\right\} \qquad (87)$$

where b_4 and b_5 are defined by Equation (83) and $\delta = D_A/K_0$.

3.4.3 Penetration Model

Assuming flat concentration profiles for both CN^- and CNO^-, the unsteady state ozone mass balance can be expressed as (cf. Equation (4))

$$D_A \frac{\partial^2 C_A}{\partial x^2} = \frac{\partial C_A}{\partial t} + KC_AC_{Bo} + 3.25\ K_BC_AC_{Co} + K_D \ , \qquad (88)$$

The solution to this partial differential equation is shown in Equation (28)

$$K_L = \frac{RT}{C_{As}S} = \sqrt{K_1D_A}\left\{\text{erf}\sqrt{K_1\theta}\left[1 + \frac{1}{2K_1\theta}\right] + \frac{\exp(-K_1\theta)}{\sqrt{\pi K_1\theta}}\right\} \qquad (89)$$

where

$$K_1 \equiv KC_{Bo} + 3.25\ K_BC_{Co} + K_D$$

$$\theta \equiv \frac{4D_A}{\pi K_0^2}$$

$$\text{erf}\, x = \frac{2}{\sqrt{\pi}} \int_0^x \exp(-x^2)\, dx \quad .$$

The penetration model differs from the film model only by the expression for K_L.

CHAPTER 4

EXPERIMENTAL

4.1 Equipment Description

4.1.1 Reactor and UV Lamp Assembly

The reactor is shown schematically in Figure 1. The reactor is a QVF glass section, 18.6 cm in height and 10.84 cm in diameter. It is sealed by silicone rubber gaskets between a stainless steel plate at the top and a quartz plate at the bottom. A stainless steel ring of inner diameter 10.3 cm (4 in) is used to hold the quartz plate (12.7 cm diameter, 7 mm thickness) in place by 6 bolted rods from the stainless steel plate to the ring at the bottom. Another silicone rubber gasket is inserted between the steel ring and the quartz plate. The bolts have to be tightened gently and evenly with extreme care. Excessive torque on any one of the bolts would create strain and probably crack the quartz plate. The quartz plate is used because it is transparent to UV.

The stirrer is also constructed of stainless steel. The end of the shaft (1 cm diameter) is slotted into a Teflon bearing (1.6 cm × 2.54 cm diameter) glued at the center of the quartz plate and three sets of stirring blades are attached to the shaft. An upper propeller is used to provide uniform mixing in the gas phase; a stirrer located slightly above the liquid surface is used to

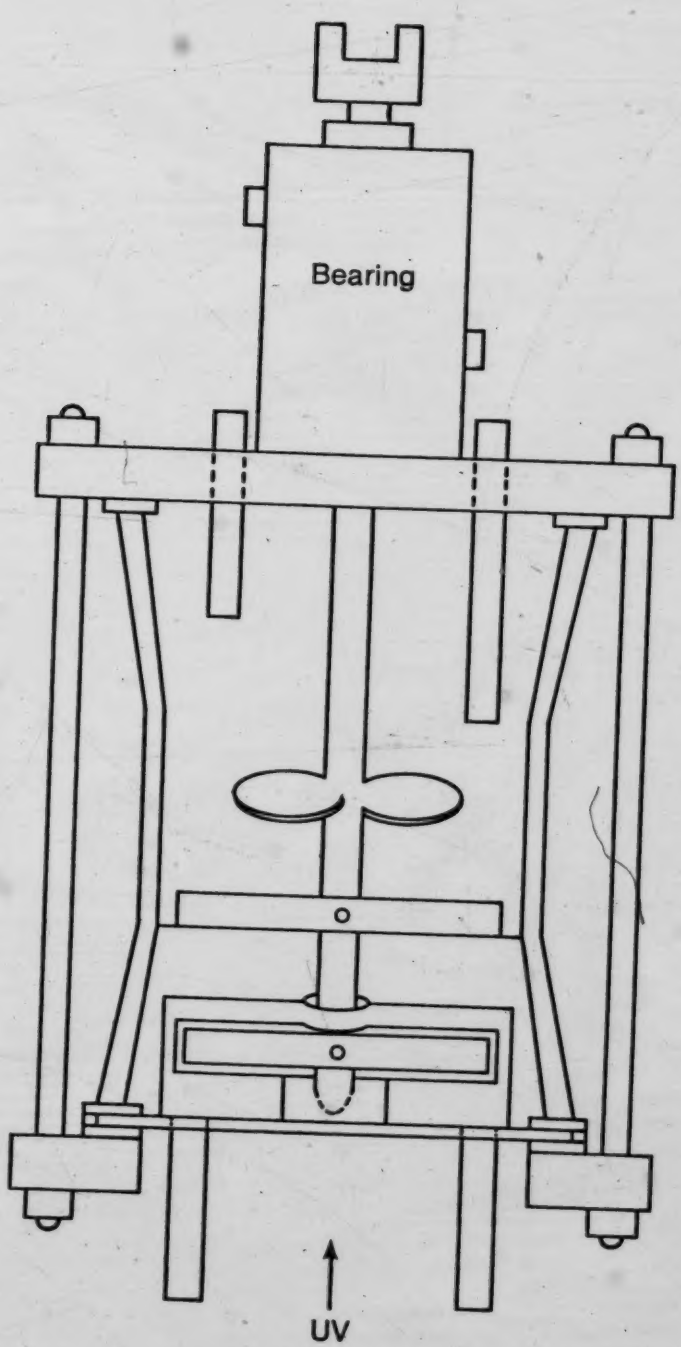

Figure 1 QVF photochemical reactor for the O_3/Ferricyanide/UV reaction

minimize the gas phase resistance, and the bottom stirring blades (7.3 cm × 0.95 cm) are used to agitate the liquid. The stirring speed can be set precisely by changing the gear ratio. A stainless steel baffle of dimension 8.9 cm × 4.13 cm is used to eliminate ripples and vortex formation in the liquid phase. It is possible to have a well mixed liquid phase and yet maintain a quiescent interfacial area in the experiment, thus the interfacial area can be approximated by the geometrical surface area. The internal diameter at the liquid surface is 10.392 cm as measured by a Vernier scale, so the surface area is equal to 84 cm^2 after accounting for the stirring shaft.

Two pieces of stainless steel tubing of 4.76 mm i.d. are glued into the two holes drilled on the quartz plate as the inlet and outlet for the solution. Likewise, two tubes are screwed into the top plate for ozone. It is crucial to maintain a reproducible liquid level and surface area in the experiments, thus a mark is placed on the side of the reactor to indicate the proper liquid level.

A 200 watt Hanovia medium pressure Mercury lamp (model 65410) is mounted on an aluminum reflector of dimension 44.5 cm length × 10.16 cm height × 5.08 cm width. The reactor is seated 2 cm above the reflector. To avoid stray UV light, the whole reflector is enclosed by metal except for a 11.43 cm × 5.08 cm space via which UV light

is directed through the quartz bottom plate of the reactor. One end of the reflector is open while the other end is slightly widened to house an air fan used to dissipate the heat generated by the UV lamp. The UV lamp is hooked to a Hanovia UV ballast transformer. The whole reflector assembly is mounted firmly on a pole, and the position and orientation are carefully marked so that it can be placed in the same position for each run. Screens, placed between the reactor and the reflector, are used to vary the intensity of the UV radiation.

In addition to the forced turbulent mixing, the dispersion of ozone is further augmented by the upper propeller and the middle interface stirring blade. The latter can also reduce the gas phase resistance in the reactor.

4.1.2 General Description of the Set-up and Flow Diagram

The reactor is a CSTR with continuous flows of O_3 and cyanide solution. The UV lamp is directly beneath the reactor. The set-up is shown schematically in Figure 2, and the following instruments and symbols are used:

Ozonator: PCI Ozone Corp., model C2P-9C4
Stanford, Conn., U.S.A.
Capacity 9 gO_3/hr from dry air.

Gas-dryer: Drierite $CaSO_4$
W.A. Hammond Drierite Co.
Xenia, Ohio, U.S.A.

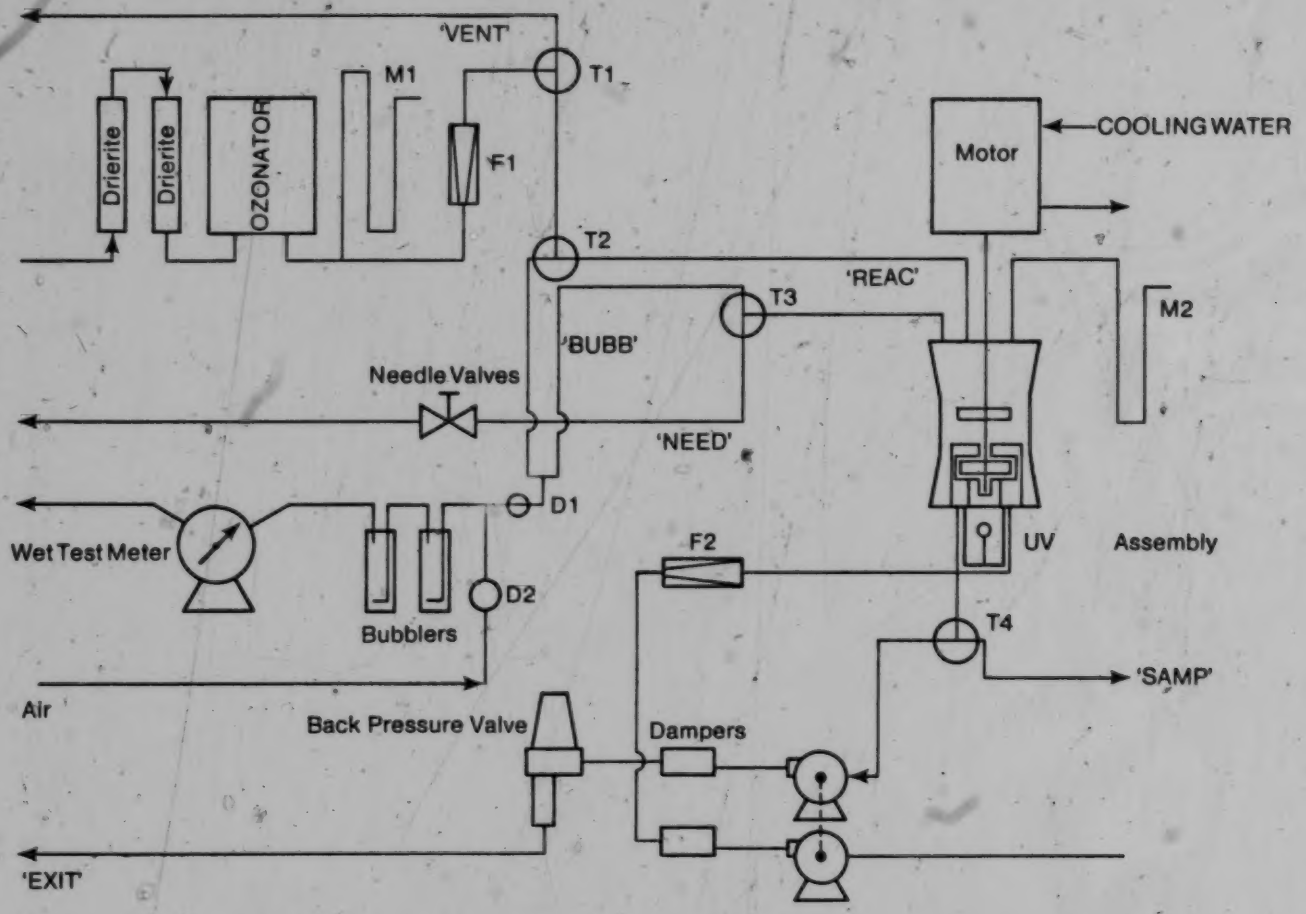

Figure 2 Schematic representation of the general set-up for the O_3-Ferricyanide-UV reaction

T : Whitey, 3 way ball valves, 316 stainless steel body.

D : Whitey, on-off valves, 316 stainless steel body.

Needle valve: NUPRO, 'S' series, 216 stainless steel.

M : Manometer.

The functions of various components of the set-up are described as follows:

Drierite : absorbs the moisture in the air that otherwise may cause damage in the ozonator.

Cooling water: removes the heat generated in the bearing.

M1 : gives the pressure at the gas inlet.

M2 : gives the reactor pressure.

Needle valve: is located at the gas outlet to control the reactor pressure in such a way that the pressures in the reactor should be the same in the run and the outlet gas sampling, so that the steady state will not be disturbed by sampling.

Back pressure valve: holds the liquid in the reactor so that the liquid will not drain out by gravity or by pressure.

Dampers: serve to smooth the pulse of circulating liquid resulting from the positive displacement pumps.

Bubblers with fritted disc gas disperser: contains 4% KI solution for ozone sampling.

Wet test meter: records the inert air flow rate after ozone is stripped by the bubblers.

T1: stops the ozone supply by connecting to 'VENT' position.

T2: samples inlet O_3 by turning to 'BUBB' position from 'REAC'.

T3: samples outlet O_3 by turning to 'BUBB' from 'NEED'.

T4: samples outlet liquid by turning to 'SAMP' from 'EXIT'.

D1: closes to stop O_3 to the bubblers.

D2: opens to purge the O_3 trapped in the tubings by air.

Polyflo tubing deteriorates slowly in the presence of O_3 and must be replaced periodically. A detailed operating procedure is given in Appendix 2.

4.1.3 Safety Measures

Ozone is a poisonous gas, so care should be taken to avoid ozone escaping into the working area. The ozonation experiment has to be done inside a well-ventilated fume hood. If the characteristic odor of ozone is sensed, the ozonator should be shut down immediately until the faulty part is fixed. Cyanide should also be handled with

extreme care; gloves should be worn to protect hands from direct contact with cyanide or its solution. Cyanide solutions must be kept at a pH higher than 12 to avoid formation of the volatile compound HCN. After the cyanide solution is drained, sufficient water should be used to rinse the sink as well as to dilute the cyanide solution. It is a good practice to immerse the ozone outlet into the waste cyanide solution so that the cyanide level is lowered by ozone oxidization before it is discharged. Hands should be washed after experiment.

4.2 Reactor Characterization

4.2.1 Mixing Pattern

Since the analyses of results depend on the assumption of ideal mixing in the continuous flow stirred tank reactor, this assumption has to be justified before further work can be done. Should any non-ideal mixing pattern be detected, the reactor has to be redesigned to facilitate more efficient mixing until the requirement is met. Ideal mixing refers to the case of complete mixing so that the properties of the reaction mixture are uniform in all parts of the vessel and are the same as those in the exit stream. In other words, there would be no concentration or temperature gradient in the reactor.

The mixing behavior of a CSTR can be studied by a residence time distribution RTD experiment[59,60] in which a 'step function' input is imposed on the reactor,

and the response in the exit stream is recorded. The residence time $\bar{t}_R$ is the average time the molecules spend in the reactor. In this experiment, diluted HCl was used to provide the step change, and a pH meter and glass electrode were used to monitor the exit pH. Details are given in Appendix 3.

A typical recorder output for a stirring rate of 85 rpm is shown in Figure A1. The time delay t_L is indicated in the time axis by a sudden drop in pH, and equal to 2.48 min as measured directly from the recorder output. At time larger than t_L, the pH drops down exponentially and then levels off after 8 minutes. $\text{Log}(C_f - C)/(C_f - Co)$ at different stirring rates are plotted against t in Figures A2-A5. For the first three graphs (Figures A2-A5) for which the stirring rates are greater than 0 rpm, straight lines can be drawn through the points. t_L can be measured readily from the graphs as the time at which the lines bend sharply from a zero slope to some negative values. The values of t_L for all four cases including the one without stirring are 2.48 minutes. The mean residence times $\bar{t}_R$ are calculated correspondingly from the slopes of the lines and found to be 7.84, 7.87 and 7.46 minutes for 102, 85 and 59.5 rpm.

The results are tabulated in Table 1. The values of t_L and $\bar{t}_R$ from graphical methods (Figures A2, A3, A4, A5 in Appendix 3) are compared with those by calculation (Equations (A22), (A23) in Appendix 3), and good agreement

RPM	Graphical method		CSTR assumption
	t_L, min	$\bar{t}_R$, min	
102	2.5	7.84	good
85	2.5	7.87	good
59.5	2.5	7.46	?
0	4.82	6.07	no

Liquid flow rate, F_L 71 ml/min

Reactor volume, V 533 ml

Inlet void volume (from the feed tank to the reactor) 66 ml

Outlet void volume (from the reactor to the glass electrode) 110 ml

Calculated time delay, $t_L = (66 + 110)/71 = 2.48$ min

Calculated average residence time, $\bar{t}_R = 533/71 = 7.51$ min

Table 1. Comparison of $\bar{t}_R$ and t_L from graphical method and direct calculation at different stirring rates.

can be seen. Finally, it can be concluded that the mixing is perfectly ideal with stirring rate down to 70 rpm; a slight deviation from ideal mixing begins to show up at 59.5 rpm which causes a decline of $\bar{t}_R$ from 7.87 to 7.46 minutes. The assumption of ideal CSTR that has been made earlier is valid at a stirring rate higher than 70 rpm.

4.2.2 Physical Mass Transfer

The physical mass transfer coefficient for O_2 in water, K_0, can be measured either directly or indirectly. The first method involves measurements of the partial pressure and the concentration of the gas component in the gas and solution phase, while the latter the correlation of K_0 of the gas component to that of CO_2 by the assumption of equal contact time θ in the penetration model. Being able to yield K_0 without making use of any model, the direct method is deemed to be better than the indirect one. However, the indirect (H_2O-CO_2) method should be as good as the direct one if the contact time θ only depends on the hydrodynamic conditions such as the detailed design of the reactor and the way the solution is stirred, but not on the nature of the gas molecules itself. CO_2-H_2O method has received wide-spread acceptance, and finds use in cases where the gas does not dissolve enough in water to give a detectable concentration in water, or no suitable analytical method exists, or the gas reacts instantaneously with water so that K_0 cannot be obtained. CO_2 is

particularly used because there is no gas phase resistance nor any known fast chemical reactions which may enhance the transfer.

The O_3-H_2O method is quite straightforward. O_3 was in contact with distilled water in the continuous flow well stirred reactor shown in Figures 1 and 2 and the ozone concentration in the outlet water was measured. O_3 was measured by iodometric method while CO_2 was by acid base titration. The detailed operating procedure, theory and calculation are shown in Appendix 4.

The K_0 from indirect (CO_2-H_2O) and direct (O_3-H_2O) measurements are plotted in Figure 3 as a function of stirring speed. Two straight lines can be seen, with the indirect value 3.8% lower. The close agreement between these two values validates the CO_2 correlation approach, which is indeed a powerful tool whenever the direct measurement method is not feasible. The slopes of these two lines are both 0.744 as compared with 0.8 from Sata's work[61]. The physical mass transfer coefficient of ozone is correlated with the stirring rate by the following expression:

$$\log K_0 = -4.172 + 0.744 \log \text{rpm} \quad . \qquad (90)$$

The values of K_0 by the two methods are also compared in Table 2. It can be observed that K_0 depends strongly on the degree of agitation. The increase of K_0 with stirring rate is comprehensible, because the surface renewal rate is enhanced in the penetration model point of view, or the film

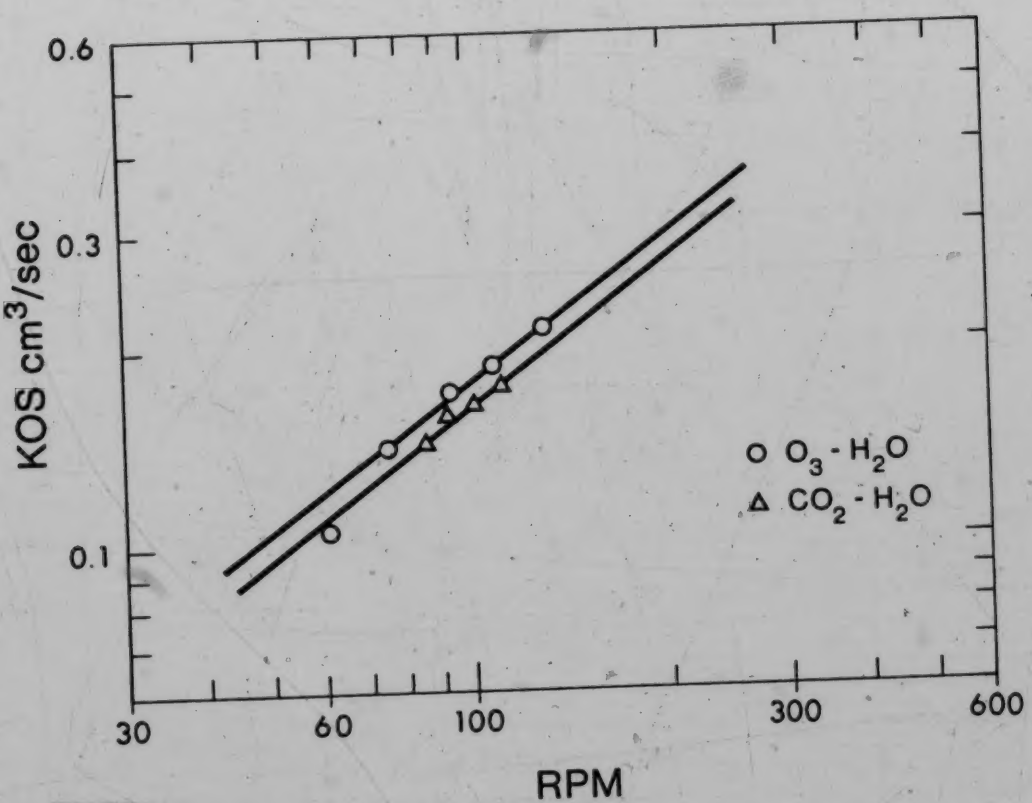

Figure 3. Plots of log K_0S by both O_3-H_2O and CO_2-H_2O methods vs log rpm at 22°C.

RPM	T	K_0 (O_3-H_2O)	K_0 (CO_2-H_2O)
	deg C	10^{-3} cm/s	10^{-3} cm/s
131	20.67	2.527	----
112	20.67	2.239	----
	21.17	----	2.086
102	20.00	----	1.974
93.6	20.67	2.043	----
92.7	21.17	----	1.887
86.0	20.00	----	1.706
74.7	20.67	1.667	----
60.8	20.67	1.246	----
60.2	21.17	----	1.273

Table 2. Comparison of K_0 of ozone measured by O_3-H_2O and CO_2-H_2O systems.

thickness decreases in terms of the film model. Besides the stirring rate, the physical mass transfer coefficients were measured at different stirring blade positions; a gradual decrease in transfer coefficient from 10.69 cm/sec with the blades 1 mm below the surface, to 7.45 cm/sec at the surface and 1.998 cm/sec just slightly above the surface was observed. This phenomenon proves that the proper maintenance of surface level is not trivial at all. The increase in K_0 with the blades touching the solution is due to the increased mixing at the interface as well as the increased area caused by the ripple and vortex.

It is known that CO_2 may react with water chemically according to the following consecutive reversible reactions

$$CO_2 + H_2O \rightleftarrows H_2CO_3 \rightleftarrows H^+ + HCO_3^-$$

A question might rise concerning whether the $K_0(CO_2)$ measured is entirely due to physical absorption or a combination of physical and chemical processes. The CO_2 system had been studied thoroughly by Danckwerts[62]; it was found that these reactions were relatively slow compared with the physical absorption process. Technically, the system is classified in a 'slow reaction regime' where the mass transfer coefficient K_L is the same as K_0.

The low partial pressure (2×10^{-2} atm at most) and solubility of ozone create problems in analysis. Even when a micro burette is used, serious scattering is observed at low stirring rates because of the low solubility. There is

no interference other than the possible decomposition of O_3. However, since the background pH of the distilled water is 5, the effect of decomposition is deemed to be negligible (cf. Equations (1) and (2)). The assumption of zero gas phase resistance is justified by the value of the gas phase resistance measured by J. Rowley[85].

4.2.3 Characterization of UV Intensity

In order to study the UV effect on the O_3-Ferricyanide reaction, the effective UV intensity, E, in the reactor for different screens had to be measured. A sensitive chemical actinometer (potassium ferrioxalate) which produced an easily analyzable product (Fe^{2+}) upon the absorption of UV was used for UV measurement. The Fe^{2+} produced was analyzed by the absorbance of the red Fe^{2+}-1,10-phenanthroline complex. The details are given in Appendix 5.

The concentrations of Fe^{2+} and the corresponding absorbances are shown in Table A3 in Appendix 5. A calibration curve is also constructed by plotting the absorbance against the concentration of Fe^{2+} and is given in Figure A6 in Appendix 5. This is a straight line passing through the origin with a slope equal to $\varepsilon\ell$, the product of molar absorptivity and the light path. From Figure A6, the term $\varepsilon\ell$, the product of molar absorptivity, and path length is found to be $1.73 \times 10^4\ M^{-1}$.

The net absorbance, the corresponding Fe^{2+} concentration, the number of moles of Fe^{2+} produced, n_B, the number of

quanta absorbed by the ferrous complex per unit time, I_0, the equivalent wattage, E, and the relative intensity are tabulated in Table 3. E was also measured directly by a Black Ray UV intensity meter. The results are given in Table 4. For this method, E is calculated by multiplying the reading on the meter by the area of the opening, which is measured to be 11.4 cm × 5 cm = 57 cm^2. Comparing the results from these two methods, the values of E from meter measurement are lower owing to the fact that the meter cannot respond to wavelengths larger than 2700°A. The values of E by chemical method give the total incident energy with wavelengths smaller than 5400°A, whereas the readings from the UV meter give only the fraction of energy with wavelengths not greater than 2700°A. In spite of the difference in absorptivity, the relative intensities based on full UV (as 100%) are expected to be the same for both methods for a given light source; however, they differ substantially as revealed in Tables 3 and 4. The discrepancy comes from the uncertainty in the reading of scale from the UV meter at full UV intensity, because it is just at the edge of the scale. It is confirmed by comparing the ratios of E(fine) to E(coarse), and they are found to be 2.6 and 2.4 for the chemical method and meter method respectively, so the error must originate from the measurement in the 'full UV' case.

The possible error sources for the chemical method are:

Table 3. Characterization of UV intensities by ferrioxalate actinometer at 21°C

UV	Exposure time sec	Absorbance	Absorbance net	Concentration 10^{-5} M	n_B 10^{-5} mole	10^{17} I_o quanta per sec	E watt	Rel. %
Full	85.2	0.665	0.642	3.73	9.33	5.28	0.319	100%
Fine	91.3	0.302	0.279	1.61	4.03	2.13	0.129	40.4%
Coarse	150.2	0.200	0.177	1.02	2.55	0.818	0.0495	15.5%
No	150.4	0.023	0.0	0	0	0	0	0%

Table 4. Characterization of UV intensities by Blak-Ray UV intensity meter

UV	Center intensity 100 μ watt/cm^2	Edge intensity 100 μ watt/cm^2	Average intensity 100 μ watt/cm^2	E watt	Relative %
Full	42	36	39	0.2223	100%
Fine	12	10.6	11.3	0.0644	29.0%
Coarse	5	4.4	4.7	0.0268	12.1%
No	0	0	0	0	0

Area of the opening $11.4 \times 5 = 57$ cm^2 .

i) the undesired photo-decomposition of ferrioxalate after it is taken out from the reactor. The dim light used in performing experiment and the light source in Spectronic 20 may cause further reaction of ferrioxalate.

ii) the assumption of no contribution to Fe^{2+} production for wavelengths greater than 5400°A. For more accurate work, the values of ϕ_B has to be known continuously for all wavelengths, or a monochromatic light source must be used.

iii) the error in $\bar{\nu}$ due to the uncertainty in the energy distribution function. To obtain a better result requires the knowledge of continuous energy distribution function or the use of monochromatic light.

In spite of the uncertainty in the chemical method, the values of the relative intensities measured using this method are thought to be more reliable and are used for the subsequent experiments.

4.3 Analytical Procedures

4.3.1 Ozone Analysis

Ozone was measured by a well-documented iodometric method[77]. In this method, the gas was bubbled through a neutral 4% KI solution and ozone reacted to liberate iodine

$$H_2O + 3I^- + O_3 \longrightarrow O_2 + I_3^- + 2OH^- \quad .$$

Under neutral or alkaline conditions, the interference of O_2 is minimal. The neutral I_2 solution (e.g. in bubbler B1)

was then acidified by 30 ml 1:10 H_2SO_4 solution, and titrated immediately by 0.1 N $Na_2S_2O_3$ solution which had been standardized against standard 0.1 N I_2 solution (Fisher Scientific Co.). Since the I^- in the solution was subject to air oxidation after acidification, the titration must be finished quickly. A magnetic stirrer was used to facilitate thorough mixing. Starch solution, as recommended by Taras et al.[45], was not sensitive enough to give a noticeable change at the end point; the end point was indicated by the complete decolorization of the I_2 solution, which would usually be reached in 30 ml of the titrant added. It had a remarkable sensitivity of ±1 drop.

The ozone in the second bubbler, B2, was measured similarly. The volume of titrant required was generally around 3 drops and seldom exceeded 10 drops. The blank was prepared by passing the same volume of air through the bubblers, and the blank solution was titrated for I_2. The blank was approximately 0.05 ml, and was subtracted from the volumes measured above. After correcting for background, the sum of the titrant used should indicate the total amount of I_2, and thus O_3, in the bubblers. Detailed calculation and gas phase sampling are shown in Appendix [illegible].

4.3.2 Analytical Method for Free Cyanide Determination

The measurement of free cyanide is well documented in the literature[77]. Free cyanide can be isolated from the interfering matrix by simple distillation in an acid medium,

and then determined by titration, colorimetric measurement[78] or cyanide selective electrode monitoring[79]. Titration is deemed to be the better method as far as convenience and accuracy are concerned, thus it was used for this research project. The procedure for CN^- titration has been described in full detail in reference (77).

Standard 0.01 N $AgNO_3$ was prepared by dissolving 3.4 g of $AgNO_3$ in a 2 liter volumetric flask, and the indicator solution by dissolving 0.02 g paradimethylaminobenzyl rhodanine in 100 ml acetone. The titration was carried out at pH 11 or above, seven drops of indicator solution were added to the receiving flasks, the color of the solution was canary yellow and would change to salmon pink at the end point. The color change was not very sensitive, thus a white background helped to improve the sensitivity significantly.

The blank was prepared by diluting 50 ml of 2 N NaOH solution to 250 ml and the same procedure as above was used to titrate the blank solution. The blank should be around 1 drop.

This modified Liebig method, when used at a cyanide level above 1 ppm, has a coefficient of variation of 2% for distilled samples, and the sensitivity is approximately 0.1 ppm of CN^-. However, the color change is not distinct at this point. At 0.4 ppm, the coefficient of variation is four times that at a concentration level greater than 1 ppm.

The reaction between Ag^+ and CN^- can be shown as

$$Ag^+ + 2CN^- \rightleftharpoons Ag(CN)_2^-$$

so the concentration of cyanide in solution is

$$\frac{2x[Ag^+](\text{volume of } Ag^+ \text{ used} - \text{blank})}{\text{sample volume}} \quad . \qquad (91)$$

4.3.3 Ferricyanide Analysis

IR[80], ion exchange chromatography[81], NMR[82] and cyanide distillation[77,83,84] are all considered to be feasible for determining ferricyanide in solution. The first three methods require expensive instruments yet the accuracy is at most on the same order as that for distillation[77]. The measurement of total cyanide content in ferricyanide by cyanide distillation is involved due to the stability and the inertness of the complex towards reactions. Ferricyanide can liberate HCN only under drastic conditions such as high acid concentration, reflux, presence of catalyst or strong complexing agent. A procedure of air circulation to remove HCN liberated from the boiling ferricyanide solution has been proposed by Gould, Afghan and Brooksbank[83] who claimed that a sensitivity of 0.5 µg CN in 15 ml of sample and a recovery of 100% at CN concentration above 1 µg/ℓ could be obtained by titrating the liberated HCN with Ag^+. However, the experiments were repeated using exactly the same set-up and procedure as recommended by the authors and the result as claimed could

not be reproduced. The percentages of recovery were sporadic, and ranged from 40% to 80% even when air was bubbled through the solution for more than 2 hours. The unrecovered portion of CN was found to be left in the solution and it could be driven out by boiling. Even though the ferricyanide had been broken down completely into HCN, the experiments with recirculating air failed because of the high solubility of HCN gas in cool water. A large percentage of HCN in the carrying air redissolved into the water condensate near the top of the distillation column and thus returned to the bulk solution. A combination of long bubbling time and large air recirculating rate might drive the process to completion.

It has been possible to develop a method that does give quantitative results by modifying the method of Gould et al. A schematic of the distillation apparatus used is shown in Figure 4. In this new method, the HCN formed by decomposition of ferricyanide was carried out of solution with steam, and dissolved in the condensate which was then mixed with 2 N NaOH solution in the receiving flask. An appropriate volume of the condensate should be collected, too large a volume might cause an insensitive indicator color change at the end point while an insufficient volume might lead to a low recovery. The volume to be collected could either be determined by a CN^- probe to monitor the CN level, or just by trial and error. A volume of 150 to 200 ml was recommended.

i) Reagents

Sulfuric acid conc., 'Baker Analyzed' Reagent, BDH

Sodium hydroxide, Fisher Scientific Co.,

Silver nitrate, Analab

Potassium cyanide, 'Baker Analyzed' Reagent, BDH

Potassium ferricyanide, 'Baker Analyzed' Reagent, BDH

Magnesium chloride·$6H_2O$, Fisher Scientific Co.,

Mercuric chloride, 'Baker Analyzed' Reagent, BDH

5-(P-Dimethylaminobenzylidene) rhodanine,

Eastman Organic Chemicals.

ii) Apparatus

Any common open distillation set-up could be used for complex cyanide distillation. Being a distillation device for HCN, it also served as a reactor in which the breaking down of the complex cyanide took place (Figure 4). The joints used in the apparatus were all of the size 24/40; a 3 neck round bottom flask with 2 stoppers was used to contain the solution to be distilled. A 380 watt Canlab heating mantle acted as a heating source. A magnetic stirrer provided adequate agitation during the run. The flask was connected to a condenser through an elbow, and the condenser was placed at a slightly inclined angle so that the condensate together with the HCN could drain by gravity into the receiver containing 2 N NaOH solution. The tip of the condensate drainage tube was dipped into the NaOH solution to prevent HCN from escaping into the air.

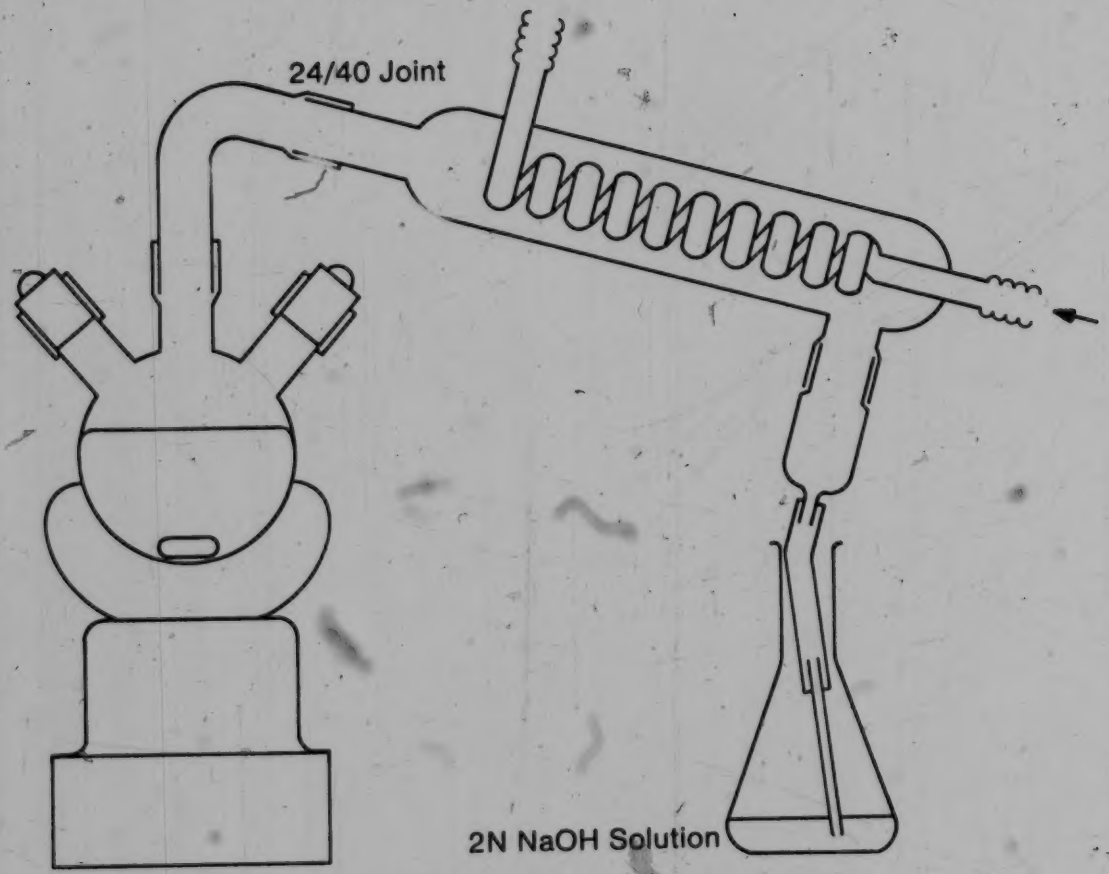

Figure 4 Apparatus for cyanide open distillation

An enlarged section was placed between the condenser and the rubber tubing leading to the receiver, so that the solution in the receiver would not be sucked back into the condenser in case of sudden cooling of the condenser and the flask.

The presence of grease in the condensate might interfere seriously with the cyanide titration. It was recommended that grease should only be used when needed, and a small amount of grease should be enough to stop leaking. As a matter of fact, the joints were only greased when they were new, and there was no sign of leaking thereafter due to insufficient greasing.

The tip of the condensate delivery tube was dipped into the 2 N NaOH solution (approximately 50 ml) in the receiver. The cooling water was turned on and all the joints were tightened firmly to avoid any leakage during the run. One stopper was pulled out, and a known volume of ferricyanide solution was pipetted into the flask. Sufficient distilled water was added to make up the volume to approximately 600 ml. Then 20 ml 6.8% $HgCl_2$ and 10 ml 51% $MgCl_2 \cdot 6H_2O$ solutions were poured into the flask and followed by 60 ml conc. H_2SO_4. The stopper was put back into place hastily after introducing sulfuric acid into the solution.

The stirrer and the heating mantle were switched on. During the heating up of the solution, bubbles were coming

out from the tip of the delivery tube due to the expansion of air inside the system. The solution boiled in 15 minutes and the characteristic yellow color of ferricyanide disappeared after boiling for 5 minutes, which indicated that the ferricyanide complex was completely broken down. An hour of reflux as recommended by Gould et al[83] was not required. After 120 ml of condensate were collected, the receiver was tilted so that the tip of the condensate delivery tube was just above the solution. Another 100 ml of condensate were collected. the purpose of this step was to wash out any HCN remaining on the wall of the condenser and the tube by the condensate. Then the receiver was removed and another receiver containing fresh NaOH solution was immediately put into place to collect further condensate to ensure that there was no cyanide left in the system. The distillation was stopped after 100 ml of condensate had been collected in the second receiver.

The contents in the receivers were titrated for CN^- by standard silver nitrate solution as mentioned in 4.3.2 Analytical Method for Free Cyanide Determination.

iii) Evaluation of Method

V_a the volume of ferricyanide sample added, ml

V_1 the volume of titrant for the first receiver, ml

V_2 the volume of titrant for the second receiver, ml

V_b the blank, ml

$[CN]_o$ the concentration of cyanide in the stock ferricyanide solution, M

The reaction between Ag^+ and CN^- can be shown as

$$Ag^+ + 2CN^- \rightleftharpoons Ag(CN)_2^-$$

so the amount of CN^- recovered is

$$2(V_1 + V_2 - 2V_b)[Ag^+] \quad .$$

The percentage of recovery R is

$$R = \frac{\text{amount of } CN^- \text{ recovered}}{\text{amount of } CN^- \text{ added}} \times 100\%$$

$$= \frac{2(V_1 + V_2 - 2V_b)[Ag^+]}{V_a[CN]_o} \times 100\% \quad . \qquad (92)$$

The results are tabulated in Table 5 and the amount of CN added (column 6, Table 5) is plotted against the amount measured (column 5, Table 5) in Figure 5. It is found that in the range of 3.155 m mole to 0.2984 m mole CN^-, the average percentage recovery is 98.7%, which can be regarded as quantitative.

At a cyanide level lower than 0.06231 m mole, only a portion of cyanide can be recovered as revealed by the downward deviation from the ideal line in Figure 5. The yield drops from 95.9% at 0.06231 m mole of CN to 90.5% at 0.0249 m mole, and would be expected to drop further at reduced cyanide contents. The loss of cyanide at low concentration might be due to the hydrolysis of cyanide catalyzed by Hg^{2+} or Mg^{2+}.

It can be concluded that the proposed open distillation method for complex cyanide determination is considered to be valid at cyanide contents higher than 0.07 m mole in

$[CN]_o$ M	V_a ml	V_1 ml	V_2 ml	CN measured m mole	CN added m mole	R%
0.1246	25	150.92	0.30	3.061	3.155	98.24
	10	59.28	1.95	1.239	1.246	99.45
	5	30.04	0.10	0.6100	0.6231	97.90
	2	11.92	0.15	0.2443	0.2492	98.03
1.246×10^{-3} *	50	5.997	0.060	0.05976	0.06231	95.91
	20	1.717	0.020	0.02256	0.02492	90.52
0.1493	25	182.51	1.15	3.697	3.734	99.03
	10	72.22	0.30	1.468	1.493	98.29
	2	14.64	0.10	0.2987	0.2984	99.91
					AVG	98.70

$[Ag^+] = 0.01012$ M

$V_b = 0.0$

* Titrated by micro-burette

Table 5. Percentage of cyanide recovery at various levels of ferricyanide by the open distillation method.

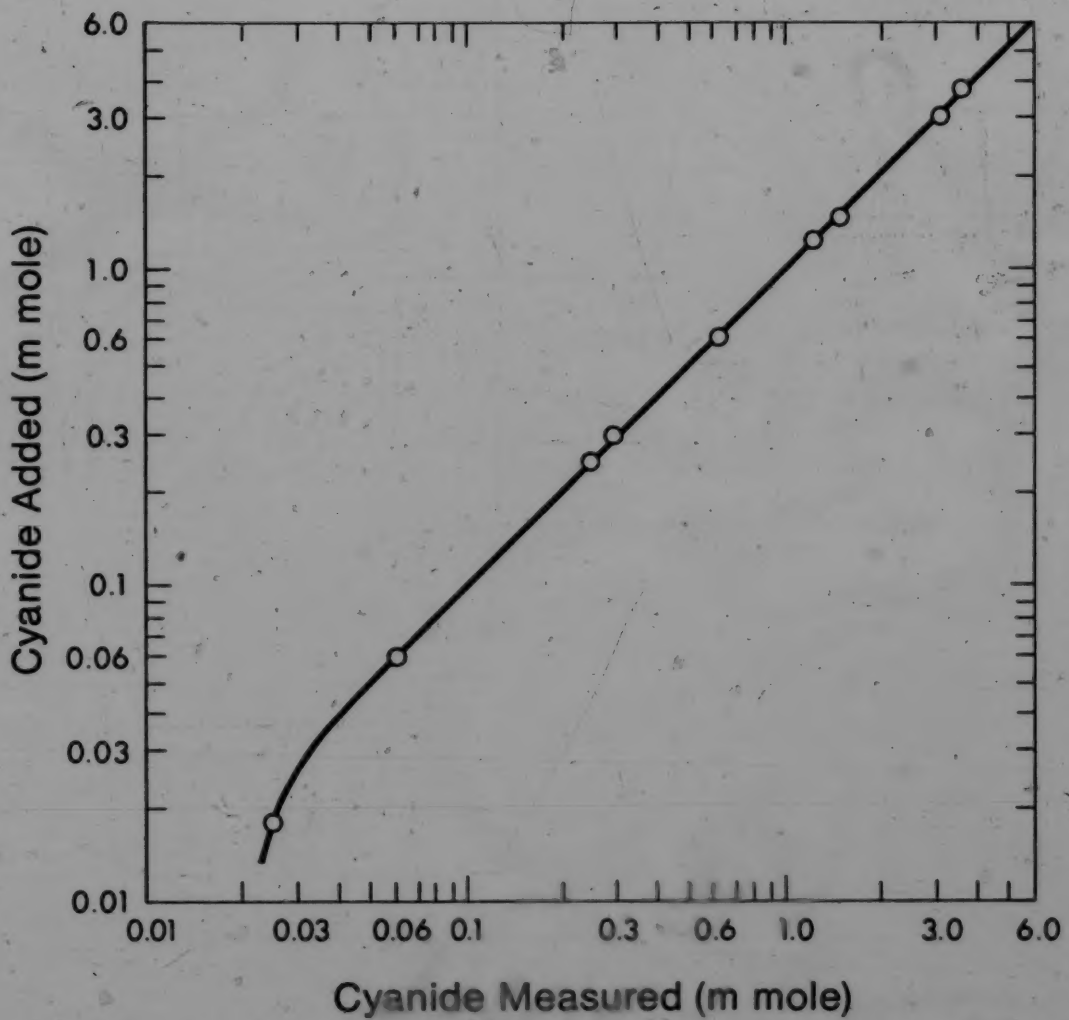

Figure 5. Plot of cyanide content measured vs cyanide content added in the determination of ferricyanide at 22 C.

700 ml solution, beyond which an accurate calibration curve is required.

4.4 Experimental Procedure - CN^-/O_3/UV Reaction

The experimental procedure is described fully in Appendix 2, General Operating Procedure. The inlet and outlet cyanide concentrations, the gas phase ozone concentrations in the inlet and outlet streams, pH, and the gas and the liquid flow rates were measured. The cyanide feed solutions were prepared by dissolving 0.6-5 gm of KCN powder ('Baker Analyzed' Reagent, J.T. Baker Chemical Co.) and 10.00 gm NaOH (Fisher Scientific Co.) in 9.435 liters of distilled water. The pH was measured by a Fisher Accumet Digital pH meter. The experiments were run at 108.6 rpm, 0 and 100% UV. The gas phase analysis is described in Appendix 2. Cyanide was measured by silver nitrate titration (cf. 4.3.2 Analytical Method for Free Cyanide Determination).

The experiments were carried out at a liquid feed rate of 0.765 ml/sec, a cyanide concentrations of 1.147×10^{-3}, 1.84×10^{-3}, 3.701×10^{-3}, 0.6113×10^{-3}, 7.694×10^{-3} M, and UV intensities of 0 and 100%. Then it was repeated at the feed rate of 1.094 ml/sec and five different cyanide concentrations from 1.140×10^{-3} to 7.880×10^{-3} M without UV.

4.5 Experimental Procedure - Ferricyanide/O_3/UV Reaction

The detailed operating procedure is given in Appendix 2, General Procedure. The ferricyanide concentrations of the feed and the outlet stream, the gas phase ozone inlet and outlet partial pressures, the liquid flow rate, the temperature and the pH were measured. The ferricyanide feed solutions were prepared by dissolving 0.2 to 40 grams of potassium ferricyanide solid $K_3Fe(CN)_6$, 'Baker Analyzed' Reagent, BDH, in 19.95 liters of distilled water. Sodium hydroxide or phosphate buffer was used to keep the pH of the solutions at 12 and 7 respectively according to the scheme shown below.

pH	Ferricyanide	Chemical used
7	concentrations below 500 ppm 19.95 ℓ of solution	Fisher Scientific, pH 7, buffer concentrate, 100 ml.
7	concentrations above 500 ppm 19.95 ℓ of solution	buffer concentrate, 300 ml.
12	all concentrations 9.435 ℓ of solution	sodium hydroxide 10 g.

The pH of the inlet and outlet solutions were measured by a Fisher Accumet Digital pH meter. The experiments were run at a stirring rate of 108.6 rpm and 4 different UV intensities ranging from 0% (UV lamp off) to 100% (0.319 watts), with the ozonator setting at 100%.

CHAPTER 5

DATA TREATMENT

The reactor system has been modelled to relate the unknown variables e.g. RT, C_{Co}, K_L and K to the measurable quantities such as cyanide depletion, temperature and ozone concentration. The ozone usage, RT, can be obtained from a gas phase mass balance or it can be obtained by the simultaneous solution of the equations that relate RT to the amount of cyanide oxidized and the reaction rate constant. These model equations depend on the reaction regime, mechanism and stoichiometry assumed.

5.1 Summarization of the Equations to be Solved for the Rate Constant

For the transition from slow to fast reaction regime (cf. 3.3.1 Transition from Slow to Fast Reaction Regime - Film Model) and for the reaction scheme outlined in Section 3.2, the following equations apply:

$$*_{RT} = \frac{D_A S a_1}{\sinh(a_1 \delta)}[\cosh(a_1 \delta) - 1][C_{As} + C_{Ao}] + K_1 C_{Ao} V \qquad (47)$$

$$a_1 = \sqrt{\frac{K_1}{D_A}}$$

$$K_1 = K_f C_{Bo} + 3.25\ K_B C_{Co} + K_D$$

$$\delta = \frac{D_A}{K_0}$$

$$*_{RT} = \frac{S D_A a_1 [C_{As} \cosh(a_1 \delta) - C_{Ao}]}{\sinh(a_1 \delta)} - F_L C_{Ao} \quad (48)$$

$$C_{Co} = \frac{1}{\frac{K_B}{K_f C_{Bo}} + \frac{1}{C_{Bi} - C_{Bo}}} \quad (52)$$

$$RT = \left(\frac{K_D + K_f C_{Bo} + 3.25\ K_B C_{Co}}{K_f C_{Bo}} \right) F_L (C_{Bi} - C_{Bo}) \quad (55)$$

$$*K_f = 5.1\ K_B \quad (34)$$

$$\text{or} \quad RT = S_0 F_L (C_{Bi} - C_{Bo}) \quad (94)$$

$$\text{or} \quad RT = RO \quad (56)$$

$$C_{As} = \frac{P_A}{H} \quad (95)$$

$$H = 67680 + 2870(T - 20) \ \text{atm/g mole/cc} \quad (96)$$

$$*K_D = 242[OH]^{0.75} = 15.3 \ \text{sec}^{-1} \ \text{at pH 12} \quad (1)$$

$$S = 84 \ \text{cm}^2 \quad (97)$$

$$V = 499 \ \text{ml} \quad (98)$$

$$*F_L = 0.765 \ \text{ml/sec} \quad (99)$$

$$D_A(T) = 1.805 \times 10^{-5} \left(\frac{T + 372.2}{293.2} \right) \left(\frac{\mu(20°C)}{\mu(T)} \right) \quad (100)$$

$$\log \frac{\mu(T)}{\mu(20°C)} = \frac{1.3272(20 - T) - 0.001053(T - 20)^2}{T + 105} \quad (101)$$

$$K_0(T) = 2.191 \times 10^{-3} \sqrt{\frac{D_A(T)}{1.8389 \times 10^{-5}}} \quad (102)$$

where the number 1.8389×10^{-5} is the diffusivity of ozone at 20°C calculated by Equation (90), and the asterisk * indicates that the values of these variables may change with models and experimental conditions.

There has been difficulty in obtaining a reliable gas-phase mass balance for ozone because the inlet ozone concentration does not differ significantly from the outlet one. Therefore, an average ozone consumption ratio S_0, which is obtained by averaging the values for all runs, is used to smooth the values of RT in Equation (94). By using Equation (94), RT has been smoothed and the idea of the gas phase material balance is still preserved. Zero gas phase resistance is also assumed in the above derivation.

Equations (47), (48) or its equivalent, which describe the transfer of ozone across the interface for a defined regime, are obtained directly by solving the differential equations; no experimental work is involved. Equation (55) is to relate ozone consumption to the amount of cyanide oxidized, which can be measured accurately. RT can also be calculated by the gas phase ozone mass balance, i.e. Equations (56) and (94), so that there are three RT's from three independent sources. If C_{Ao} is equal to zero, Equations (47) and (48) can be reduced to a single equation (Equation (57)). The unknowns RT, K_B and K can be solved from these three RT equations (Equations (57) and (55) and one of (34), (94)). If C_{Ao} is not equal to zero, there

would be one more unknown and one more RT equation (Equations (47) and (48) instead of (57)), the unknowns can still be solved readily. However, one of the RT equations is not required if the assumption of

$$K_f = 5.1\ K_B \qquad (34)$$

is made. It is a logical decision to drop the RT obtained from the gas phase mass balance (Equations (56) and (94)) because it is the most uncertain one. Equation (52) is derived from the well-mixed model, and provides the relationship between cyanate concentration and the rate constants K_B, K_f. Equations (96) and (1) are from the literature (cf. 2.1.1 Ozone Chemistry and 2.2.1 Solubility of Ozone in Aqueous Media), while (97), (98), (99) are from direct measurement. Equations (100), (101) give the value of diffusivity (cf. Appendix 4 Detailed Physical Mass Transfer Measurement) and Equation (102), the value of physical mass transfer coefficient (cf. Appendix 4) at various temperatures.

The variables P_A, T, C_{Bi}, C_{Bo}, F_L, V, S, $[OH^-]$, K_0 and D_A are measurable. Inserting the values of these variables into the key equations (Equations (47), (48), (52), (55) and one of (34), (94) and (56), K_f can be solved by Mueller's method[54,55] (cf. Appendix 1).

5.2 $CN/O_3/UV$ Reaction

5.2.1 Fast Reaction Regime

The theory developed in 3.3 Modelling of the $CN^-/O_3/UV$ Reaction can be greatly simplified by assuming zero ozone concentration in the bulk phase, which is valid for fast reaction. Equation (25) in 3.3.3 Fast Reaction Regime can be used

$$K_L = \sqrt{D_A K_1} \qquad (58)$$

where

$$K_1 = K_f C_{Bo} + 3.25\, K_B C_{Co} + K_D \,.$$

K_L can then be related to RT after correcting for the gas phase mass transfer resistance (kg,cm/sec) which is equal to 2.15 cm/sec at 22°C as measured by Rowley[85] using the same reactor configuration and operating conditions

$$\frac{RT \cdot H}{SP_A} = \frac{\frac{HK_g}{RT} + \sqrt{D_A K_1}}{\frac{HK_g \sqrt{D_A K_1}}{RT}} \,. \qquad (103)$$

The process variables P_A, T, C_{Bi}, C_{Bo}, F_L, V, S and pH are measurable, and D_A, H, K_D, C_s can be generated by Equations (95) to (102) listed in 5.1 Summarization of the Equations to be Solved for the Rate Constant.

Four different cases are tried in this regime (cf. Section 5.1).

Case A: RT is obtained directly from the gas phase mass balance

$$RT = RO \tag{56}$$

K_f and K_B can be solved simultaneously by Equations (103), (56), (52) and (55).

Case B: RT is calculated from R multiplied by the average measured ozone consumption ratio S_0

$$RT = 1.5\ R = 1.5\ F_L(C_{Bi} - C_{Bo}) \tag{94a}$$

Case C: Rowley[85] obtained a S_0 value of 1.2; 1.2 is used instead of 1.5 in this case

$$RT = 1.2\ F_L(C_{Bi} - C_{Bo}) \tag{94b}$$

Case D: The gas phase mass balance is ignored in this case, a constant ratio of K_B/K_f is assumed

$$K_B/K_f = 1/5.1\ . \tag{34}$$

Equations (103), (34), (52) and (55) are used to solve K_B and K_f. The key equations are Equation (103),

$$RT = \frac{\frac{K_g H}{RT} + \sqrt{DT \cdot K_1}}{\frac{K_g H}{RT}\sqrt{DT \cdot K_1}} \cdot ARA \cdot \frac{P_A}{H} \tag{103}$$

where

$$K_1 = K_f \cdot CNF + K_D + 3.25\ K_B \cdot CNO\ .$$

Equations (55), (52) and one of the Equations (56) to (34).

$$\begin{cases} RT = RO & \text{case } \underline{A} \quad (56) \\ RT = 1.5\, F_L (CNI - CNF) & \underline{B} \quad (94a) \\ RT = 1.2\, F_L (CNI - CNF) & \underline{C} \quad (94b) \\ K_B = K_f / 5.1 & \underline{D} \quad (34) \end{cases}$$

K_f and K_B can be solved by the computer program THES using Equations (103), (55), (52) and one of the equations from (56) to (34) in addition to the basic equations from (95) to (102). The input variables are surface area ARA, inlet and outlet cyanide concentrations CNI, CNF, rate of ozone consumption $\dot{n}_{Ai} - \dot{n}_{Af}$, ozone partial pressure P_A, pH, temperature T and liquid flow rate F_L.

The whole computer program THES as listed in Appendix 7 consists of a main program and two subroutines, MULR and FMU. MULR is the program for Mueller's method, which requires the inputs of initial guess XLI and XRI, maximum number of iterations IEND, convergency testing number EPS and the other experimental numbers to be fed into FMU, for instance, diffusivity DT, outlet cyanide concentration CNF, physical mass transfer coefficient KO, interfacial ozone concentration (saturated) CS, amount of cyanide reacted per unit time R, measured ozone consumption RO, initial concentration CNI, ozone decomposition rate constant XKD and an indicator II, which varies from 1 to 4 denoting cases A to D. Equations (103), (52), (55) and (56) to (34) are stored in the subroutine FMR.

The general algorithm for cases A to C is to use Equation (56) for case A, (94a) for case B and (94b) for case C to generate the value of RT; Equation (52), the value of CNO; and Equation (104), a combination of Equations (52) and (55), the value of K_B,

$$K_B = \left(\frac{1}{\frac{3.25}{K_f \cdot CNF \cdot (\frac{RT}{R} - 1) - K_D} - \frac{1}{K_f \cdot CNF}} \right) \left(\frac{1}{CNI - CNF} \right) . \qquad (104)$$

Once a tried K_f value is fed from the program MULR into FMU, first K_B and then CNO are defined. Another comparison function F is introduced in FMR where

F = RT(from Equation(103)) - RT(from Equations (56) or (94a) or (94b)).

The value of F is brought back to MULR for comparison and generation of a new K_f value which is then fed into FMU until F is less than the set limit, EPS.

The algorithm for case D is less involved. The values K_B and CNO are obtained from Equations (34) and (52) respectively.

F = RT(from Equation (103)) - RT(from Equation (55)).

These equations are stored in FMU and the same trial and error method is used to solve for K_f.

5.2.2 Transition from Fast to Instantaneous Reaction Regime

The same THES program can be applied to this regime with modifications. The key equations are Equations (34), (52), (55), (68) and (32) (cf. 3.3.4 Transition from Fast to Instantaneous Reaction Regime). M and E_i are functions of K_f and CNO, which, in turn, is a function of K_f.

F = RT(Equation (68)) - RT(Equation (55))

Two additional subroutines FNU and NULR are required in this regime because Equation (68) is an implicit function of EN, the enhancement factor. The initial bounds of K_f are set in MULR, which then directs a tried K_f value to FMU to define E_i and M. Then, EN is solved by the other subroutines FNU and NULR based on the same principle as that of FMU and MULR. The initial guesses of K_f and EN are critical in this program, as an improper choice of initial conditions will render a negative value to the term $M(E_i - EN)/(E_i - 1)$. The square root of a negative number is not defined, and thus the value of EN does not converge. Several sets of initial K_f and EN values have to be tried in order to get the results converged for the cyanide concentrations studied; a unique general set of initial conditions applicable to the whole cyanide concentration range covered in the experiment does not exist.

5.3 Ferricyanide/O_3/UV Reaction

The reaction scheme and the mass transfer model have been developed in Sections 3.2.3 and 3.4. As it has been shown in the O_3/CN^- reaction that the gas phase mass transfer resistance only accounts for 2% of the total resistance, the correction for the gas phase resistance is not necessary in this experiment because the O_3/UV/Ferricyanide reaction is substantially slower. The same THES program is used to solve for K except the following differences:

i) The ozone consumption cannot be obtained from the gas phase measurement, the outlet ozone concentration is essentially equal to the inlet concentration owing to the slow reaction, the insignificant ozone usage makes the gas phase ozone mass balance impossible. The ozone consumption is calculated from the liquid phase cyanide mass balance by Equation (55).

ii) K_B has a value of 3740 $M^{-1}sec^{-1}$, which is about 1/5.1 of the K_f measured in the O_3/CN^- reaction (19083 $M^{-1}sec^{-1}$).

The key equations for the flat CNO profile are Equation (105)

$$RT = \frac{K_0 \tanh\sqrt{DT \cdot K_1}}{\sqrt{DT \cdot K_1}} \cdot ARA \cdot C_{As} \qquad (105)$$

where

$$K_1 = K \cdot CNF + K_D + 3.25 \times 3740 \times CNO$$

$$= K \cdot CNF + K_D + 12155\ CNO$$

and Equations (55) and (52). K can be solved by using these 3 equations in addition to the general basic equations from (95) to (102) in Section 5.1. The algorithm is identical to that used in the free cyanide case.

RT is expressed in another form if a quadratic CNO profile is assumed (cf. Section 3.4.2)

$$RT = \frac{ARA \cdot DT\sqrt{b_4}}{\sinh\sqrt{b_4}\,\delta}\left\{\frac{b_5}{b_4} + \left[C_{As} - \frac{b_5}{b_4}\right]\cosh(\sqrt{b_4}\delta)\right\} \qquad (106)$$

$$b_4 \equiv \frac{4.25\ K \cdot CNF + K_D}{DT}$$

$$b_5 \equiv \frac{3.25\ F_L CNO}{DT \cdot ARA \cdot \delta}$$

$$\delta = \frac{DT}{K_0}$$

where Equation (106) is obtained by combining Equations (85) and (86). Equation (105) for the flat CNO profile is replaced by Equation (106) for the quadratic CNO profile, and the computational procedure would be the same in both cases.

Equation (89) is used for the penetration model (cf. Section 3.4.3)

$$RT = ARA \cdot C_s\sqrt{DT \cdot K_1}\left\{\text{erf}\sqrt{K_1 DT}\left[1 + \frac{1}{2K_1\theta}\right] + \frac{\exp(-K_1\theta)}{\sqrt{\pi K_1\theta}}\right\} \qquad (89)$$

$$K_1 \equiv K \cdot CNF + 12155\ CNO + K_D$$

$$\theta \equiv \frac{4DT}{\pi K_0^2}$$

$$\text{erf}\ x = \frac{2}{\sqrt{\pi}}\int_0^x \exp(-x^2)\,dx$$

In addition to the subroutines MULR and FMU, another subroutine INTG is used to integrate the function $\exp(-x^2)$, which is declared as FUNCTION FCT(x) in the computer program THES to provide the error function.

CHAPTER 6

RESULT AND DISCUSSION

6.1 CN^-/O_3/UV Reaction

The input variables and directly measurable data are tabulated in Tables 6 and 7; data for a flow rate of 0.765 ml/sec are in Table 6, and a flow rate of 1.094 ml/sec in Table 7. CNI, CNF are the feed and outlet cyanide concentrations respectively. P_A is the ozone partial pressure, T the temperature and RO the amount of ozone consumed per unit time, as calculated by the gas phase ozone mass balance. Utilizing these numbers, the rate constant of the free cyanide/O_3 reaction, K_f, can be evaluated by the computer program THES listed in Appendix 7. A brief explanation of the program can be seen in Chapter 5 Data Treatment. Four different methods as mentioned in Chapter 5 are used to obtain K_f, and the results are shown in Tables 8 and 9, in which A designates the case based on the ozone consumption RT directly from the gas phase ozone mass balance RO; B, RT from the cyanide consumption, R, multiplied by an ozone consumption ratio of 1.5; C, RT from R multiplied by 1.2 and D, $K_B = K_f/5.1$ instead of RT. All cases are regarded to be in the fast reaction regime.

The variables and parameters of interest for the case D e.g. the physical mass transfer coefficient K_0, cm/sec; the interfacial ozone concentration CS, M; the calculated

Table 6

DIRECTLY MEASURABLE EXPERIMENTAL VARIABLES FOR THE $CN^-/O_3/UV$ REACTION AT A FLOW RATE OF 0.765 ML/SEC, OZONATOR SETTING OF 100%, pH 12 AND TEMPERATURE 21°C

Run	UV	Temp (°C)	Ozone Pressure (PA) (atm x 10^2)	Cyanide Feed (CNI) (M x 10^3)	Concentration Product (CNF) (M x 10^3)	RO (1) (mol/s x 10^6)
1	No	23.6	1.874	1.147	0.746	0.200
2	No	23.6	1.889	1.147	0.753	0.300
3	Full	23.6	1.852	1.147	0.755	0.783
4	No	23.4	1.831	1.840	1.344	0.683
5	No	23.4	1.844	1.840	1.341	0.767
6	Full	23.4	1.867	1.840	1.342	1.049
7	Full	23.4	1.816	1.840	1.342	0.400
8	No	22.5	1.925	3.701	2.925	0.050
9	No	22.5	1.910	3.701	3.011	1.999
10	No	22.5	1.910	3.701	2.967	0.850
11	Full	22.5	1.902	3.701	3.009	1.083
12	Full	22.5	1.915	3.701	2.965	0.533
13	No	22.5	1.775	6.113	5.146	0.150
14	No	22.5	1.774	6.113	5.146	0.683
15	No	22.5	1.860	6.113	5.135	2.816
16	Full	22.5	1.820	6.113	5.153	0.567
17	Full	22.5	1.860	6.113	5.151	2.649
18	No	22.8	1.544	7.694	6.663	1.083
19	No	22.8	1.862	7.694	6.665	1.099
20	Full	22.8	1.880	7.694	6.665	1.233
21	Full	22.8	1.871	7.694	6.700	1.016

(1) RO = rate of disappearance of ozone based on an ozone balance

Table 7

DIRECTLY MEASURABLE EXPERIMENTAL VARIABLES FOR THE CN^-/O_3/UV REACTION AT A FLOW RATE OF 1.094 ML/SEC, OZONATOR SETTING OF 75%, pH 12 AND TEMPERATURE 21°C

Run	UV	Temp (°C)	Ozone Pressure (PA) (atm x 10^2)	Cyanide Feed (CNI) (M x 10^3)	Concentration Product (CNF) (M x 10^3)	RO (1) (mol/s x 10^6)
1	No	22.3	1.656	1.140	0.922	2.316
2	No	22.3	1.749	1.140	0.917	1.433
3	No	22.3	1.518	1.959	1.623	2.478
4	No	22.3	1.776	1.959	1.673	2.211
5	No	22.3	1.499	4.056	3.513	2.066
6	No	21.1	1.639	6.147	5.448	1.216
7	No	21.1	1.599	6.147	5.502	1.633
8	No	22.8	1.620	7.880	6.468	2.408
9	No	22.8	1.620	7.880	6.605	2.408

(1) RO = rate of disappearance of ozone based on an ozone balance

cyanate concentration CNO, M; the reaction and diffusion time TR, sec, TD, sec; the reaction diffusion time ratio, TRD; the calculated ozone consumption O3, mole/sec; the measured and calculated ozone consumption ratios S_0 and S_1; the rate of cyanide reacted R, mole/sec; the fractions of ozone consumed by decomposition and cyanate oxidation FRD and FRC are printed out in Tables A4 and A5 in Appendix 6, Detailed Analyses of the Ozonation Reactions, where

$$S_0 = \frac{RO}{R} \tag{107}$$

$$S_1 = \frac{O3}{R} \tag{108}$$

$$FRD = \frac{K_D}{K_D + 3.25\ K_B \cdot CNO + K_f \cdot CNF} \tag{109}$$

$$FRC = \frac{3.25\ K_B \cdot CNO}{K_D + 3.25\ K_B \cdot CNO + K_f \cdot CNF} \tag{110}$$

Comparing the values of K_f from the four different methods (A to D, Tables 8 and 9), it is found that the one from ozone material balance (A) does not furnish any useful information due to the scattering. Owing to the large uncertainty in the term RO, the amount of ozone reacted, some K_f values are negative. The assumption of constant ozone consumption ratio is questionable. As the cyanide concentration increases, ozone decomposition becomes a less significant factor in the whole process and the ozone consumption ratio would decrease. The values of K_f in B and C by assigning constant ozone consumption ratios and then

RUN NO.		A	B	C	D
1	K	0.1027E 05	0.2390E 05	0.1906E 05	0.3150E 05
	KB	-0.8004E 04	-0.4433E 04	-0.7524E 04	0.6177E 04
	KL	0.9961E-02	0.2303E-01	0.1841E-01	0.3026E-01
	EN	0.4374E 01	0.1011E 02	0.8086E 01	0.1328E 02
2	K	0.1481E 05	0.2245E 05	0.1791E 05	0.2991E 05
	KB	-0.8423E 04	-0.4773E 04	-0.7644E 04	0.5865E 04
	KL	0.1485E-01	0.2243E-01	0.1793E-01	0.2978E-01
	EN	0.6524E 01	0.9853E 01	0.7876E 01	0.1307E 02
3	K	0.4092E 05	0.2311E 05	0.1844E 05	0.3052E 05
	KB	0.4110E 05	-0.4643E 04	-0.7689E 04	0.5985E 04
	KL	0.4002E-01	0.2279E-01	0.1821E-01	0.2999E-01
	EN	0.1757E 02	0.1000E 02	0.8000E 01	0.1317E 02
4	K	0.2560E 05	0.2118E 05	0.1687E 05	0.2402E 05
	KB	0.8543E 04	-0.6875E 03	-0.5826E 04	0.4711E 04
	KL	0.3501E-01	0.2904E-01	0.2320E-01	0.3288E-01
	EN	0.1541E 02	0.1278E 02	0.1021E 02	0.1447E 02
5	K	0.2866E 05	0.2118E 05	0.1688E 05	0.2406E 05
	KB	0.1781E 05	-0.7014E 03	-0.5794E 04	0.4717E 04
	KL	0.3908E-01	0.2901E-01	0.2318E-01	0.3289E-01
	EN	0.1720E 02	0.1277E 02	0.1020E 02	0.1447E 02
6	K	0.3868E 05	0.2056E 05	0.1638E 05	0.2349E 05
	KB	0.8519E 05	-0.9466E 03	-0.5844E 04	0.4607E 04
	KL	0.5320E-01	0.2859E-01	0.2284E-01	0.3262E-01
	EN	0.2341E 02	0.1258E 02	0.1005E 02	0.1435E 02
7	K	0.1511E 05	0.2174E 05	0.1732E 05	0.2454E 05
	KB	-0.7255E 04	-0.4690E 03	-0.5767E 04	0.4812E 04
	KL	0.2052E-01	0.2941E-01	0.2349E-01	0.3313E-01
	EN	0.9035E 01	0.1294E 02	0.1034E 02	0.1458E 02

TABLE 8. THE COMPARISON OF RATE CONSTANTS AND MASS TRANSFER COEFFICIENTS OBTAINED BY 4 DIFFERENT WAYS

A RT FROM GAS PHASE MASS BALANCE

B RT=1.5*R

C RT=1.2*R

D KB=K/5.1, RT FROM B

RUN NO.		A	B	C	D
8	K	0.1129E 04	0.2083E 05	0.1656E 05	0.1978E 05
	KB	-0.2684E 04	0.6460E 04	-0.2147E 04	0.3879E 04
	KL	0.2317E-02	0.4197E-01	0.3349E-01	0.3988E-01
	EN	0.1032E 01	0.1870E 02	0.1492E 02	0.1777E 02
9	K	0.4323E 05	0.1619E 05	0.1288E 05	0.1578E 05
	KB	0.8710E 06	0.4244E 04	-0.3173E 04	0.3095E 04
	KL	0.9754E-01	0.3753E-01	0.2996E-01	0.3660E-01
	EN	0.4347E 02	0.1673E 02	0.1335E 02	0.1631E 02
10	K	0.1883E 05	0.1863E 05	0.1481E 05	0.1787E 05
	KB	0.6073E 04	0.5504E 04	-0.2608E 04	0.3504E 04
	KL	0.4040E-01	0.3997E-01	0.3190E-01	0.3836E-01
	EN	0.1800E 02	0.1781E 02	0.1421E 02	0.1710E 02
11	K	0.2274E 05	0.1643E 05	0.1307E 05	0.1598E 05
	KB	0.3353E 05	0.4405E 04	-0.3122E 04	0.3134E 04
	KL	0.5198E-01	0.3780E-01	0.3018E-01	0.3678E-01
	EN	0.2316E 02	0.1685E 02	0.1345E 02	0.1639E 02
12	K	0.1163E 05	0.1865E 05	0.1483E 05	0.1789E 05
	KB	-0.6209E 04	0.5491E 04	-0.2600E 04	0.3508E 04
	KL	0.2510E-01	0.3997E-01	0.3190E-01	0.3838E-01
	EN	0.1119E 02	0.1781E 02	0.1422E 02	0.1710E 02
13	K	0.2837E 04	0.2193E 05	0.1738E 05	0.1853E 05
	KB	-0.5467E 04	0.1465E 05	0.8326E 03	0.3634E 04
	KL	0.7557E-02	0.5711E-01	0.4551E-01	0.4845E-01
	EN	0.3368E 01	0.2545E 02	0.2028E 02	0.2159E 02
14	K	0.1326E 05	0.2195E 05	0.1740E 05	0.1855E 05
	KB	-0.5973E 04	0.1467E 05	0.8393E 03	0.3638E 04
	KL	0.3488E-01	0.5714E-01	0.4553E-01	0.4847E-01
	EN	0.1554E 02	0.2547E 02	0.2029E 02	0.2160E 02
15	K	0.5558E 05	0.2043E 05	0.1620E 05	0.1744E 05
	KB	0.1468E 07	0.1304E 05	0.4248E 03	0.3420E 04
	KL	0.1439E 00	0.5507E-01	0.4389E-01	0.4717E-01
	EN	0.6417E 02	0.2454E 02	0.1956E 02	0.2102E 02
16	K	0.1030E 05	0.2049E 05	0.1625E 05	0.1745E 05
	KB	-0.7583E 04	0.1341E 05	0.4677E 03	0.3421E 04
	KL	0.2810E-01	0.5525E-01	0.4403E-01	0.4720E-01
	EN	0.1252E 02	0.2462E 02	0.1962E 02	0.2104E 02

Table 8. (cont'd)

RUN NO.		A	B	C	D
17	K	0.5087E 05	0.1969E 05	0.1562E 05	0.1685E 05
	KB	0.9790E 06	0.1261E 05	0.2543E 03	0.3305E 04
	KL	0.1349E 00	0.5414E-01	0.4315E-01	0.4650E-01
	EN	0.6013E 02	0.2413E 02	0.1923E 02	0.2072E 02
18	K	0.2389E 05	0.2620E 05	0.2071E 05	0.2082E 05
	KB	0.1441E 05	0.2446E 05	0.3775E 04	0.4083E 04
	KL	0.6523E-01	0.7134E-01	0.5677E-01	0.5706E-01
	EN	0.2894E 02	0.3165E 02	0.2519E 02	0.2532E 02
19	K	0.1648E 05	0.1773E 05	0.1405E 05	0.1468E 05
	KB	0.9212E 04	0.1469E 05	0.1039E 04	0.2880E 04
	KL	0.5466E-01	0.5870E-01	0.4677E-01	0.4884E-01
	EN	0.2425E 02	0.2605E 02	0.2075E 02	0.2167E 02
20	K	0.1823E 05	0.1738E 05	0.1378E 05	0.1443E 05
	KB	0.1853E 05	0.1429E 05	0.9278E 03	0.2830E 04
	KL	0.6087E-01	0.5813E-01	0.4631E-01	0.4847E-01
	EN	0.2701E 02	0.2579E 02	0.2055E 02	0.2150E 02
21	K	0.1444E 05	0.1627E 05	0.1290E 05	0.1357E 05
	KB	0.5669E 04	0.1356E 05	0.6191E 03	0.2661E 04
	KL	0.5017E-01	0.5638E-01	0.4493E-01	0.4722E-01
	EN	0.2226E 02	0.2501E 02	0.1993E 02	0.2095E 02

Table 8. (cont'd)

RUN NO.		A	B	C	D
1	K	0.1001E 06	0.1396E 05	0.1114E 05	0.1894E 05
	KB	-0.6834E 06	-0.1034E 05	-0.1338E 05	0.3715E 04
	KL	0.1311E 00	0.1923E-01	0.1537E-01	0.2601E-01
	EN	0.5863E 02	0.8598E 01	0.6875E 01	0.1162E 02
2	K	0.5435E 05	0.1316E 05	0.1051E 05	0.1824E 05
	KB	-0.7745E 06	-0.1036E 05	-0.1293E 05	0.3577E 04
	KL	0.7493E-01	0.1862E-01	0.1489E-01	0.2572E-01
	EN	0.3349E 02	0.8325E 01	0.6657E 01	0.1149E 02
3	K	0.1139E 06	0.2270E 05	0.1808E 05	0.2324E 05
	KB	-0.1292E 07	0.2868E 04	-0.7859E 04	0.4557E 04
	KL	0.1546E 00	0.3253E-01	0.2598E-01	0.3329E-01
	EN	0.6912E 02	0.1454E 02	0.1161E 02	0.1488E 02
4	K	0.5930E 05	0.1156E 05	0.9223E 04	0.1372E 05
	KB	-0.7700E 06	-0.5591E 04	-0.1056E 05	0.2692E 04
	KL	0.1159E 00	0.2357E-01	0.1884E-01	0.2793E-01
	EN	0.5184E 02	0.1053E 02	0.8424E 01	0.1248E 02
5	K	0.7115E 05	0.2864E 05	0.2272E 05	0.2421E 05
	KB	0.1337E 07	0.2207E 05	0.3767E 03	0.4747E 04
	KL	0.1291E 00	0.5376E-01	0.4285E-01	0.4561E-01
	EN	0.5773E 02	0.2403E 02	0.1915E 02	0.2039E 02
6	K	0.2584E 05	0.2424E 05	0.1920E 05	0.1959E 05
	KB	0.3510E 05	0.2518E 05	0.2518E 04	0.3841E 04
	KL	0.6450E-01	0.6062E-01	0.4829E-01	0.4924E-01
	EN	0.2979E 02	0.2753E 02	0.2193E 02	0.2236E 02
7	K	0.3406E 05	0.2141E 05	0.1697E 05	0.1744E 05
	KB	0.1776E 06	0.2333E 05	0.1628E 04	0.3421E 04
	KL	0.8977E-01	0.5725E-01	0.4562E-01	0.4688E-01
	EN	0.4077E 02	0.2600E 02	0.2072E 02	0.2129E 02

TABLE 9. THE COMPARISON OF RATE CONSTANTS AND MASS TRANSFER COEFFICIENTS OBTAINED BY 4 DIFFERENT WAYS

A RT FROM GAS PHASE MASS BALANCE

B RT=1.5*R

C RT=1.2*R

D KB=K/5.1, RT FROM B

RUN NO.		A	B	C	D
8	K	0.1040E 06	0.9943E 05	0.7767E 05	0.7517E 05
	KB	0.9417E 05	0.7781E 05	0.1958E 05	0.1474E 05
	KL	0.1427E 00	0.1368E 00	0.1082E 00	0.1049E 00
	EN	0.6340E 02	0.6076E 02	0.4806E 02	0.4659E 02
9	K	0.9198E 05	0.7841E 05	0.6141E 05	0.5906E 05
	KB	0.1311E 06	0.6841E 05	0.1672E 05	0.1158E 05
	KL	0.1427E 00	0.1228E 00	0.9727E-01	0.9370E-01
	EN	0.6340E 02	0.5453E 02	0.4319E 02	0.4160E 02

Table 9. (cont'd)

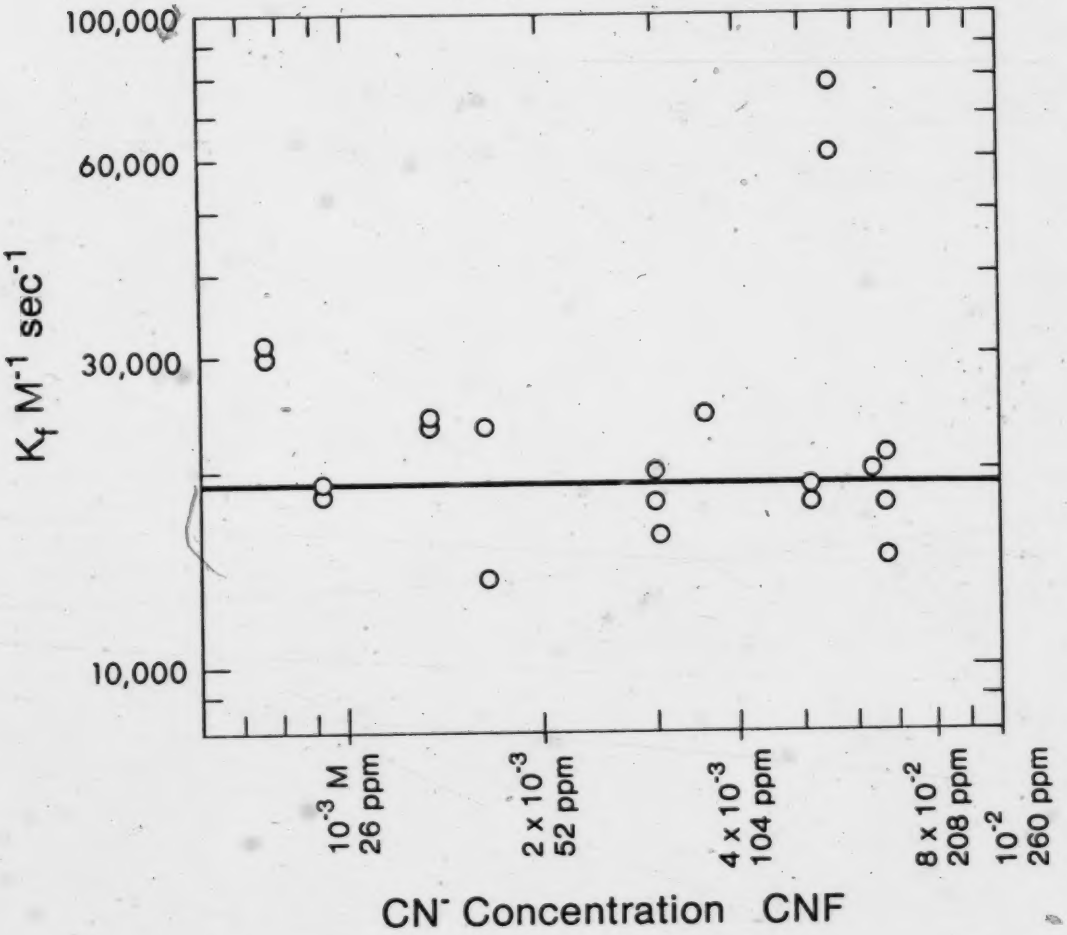

Figure 6. Plot of K_f vs cyanide concentration at 22°C and 108 rpm.

forcing the ozone mass balance are in the same order of magnitude as that of D, except that K_B varies from some negative numbers at low cyanide concentrations to a value of 13,000 M^{-1} sec^{-1} at a cyanide concentration of 6.6×10^{-3} M. It seems that models based on constant ozone consumption ratios are not valid. D is more acceptable, because a constant K_f/K_B ratio is assumed.

Despite the heavy scattering of K_f values, several conclusions can still be drawn. First, K_f is independent of cyanide concentration which is revealed by the plot of K_f vs cyanide concentration (Figure 6) where a horizontal line can be drawn through the points. The average value of K_f is 19086 M^{-1} sec^{-1} with the standard deviation of ±18%. The power law rate expression (first order in ozone and cyanide or cyanate) and the validity of the model are confirmed. Secondly, in contrast to the statement that "the unnecessary UV may slow down the reaction"[20], neither a beneficial nor a detrimental effect of UV on the reaction rate is observed which is in agreement with the observation that UV irradiation does not appreciably promote the ozone decomposition in the gas phase.

K_f is also solved using the same computer program by setting $K_D = 0$ and $q = 1.5$ instead of 15.3 and 3.25 respectively. K_f remains unchanged for cases B and C in which a constant ozone consumption ratio is assumed, while it decreases almost 25% from 20,000 M^{-1} sec^{-1} to 16,000 M^{-1} sec^{-1} in case D. The effect of q on K_f is mild, only

a 3% reduction in K_f is observed by changing q from 3.25 to 1.5. The values of K_D and q are chosen to be 15.3 sec^{-1} and 3.25 not only because they have more theoretical support but also they give an average calculated ozone consumption ratio of 1.5 (S_1 in Table A4) which is in exact agreement with the average measured value (S_0 in Table A4 and S_0 in Table A5 are not used because the ozone inlet concentrations have not been measured accurately in these experiments). The small reaction time to diffusion time ratio, (TRD $\cong 5 \times 10^{-3}$) in Tables A4 and A5 in Appendix 6 indicates that the reaction is in a fast reaction regime. The values of K_f can also be solved by the equations developed in the fast reaction regime (cf. 3.3.3 Fast Reaction Regime - Film Model).

If the reaction is found to be in the fast reaction regime using the reaction time - diffusion time ratio as the criterion, there is a good chance for the reaction to be in the transition from fast to instantaneous reaction regime; further characterization is required. The dimensionless parameter

$$\sqrt{t_D/t_R}/(1 + \frac{D_B B}{qD_A C_S})$$

is used as the criterion to differentiate the fast reaction regime from the transition from fast to instantaneous reaction regime. The reaction is said to be in an instantaneous reaction regime for a parameter value of 10 or larger, a fast reaction regime for

a value of 1/2 or less, and a transition regime for the values in between. The value of this parameter at various cyanide concentrations lies between 3.2 to 0.75, therefore the reaction would be in the transition from fast to instantaneous reaction regime. Two sets of initial guesses are used; the first set is good for Runs 1-3 in Table 6, and the second for Runs 3-21. The value of K_f calculated by assuming a transition regime is higher than that of the fast reaction regime by about 5% as shown in Table 10. The reaction, being in a fast reaction regime is still applicable. The liquid mass transfer coefficient at a cyanide concentration of 6.66×10^{-3} M is about 0.06 cm/sec, which is small compared with the gas phase mass transfer coefficient (2.15 cm/sec[85]). The gas phase resistance, which amounts to 2% of the total resistance, can be dropped without affecting the result. The effect of gas phase resistance need not be considered for the complex cyanide as the reaction is in the transition from slow to fast reaction regime.

As shown in Tables A4 and A5, the physical mass transfer coefficient, K_0, is on the order of 2×10^{-3} cm/sec, which is significantly smaller than the gas phase mass transfer coefficient (2.15 cm/sec). The calculated cyanate concentration CNO is only 1% of that of cyanide. The fraction of ozone consumed by decomposition, FRD, ranges from 14% to 34%, being more significant at low cyanide concentrations

Run	UV	CNI	K_T	K_f
		10^{-3}M	$M^{-1}s^{-1}$	$M^{-1}s^{-1}$
1	NO	1.147	32130	31500
2	NO		30460	29910
3	FULL		31110	30520
4	NO	1.840	24800	24020
5	NO		24830	24060
6	FULL		24230	23490
7	FULL		25350	24540
8	NO	3.701	20670	19780
9	NO		16340	15780
10	NO		18590	17870
11	FULL		16560	15980
12	FULL		18610	17890
13	NO	6.113	19480	18530
14	NO		19500	18550
15	NO		18300	17440
16	FULL		18300	17450
17	FULL		17600	16850
18	NO	7.694	21980	20820
19	NO		15370	14680
20	FULL		15090	14430
21	FULL		14160	13570

K_T Rate constant for free cyanide calculated by the transition regime,

K_f Rate constant for free cyanide calculated by the fast reaction regime (Case D, Table 8)

Table 10 Comparison of K_f for the $CN^{-1}/O_3/UV$ reaction calculated by assuming the transition from fast to instantaneous reaction regime and fast reaction regime.

where the bulk concentration of ozone is high. Since the decomposition is the major side reaction and strongly pH dependent, an accurate measurement of pH is warranted. On the other hand, only 13% to 7% of ozone is destroyed by the cyanate reaction (FRC). In contrast to the decomposition, it is more significant at higher cyanide concentration. The total consumption of ozone by these side reactions ranges from 27% to 41% as the cyanide concentration increases from 1.14×10^{-3} M to 7.694×10^{-3} M.

For an ideal case, RO, the number of moles of ozone reacted per second obtained by gas phase material balance, is equal to RT, the amount of ozone reacted per second calculated by cyanide balance, i.e.

$$RT = R(K_f[CN] + 3.25\ K_B[CNO] + K_D)/(K_f[CN])$$

However, the uncertainty in RO makes the comparison impossible. This can be illustrated by plotting S_0, the ratio of RO to R, against S_1, the ratio of RT to R in Figure 7 (S_0, S_1 are known as the measured and the calculated ozone consumption ratios). The points show an uninterpretable pattern scattering in a random fashion, which complies with the observation in column A, Tables 8, 9. The scattering is natural considering the subtraction of two close numbers. The mass flow rate of ozone is on the order of 2.2×10^{-5} mole/min, whereas the amount of ozone reacted is at most 1×10^{-6} mole/min, which represents a 1/22 or 5%

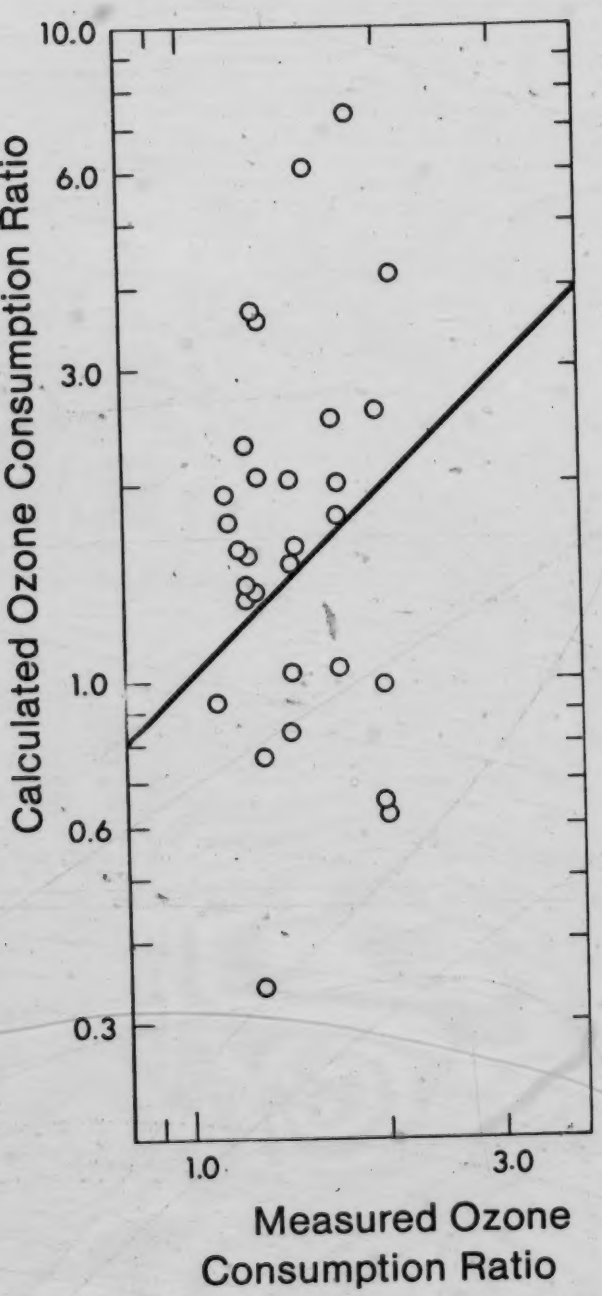

Figure 7. Plot of the measured ozone consumption ratio S_0 vs the calculated ozone consumption ratio S_1.

decrease in the exit ozone flow rate. As the relative error is concerned, it is almost impossible to obtain RO by taking the difference between the inlet and outlet ozone flow rates according to the error propagation theory

$$RO = \dot{n}_{Ai} - \dot{n}_{Af} \tag{111}$$

where $\dot{n}_{Ai}$, $\dot{n}_{Af}$ are the inlet and outlet ozone mass flow rate respectively. By a simple mathematical manipulation, the following relationship can be derived

$$\left(\frac{\Delta RO}{RO}\right)^2 = \left(\frac{\Delta \dot{n}_{Ai}}{\dot{n}_{Ai} - \dot{n}_{Af}}\right)^2 + \left(\frac{\Delta \dot{n}_{Af}}{\dot{n}_{Ai} - \dot{n}_{Af}}\right)^2 \tag{112}$$

where ΔRO denotes the uncertainty in RO caused by the measurement errors $\Delta \dot{n}_{Ai}$ and $\Delta \dot{n}_{Af}$. Assuming a 5% of measurement error,

$$\left(\frac{\Delta RO}{RO}\right)^2 \doteq 2x\left(\frac{0.05 \times 10^{-5} \times 2.2}{10^{-6}}\right)^2 = 2.42 \tag{113}$$

$$\frac{\Delta RO}{RO} = 1.56 = 156\% \quad . \tag{114}$$

156% only represents the inherent uncertainty of the term RO; the actual error including determinate errors and the errors from the data other than $\dot{n}_{Ai}$ and $\dot{n}_{Af}$ may be even larger than that. In spite of the scattering, the average measured ozone consumption ratio, S_0, agrees with the calculated one, S_1. They both indicate that an average of 1.5 mole of ozone reacts with 1 mole of cyanide.

The error in K_f comes from the following possible sources:

i) Experimental errors: Besides the measurement errors, additional errors can be caused by the irreproducible surface area and the liquid hold-up volume in the reactor. The vortex and ripple on the surface due to vigorous stirring may increase the actual surface area to a value larger than the geometrical cross section. In the ozonation experiment, liquid level was maintained by manually adjusting the liquid outlet valve, an insufficient control in liquid level may change the geometrical surface area because the cross section of the QVF column is not uniform. Furthermore, the ozone partial pressure fluctuates with the atmospheric pressure outside the building probably due to the change in oxygen content and the air compressor inlet pressure. For the best result, it is advisable to use a liquid level controller to maintain the proper liquid level and compressed oxygen as the oxygen source to generate ozone.

ii) Errors from the chemistry of the system: The order of the reaction is still controversial, a value of $1/3$[47], 0[44,45] or 1[45,46] (for cyanide) has been reported by various workers. The stoichiometric ratio q_{CNO} (moles of ozone required to react with 1 mole of cyanate) is uncertain too because a complicated mixture of N_2, NO_3^-, NH_4^+ is produced. In the

present work, an order of 1, a stoichiometric ratio of 3.25, a rate constant ratio (cyanide/cyanate) of 5.1 as observed by Balyanskii are chosen. The consistency of K_f values at various cyanide concentrations validates the choice, but still, the other possibilities cannot be excluded.

iii) The assumption of flat concentration profiles for cyanide and cyanate may introduce certain errors in the calculation. Cyanide concentration may be regarded as constant since it is the major species. As for cyanate, the same argument does not hold owing to the relatively small concentration. It is obvious that the concentration of cyanate is high inside the film where the reaction takes place and low in the bulk phase.

In conclusion, the cyanide/ozone/UV reaction is in the fast reaction regime ($t_R/t_D = 5 \times 10^{-3}$), with the first order rate constant of 19086 M^{-1} sec^{-1}. Because of large uncertainty in the ozone gas phase balance, K_f has to be calculated from the cyanide liquid phase balance correcting for the ozone decomposition and cyanate oxidation. The film and penetration models serve equally well for the above reaction. The rate constant of cyanate, K_B, which is used in the next section in the ferricyanide/ozone/UV reaction is equal to 1/5.1 of K_f, i.e. 3740 M^{-1} sec^{-1} for a measured K_f value of 19086 M^{-1} s^{-1}.

6.2 Ferricyanide/O_3/UV Reaction

The rate constants of ozone/ferricyanide/UV reaction at different UV intensities were calculated using three different models, namely, the film model with both flat and quadratic CNO concentration profiles and the penetration model with a flat CNO profile. All cases have been derived mathematically in 3.4 Modelling of the Ferricyanide/O_3/UV Reaction. A single program can be applied to all cases with minor modifications in the form of K_L. The penetration model is more complicated and it requires one more subroutine INTG to generate the error function. Since the decomposition of ozone is important at high pH, the pH of the solution has to be measured accurately and fed into the Stumm correlation incorporated in the program to get K_D. On the other hand, at pH 7, a value of 8.5×10^{-4} sec^{-1} as predicted from Stumm's correlation is accurate enough to account for the ozone decomposition. The main programs for film model, flat and quadratic CNO profiles, and penetration model all at pH 12 are listed in Appendix 7. Comparing the programs for free cyanide and ferricyanide, striking similarity can be found.

The input variables and the directly measurable data e.g. the cyanide contents of the feed and outlet ferricyanide solutions, CNI (6 times the ferricyanide concentration), and CNF, temperature T, and the ozone partial pressure P_A, are tabulated in Tables 11 and 12. Data for pH 7 and a flow rate of 0.4944 ml/sec are reported in

Table 11

DIRECTLY MEASURABLE EXPERIMENTAL VARIABLES
FOR THE FERRICYANIDE/O_3/UV REACTION AT A FLOW RATE OF
0.4944 ML/SEC, pH 7 AND TEMPERATURE 21°C

Run	UV	Temp (°C)	Ozone Pressure (PA) (atm x 10^2)	Cyanide Feed (CNI) (M x 10^3)	Concentration Product (CNF) (M x 10^3)
1	No	24.3	1.917	0.1843	0.1583
2	No	24.3	1.933	0.1843	0.1614
3	Coarse	22.3	1.925	0.1843	0.1508
4	Coarse	22.3	1.972	0.1843	0.1529
5	Fine	22.3	1.921	0.1843	0.1475
6	Fine	22.3	1.921	0.1843	0.1456
7	Full	24.3	1.826	0.1843	0.1372
8	Full	24.3	1.826	0.1843	0.1482
9	No	23.9	1.944	0.3329	0.2953
10	No	23.9	1.967	0.3329	0.2958
11	Coarse	23.4	1.997	0.3329	0.2815
12	Coarse	23.4	1.965	0.3329	0.2854
13	Fine	23.4	1.964	0.3329	0.2723
14	Fine	23.4	2.006	0.3329	0.2725
15	Full	23.9	1.977	0.3329	0.2595
16	Full	23.9	1.905	0.3329	0.2609
17	No	22.3	1.843	0.4489	0.3960
18	No	22.3	1.843	0.4489	0.4182
19	Coarse	23.6	1.984	0.4489	0.4002
20	Coarse	23.6	1.985	0.4489	0.4061
21	Fine	23.6	1.899	0.4489	0.3937
22	Full	22.3	1.823	0.4489	0.3741
23	Full	22.3	1.952	0.4489	0.3666
24	No	25.1	1.890	0.9609	0.8577
25	No	25.1	1.888	0.9609	0.8545
26	Coarse	25.8	1.810	0.9609	0.8452
27	Coarse	25.8	1.852	0.9609	0.8544
28	Fine	25.8	1.858	0.9609	0.8390
29	Fine	25.8	1.858	0.9609	0.8469
30	Full	25.1	1.967	0.9609	0.8358
31	Full	25.1	1.928	0.9609	0.8378
32	No	25.0	2.084	1.394	1.240
33	No	25.0	1.960	1.394	1.240
34	Coarse	23.6	1.961	1.394	1.172
35	Coarse	23.6	1.937	1.394	1.250
36	Fine	23.6	1.948	1.394	1.255

Table 11 (cont'd.)

Run	UV	Temp (°C)	Ozone Pressure (PA) (atm x 10^2)	Cyanide Feed (CNI) (M x 10^3)	Concentration Product (CNF) (M x 10^3)
37	Fine	23.6	1.934	1.394	1.245
38	Full	25.0	1.942	1.394	1.243
39	Full	25.0	1.907	1.394	1.234
40	No	23.4	1.936	2.272	2.044
41	No	23.4	1.908	2.272	2.042
42	Coarse	23.4	1.945	2.272	2.075
43	Fine	23.4	1.877	2.272	2.080
44	Fine	23.4	1.842	2.272	1.996
45	Full	23.4	1.881	2.272	2.118
46	Full	23.4	1.881	2.272	2.084
47	Full	23.4	1.842	2.272	2.093
48	No	24.3	1.974	5.487	5.119
49	No	24.3	1.924	5.487	5.151
50	Full	24.3	1.929	5.487	5.168
51	Full	24.3	1.937	5.487	5.166
52	Full	25.4	1.860	9.342	9.007
53	No	23.8	1.968	10.21	9.783
54	Full	23.8	1.943	10.21	9.805
55	Full	23.8	1.994	10.21	9.817
56	No	26.1	1.856	17.90	17.32
57	No	26.1	1.890	17.90	17.46
58	Full	26.1	1.874	17.90	17.39
59	Full	25.0	1.927	18.30	17.77
60	No	24.0	1.931	36.74	35.61
61	Full	24.0	1.867	36.74	36.10
62	Full	24.0	1.905	36.74	35.73
63	Full	25.7	1.908	36.82	35.92
64	Full	25.7	2.000	36.82	35.81

Table 12

DIRECTLY MEASURABLE EXPERIMENTAL VARIABLES FOR THE FERRICYANIDE/O_3/UV REACTION AT A FLOW RATE OF 0.5525 ML/SEC, pH 12 AND TEMPERATURE 21°C

Run	UV	Temp (°C)	Ozone Pressure (PA) (atm x 10^2)	Cyanide Feed (CNI) (M x 10^3)	Concentration Product (CNF) (M x 10^3)	pH
1	Full	21.9	1.844	0.9518	0.9129	12.294
2	Full	21.4	1.827	1.859	1.756	12.294
3	Full	21.4	1.857	1.859	1.777	12.294
4	Full	22.8	1.890	3.795	3.649	12.319
5	Full	22.3	2.030	5.792	5.356	12.330
6	Full	22.3	1.916	5.792	5.600	12.330
7	Full	23.6	1.810	4.876	4.640	12.202

Table 11. Table 12 gives data for pH 12 and a flow rate of 0.5525 ml/sec. The values of K calculated from the three different methods are shown in Tables 13, 14. K, KQ, KP denote the rate constants based on the film model with flat CNO profile, film model with quadratic CNO profile and penetration model with flat CNO profile respectively.

Comparing the values of K from the three different models, it is found that K is larger than KP by 8% or less, whereas KQ is slightly higher than K at low cyanide content and substantially lower than K at high cyanide content. The deviation at the high end may be as large as -100%. In order to show the trend more clearly, the rate constants from three different models, i.e. K, KP and KQ are plotted against cyanide content at various UV intensities on Figures 8, 9, 10. K can be correlated with cyanide content and UV intensity. In Figures 8, 9, K and KP at 100% UV are almost independent of cyanide content as represented by 2 horizontal lines (1100 for K, 1000 for KP) in the graphs. The effect of UV on the rate constant is not obvious until the cyanide content is below 1.5×10^{-3} M, i.e. 40 ppm, then the rate constant decreases sharply with depletion of cyanide in the absence of UV. At a fixed cyanide content (below 40 ppm), the rate constant increases gradually and finally reaches a plateau value as the UV intensity is increased to 100% (200 watt). While KP agrees with K within 8%, KQ shows a substantial discrepancy (Figure 10). The whole curve is skewed relative to that of KP and K, and

Run	K, $10^2 M^{-1} s^{-1}$	KQ, $10^2 M^{-1} s^{-1}$	KP, $10^2 M^{-1} s^{-1}$
1	0.9238	1.271	0.8415
2	0.3072	0.3898	0.2888
3	2.644	3.444	2.371
4	1.820	2.422	1.636
5	3.805	4.802	3.401
6	4.534	5.621	4.047
7	10.29	11.68	9.191
8	4.643	5.807	4.156
9	2.193	2.735	1.960
10	2.033	2.552	1.817
11	4.967	5.589	4.427
12	4.159	4.794	3.706
13	7.763	8.242	6.945
14	7.406	7.906	6.621
15	12.31	12.30	11.10
16	12.53	12.50	11.31
17	4.202	4.633	3.752
18	0.7821	10.41	0.7040
19	3.130	3.580	2.790
20	2.187	2.617	1.949
21	4.683	5.088	4.185
22	9.523	9.378	8.609
23	10.48	10.19	9.502
24	8.048	7.189	7.430
25	8.557	7.580	7.917
26	10.98	9.388	10.24
27	9.029	7.932	8.367
28	11.68	9.910	10.92
29	10.25	8.855	9.547
30	11.02	9.449	10.29
31	11.01	9.434	10.28

Table 13 Comparison of rate constants K,KQ,KP from three different models for the ferricyanide concentrations listed in Table 11.

Table 13 continued

32	9.827	8.117	9.282
33	10.77	8.768	10.20
34	20.68	15.51	19.97
35	9.213	7.659	8.679
36	8.543	7.174	8.027
37	9.851	8.117	9.302
38	10.52	8.588	9.961
39	12.07	9.662	11.47
40	12.59	9.361	12.18
41	13.08	9.666	12.66
42	9.532	7.352	9.150
43	9.588	7.371	9.202
44	19.45	13.59	18.98
45	6.363	5.169	6.027
46	9.193	7.108	8.811
47	8.665	6.744	8.289
48	11.70	7.725	11.51
49	10.30	6.899	10.11
50	9.331	6.336	9.143
51	9.378	6.366	9.191
52	6.411	4.216	6.286
53	7.854	5.010	7.748
54	7.277	4.684	7.172
55	6.621	4.330	6.518
56	9.120	5.174	12.20
57	5.349	3.283	5.286
58	7.093	4.177	9.062
59	13.02	6.417	12.99
60	13.02	6.417	12.99
61	4.814	2.713	5.703
62	10.80	5.450	10.76
63	9.226	4.729	9.189
64	10.57	5.357	10.53

Run	K, $10^2 M^{-1} s^{-1}$	KQ, $10^2 M^{-1} s^{-1}$	KP, $10^2 M^{-1} s^{-1}$
1	9.911	9.366	9.842
2	14.57	12.81	16.32
3	11.01	9.910	12.12
4	10.68	9.037	12.61
5	25.75	18.35	25.65
6	9.387	7.685	11.62
7	14.57	11.18	17.81

Table 14. Comparison of rate constants K, KQ, KP from three different models for the ferricyanide concentrations listed in Table 12.

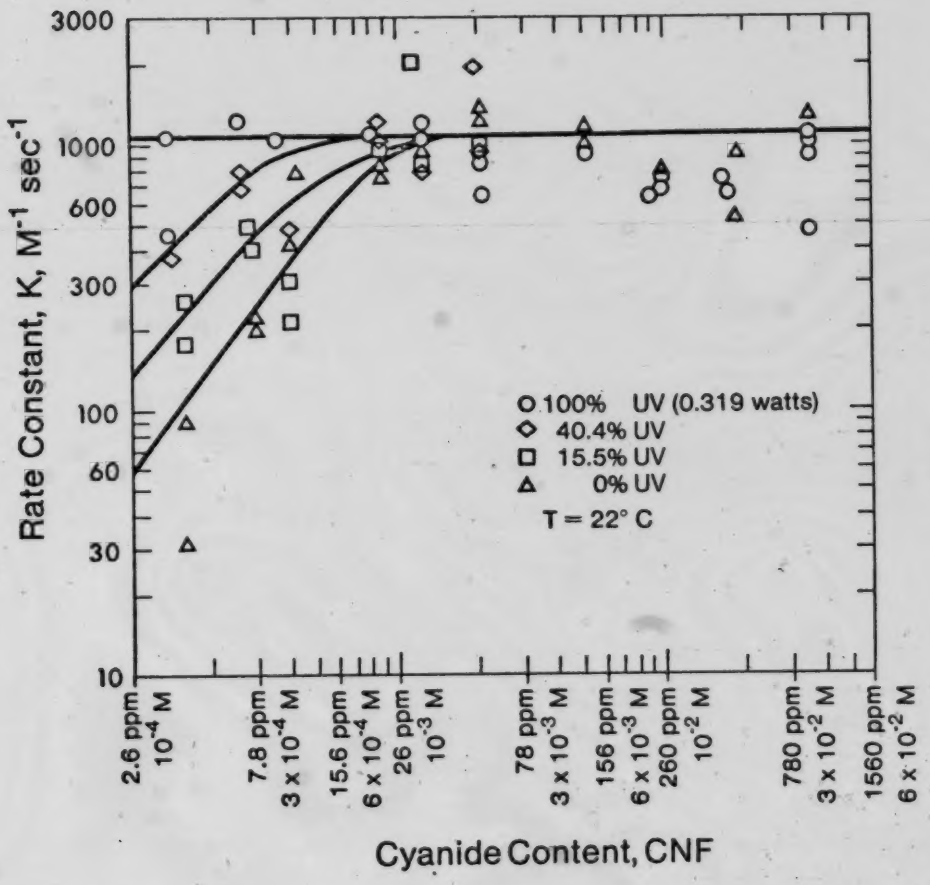

Figure 8. Plot of K from the film model, flat CNO profile vs cyanide content, CN, at 22°C, pH 7, 108 rpm and various UV intensities.

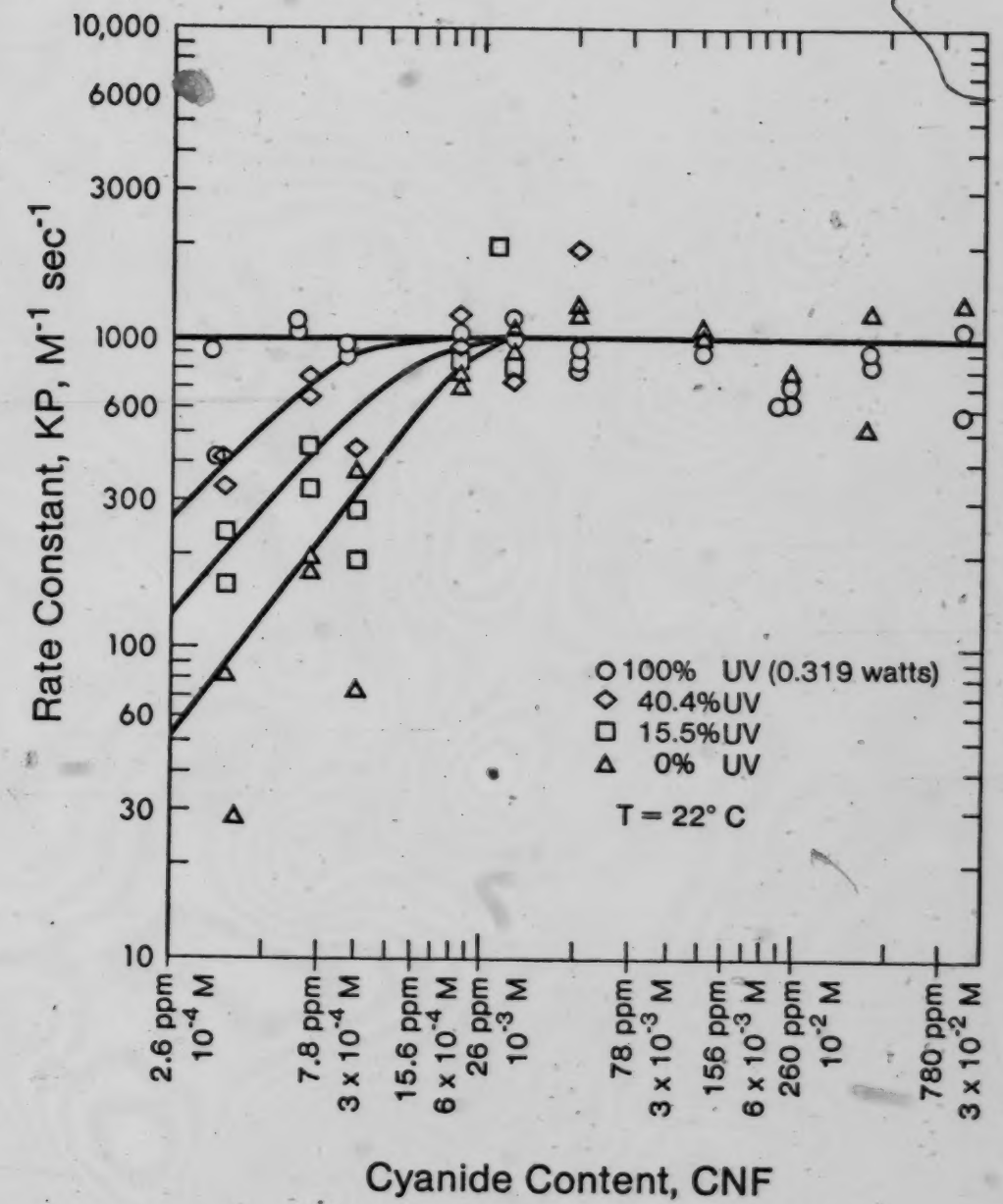

Figure 9. Plot of KP from the penetration model, flat CNO profile vs cyanide content, CN, at 22°C, pH 7, 108 rpm and various UV intensities.

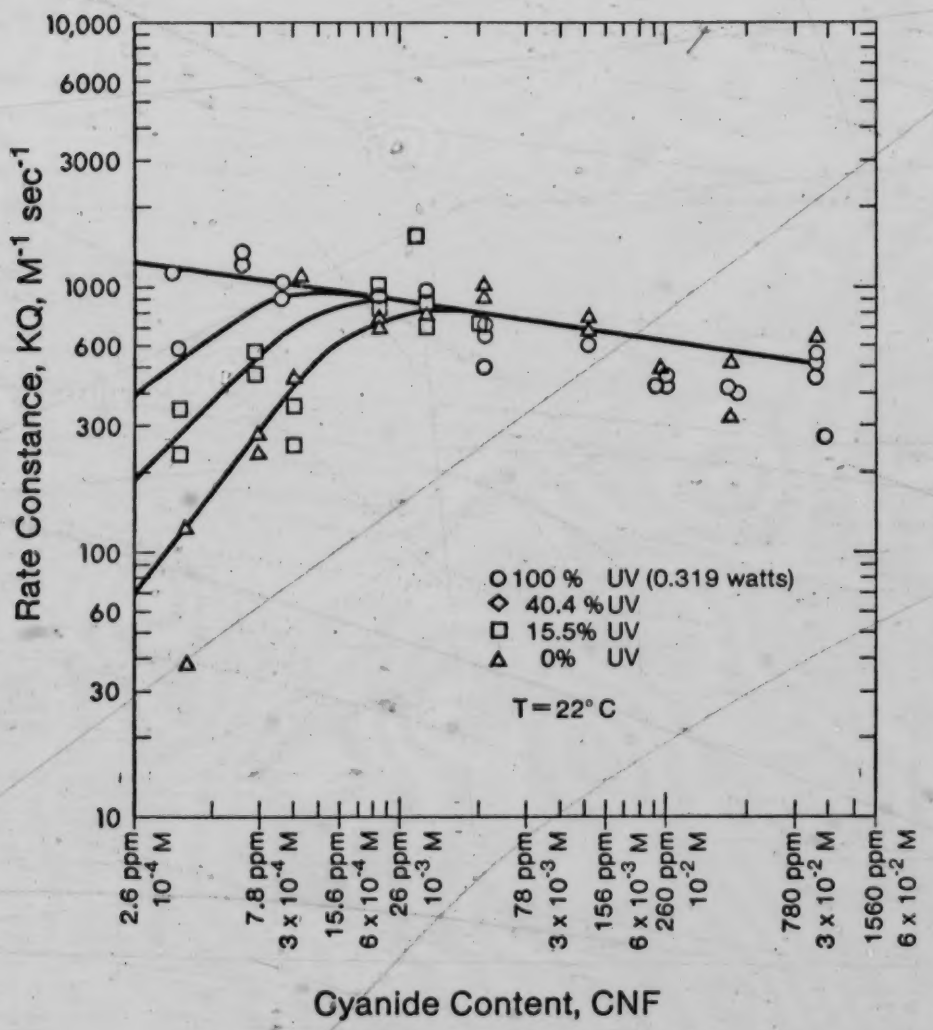

Figure 10. Plot of KQ from the film model, quadratic CNO profile vs cyanide content, CN, at 22°C, pH 7, 108 rpm and various UV intensities.

KQ depends strongly on cyanide content. It implies that the model has been over-corrected by the assumption that the CNO profile is quadratic, and the rate constants obtained by the assumption of an uncorrected flat CNO profile are more reasonable. K and KP at concentrations higher than 40 ppm (1.5×10^{-3} M) and below 40 ppm with 100% UV irradiation are independent of cyanide concentration. The effect of UV on the rate constant can be seen more clearly by transforming Figure 8 into a ln K vs % UV plot at fixed cyanide concentrations (Figure 11). K increases with UV intensity as well as cyanide content. The curves converge to the horizontal line at high cyanide level (1.5×10^{-3} M, or 40 ppm).

Similarly, K and KQ at pH 12, 100% UV are plotted against cyanide content at 22°C. In Figure 12, a horizontal line is observed for K (K = 1100) and a severely bent curve for KQ, as represented by a dotted line in the graph. The graph reveals that the flat CNO profile is more satisfactory than the quadratic one. The value of K at pH 12 agrees with that of pH 7. The agreement implies that the model and the assumptions made in the model are valid, therefore the value of K is independent of pH and ferricyanide concentration.

The fact that the rate constant apparently decreases with decreasing cyanide content at low cyanide concentrations in the absence of UV imposes a problem for the treatment of ferricyanide. The rate of oxidation diminishes in

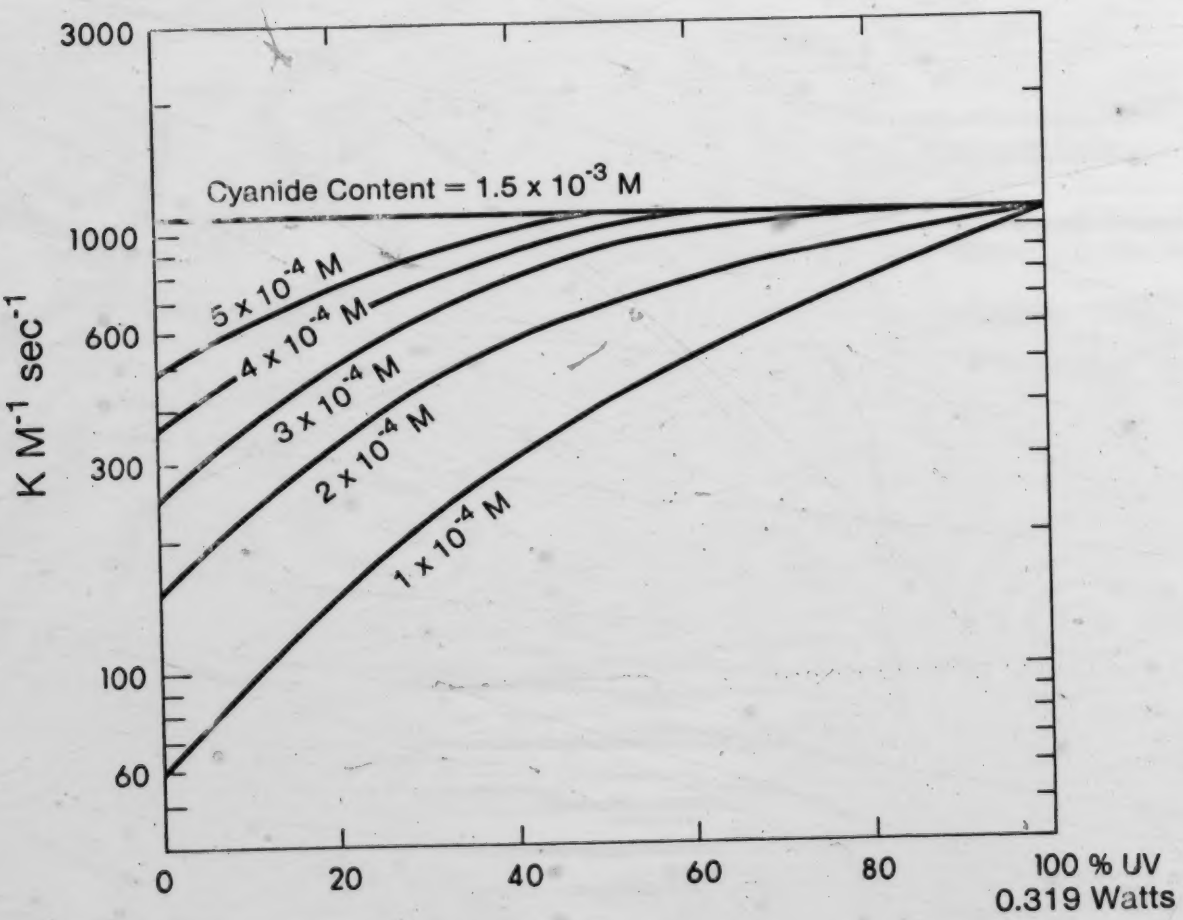

Figure 11. Plot of K vs UV intensity at 22°C, pH 7, 108 rpm and various cyanide contents.

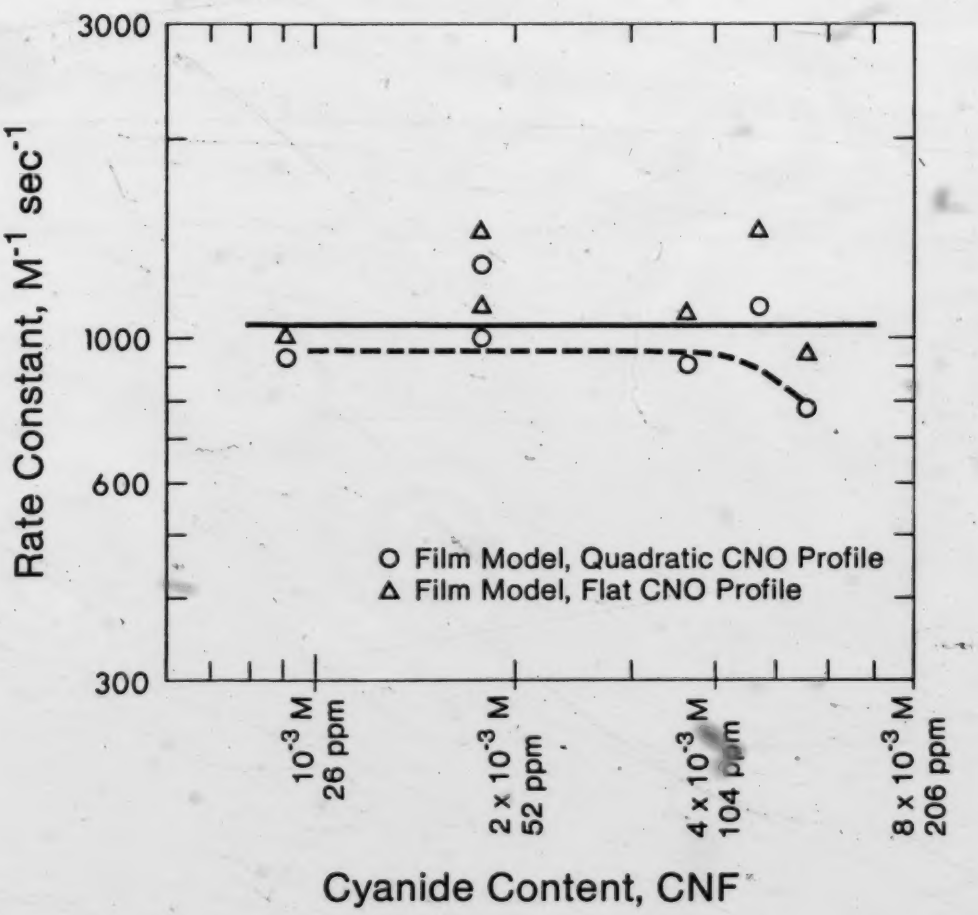

Figure 12. Plot of K, KQ vs cyanide content, CN, at 0 and 100% UV, 22°C, pH 12 and 108 rpm.

the final stage where cyanide is almost depleted; the oxidation is so slow that in the absence of UV the desired discharge standard of 1.5 ppm cannot be achieved with a reasonable contact time and flow rate. To facilitate the oxidation reaction, UV has to be applied to the reaction system at low cyanide content (40 ppm) where the effect of UV is pronounced. For instance, at 1×10^{-4} M (2.6 ppm), the rate constant with 100% UV (K = 1100) is higher than that with 40.4% UV by a factor of 3, 15.5% UV by 9, and 0% UV by 19. O_3/UV is indeed a powerful combination to reduce the wasted cyanide content to the allowable discharged level.

Most of the important parameters are shown in Tables A6, A7 in Appendix 6 for pH 7 and 12 respectively. At all UV intensities, K_0 is approximately 2.2×10^{-3} cm/sec and K_L ranges from 1.7×10^{-2} to 3×10^{-2} cm/sec, which means an enhancement factor of 7.6 to 13 irrespective of the pH of the solution. The values of EN are considerably lower than those for free cyanide, for which EN may exceed 20. The value of TRD (~0.5) indicates that the reaction is in the transition regime. The calculated cyanate concentration, CNO, varies from 3.6×10^{-6} M to 9×10^{-4} M as CN content increases from 1.8×10^{-4} to 3.6×10^{-2} M, which is also less than that for free cyanide at the corresponding concentration because of slower reaction. The trend can be observed more clearly on a log-log plot of CNO vs CN as given in Figure 13. A linear relationship exists and the lines for

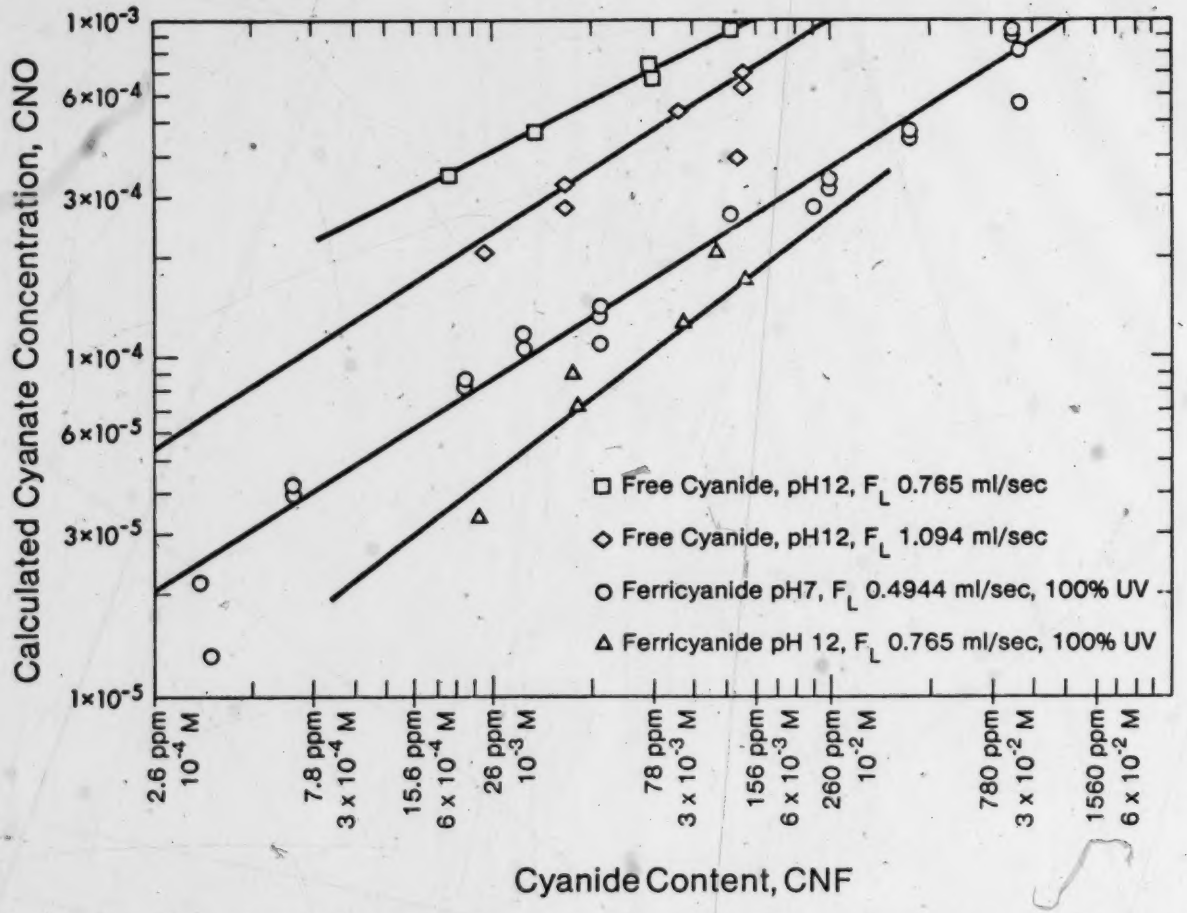
Calculated Cyanate Concentration, CNO
1×10⁻³
6×10⁻⁴
3×10⁻⁴
1×10⁻⁴
6×10⁻⁵
3×10⁻⁵
1×10⁻⁵
Free Cyanide, pH12, F_L 0.765 ml/sec
Free Cyanide, pH12, F_L 1.094 ml/sec
Ferricyanide pH7, F_L 0.4944 ml/sec, 100% UV
Ferricyanide pH 12, F_L 0.765 ml/sec, 100% UV
2.6 ppm 10⁻⁴ M
7.8 ppm 3 x 10⁻⁴ M
15.6 ppm 6 x 10⁻⁴ M
26 ppm 10⁻³ M
78 ppm 3 x 10⁻³ M
156 ppm 6 x 10⁻³ M
260 ppm 10⁻² M
780 ppm 3 x 10⁻² M
1560 ppm 6 x 10⁻² M
Cyanide Content, CNF

Figure 13. Plot of calculated cyanate concentration CNO vs cyanide content CN for ferricyanide at pH 7 and 12, 100% UV;, and for free cyanide at pH 12, flow rates of 0.4944 and 0.765 ml/s.

free cyanide lie above those for ferricyanide.

The percentage of ozone decomposed, FRD, shown in Tables A6, A7 depends strongly on the pH of the solution. At pH 7, ozone decomposition is not significant and accounts for 0.2 to 0.001% of the total ozone consumption as cyanide concentration increases from 1.3×10^{-4} M to 3.6×10^{-2} M. The decomposition of ozone can thus be ignored, so that accurate measurement of pH is not required; a K_D value of 8.5×10^{-4} can be obtained from Stumm's correlation and was used throughout the program. However, decomposition becomes the major reaction as the pH is raised to 12, under this condition, decomposition claims 70~90% of the ozone consumed. Utilizing ozone for waste water treatment at such a high pH is uneconomical. FRD for ferricyanide and free cyanide at pH 7 and 12 are plotted against cyanide content in Figures 14 and 15. Comparing the FRD for free cyanide with that for ferricyanide the decomposition reaction is still significant (40%~10%). However, it is far less than that of ferricyanide because the faster CN^-/O_3 reaction tends to reduce the ozone concentration in the solution. For all cases, FRD decreases with increasing cyanide concentration which is in agreement with the model used. An increased cyanide level will reduce the ozone concentration in solution, and thus diminish the decomposition.

The fraction of ozone reacted with CNO, FRC, is complementary to FRD, large FRD is accompanied by small

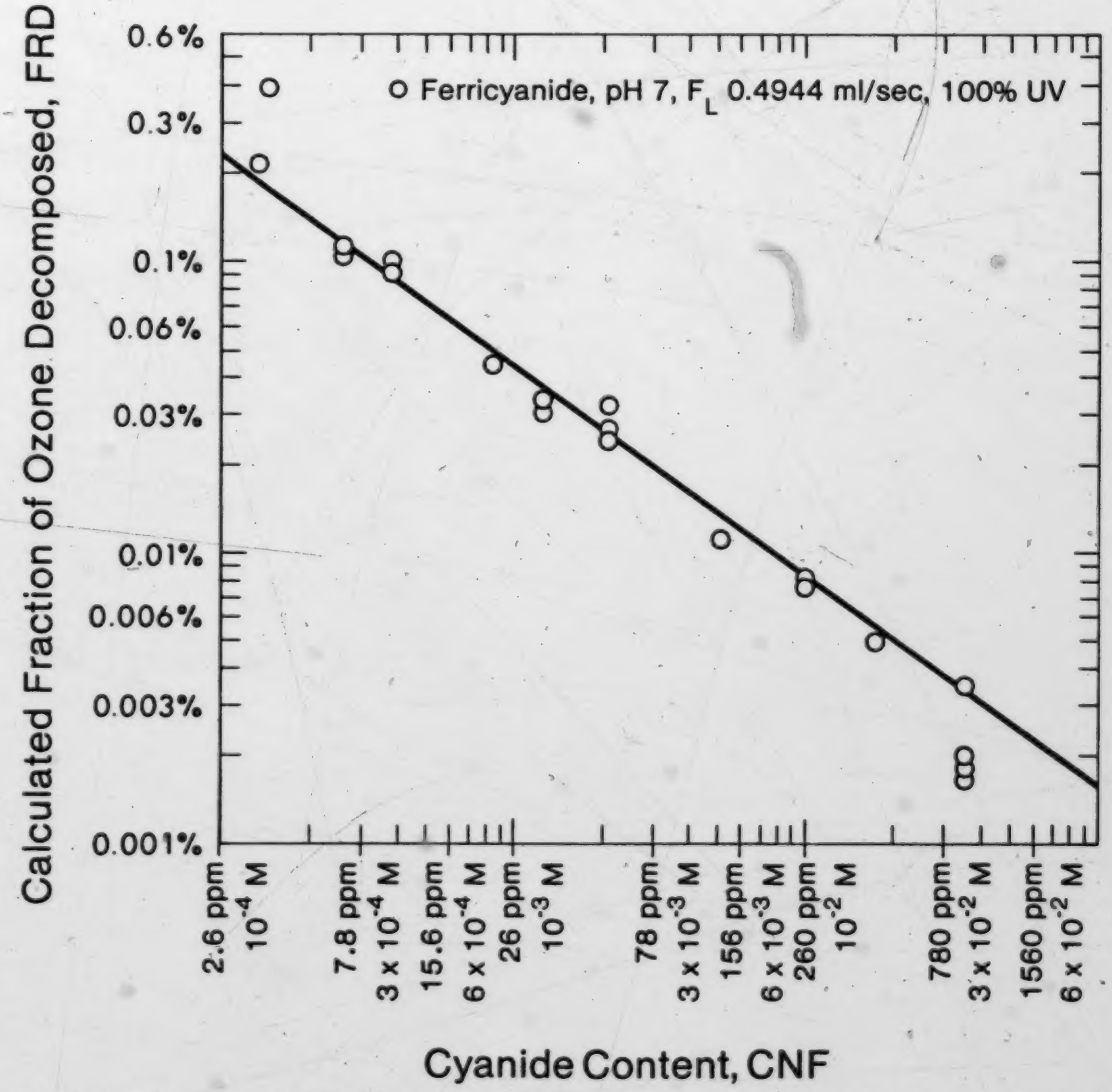

Figure 14. Plot of fraction of ozone decomposed FRD vs CN for ferricyanide at pH 7 and 12, 100% UV and for free cyanide at pH 12, flow rates of 0.4944 and 0.765 ml/sec.

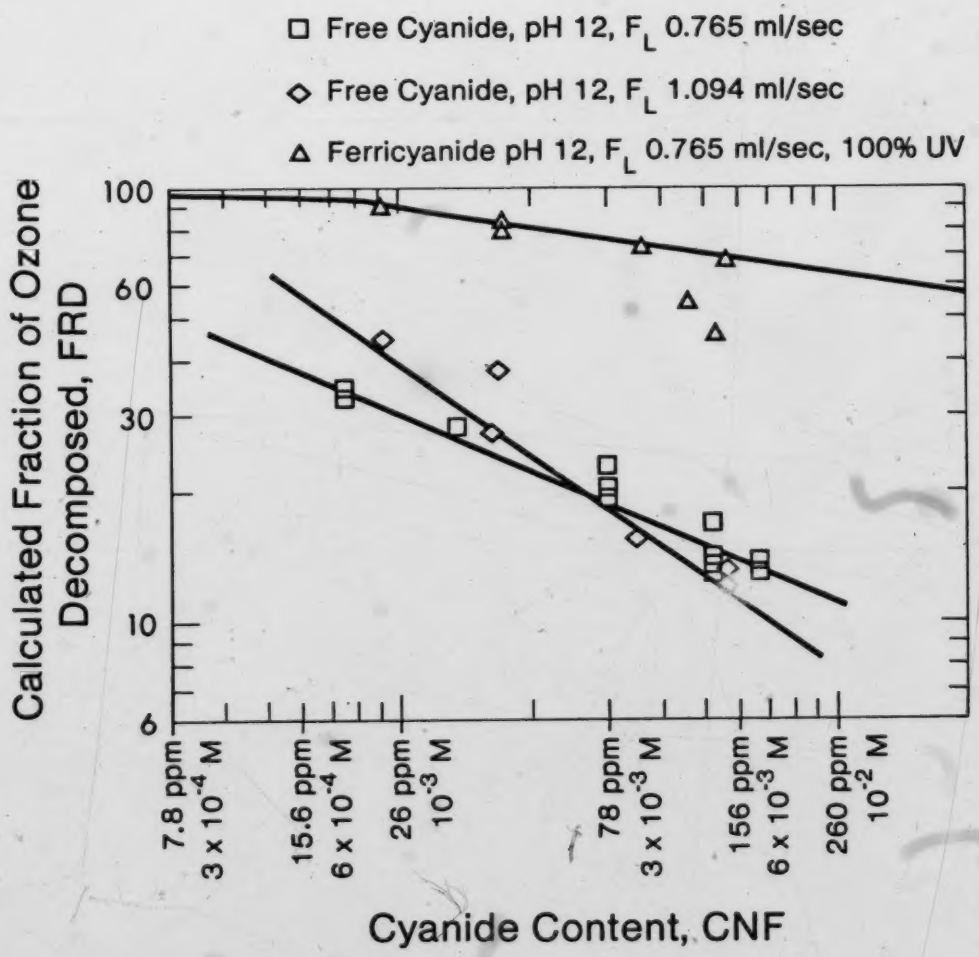
□ Free Cyanide, pH 12, F_L 0.765 ml/sec
◇ Free Cyanide, pH 12, F_L 1.094 ml/sec
△ Ferricyanide pH 12, F_L 0.765 ml/sec, 100% UV
Calculated Fraction of Ozone Decomposed, FRD
100
60
30
10
6
7.8 ppm 3 x 10^{-4} M
15.6 ppm 6 x 10^{-4} M
26 ppm 10^{-3} M
78 ppm 3 x 10^{-3} M
156 ppm 6 x 10^{-3} M
260 ppm 10^{-2} M
Cyanide Content, CNF

Figure 15. Plot of fraction of ozone decomposed FRD vs CN for ferricyanide at pH 7 and 12, 100% UV and for free cyanide at pH 12, flow rates of 0.4944 and 0.765 ml/sec.

FRC and vice versa; and it accounts for the graph obtained by plotting FRC vs cyanide content (Figure 16). FRC is determined by the cyanate concentration as well as the ozone concentration. Even though CNO increases with CN, FRC declines because the decrease in ozone concentration can more than compensate for the increase in CNO. However, the case of ferricyanide at pH 12 holds an opposite trend, it is probably due to the fact that at high pH, ozone has already decreased to such a small extent that it is not sensitive to the cyanide content, and then the shape of the curve is completely governed by CNO.

Conclusion

Comparing the ferricyanide/O_2/UV reaction at pH 7 and 12, the dissimilarity is quite striking. At pH 12, ozone decomposition is dominant and consumes 90~70% of ozone, O_3/CNO^- and O_3/ferricyanide reactions only claim the remaining 3~10% and 7~20%. On the other hand, at pH 7, O_3/CNO^- is as important as the O_3/ferricyanide reaction (70~30% and 30~70%), and the decomposition is negligible. Despite the adverse predominant reactions and diversified conditions, after correcting for decomposition and CNO^- oxidation, the same K can be obtained at both pH values (K = 1100 at 22°C, pH 7 and 12). The excellent agreement as well as the applicability of the same model to the diversified conditions prove that the model proposed is indeed valid, and the argument in the previous chapters is substantiated.

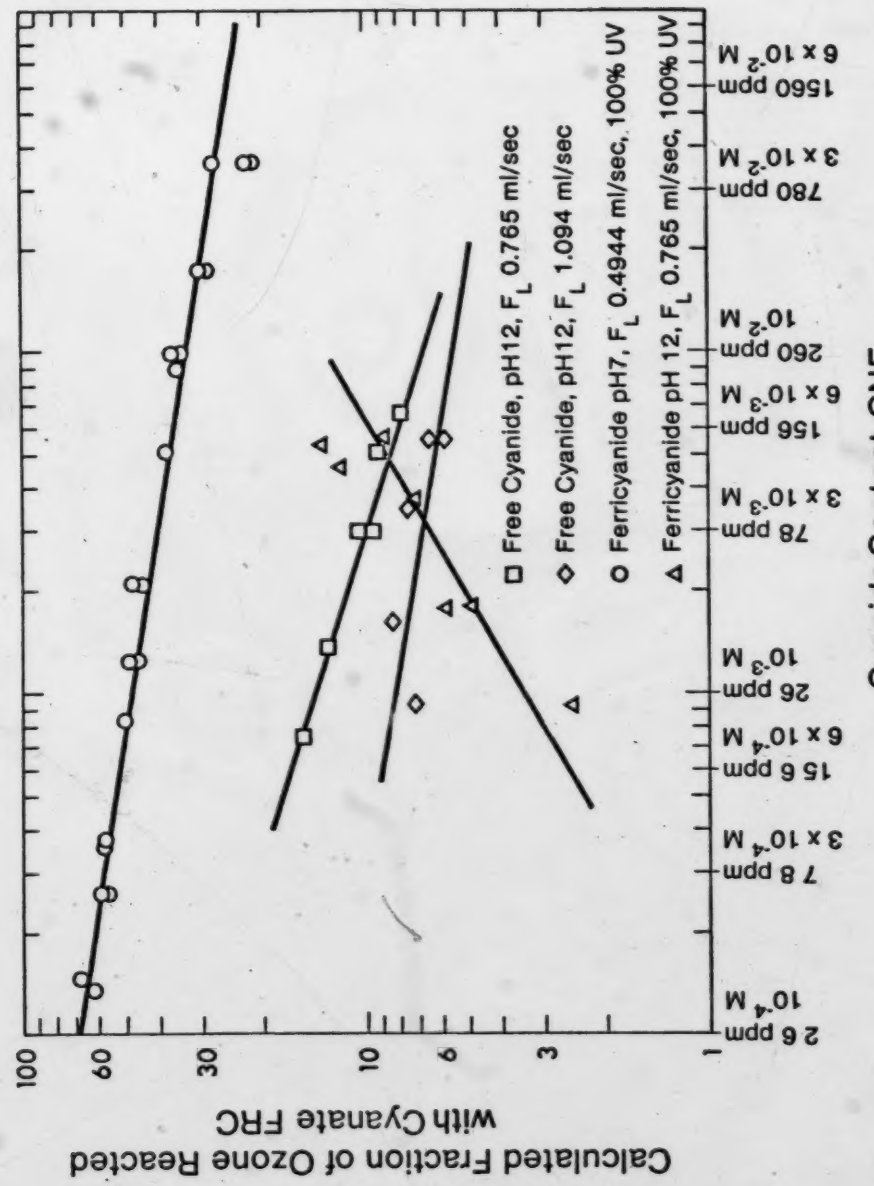
Calculated Fraction of Ozone Reacted with Cyanate FRC
100
60
30
10
6
3
1
Free Cyanide, pH12, F_L 0.765 ml/sec
Free Cyanide, pH12, F_L 1.094 ml/sec
Ferricyanide pH7, F_L 0.4944 ml/sec, 100% UV
Ferricyanide pH 12, F_L 0.765 ml/sec, 100% UV
2.6 ppm 10^{-4} M
7.8 ppm 3×10^{-4} M
15.6 ppm 6×10^{-4} M
26 ppm 10^{-3} M
78 ppm 3×10^{-3} M
156 ppm 6×10^{-3} M
260 ppm 10^{-2} M
780 ppm 3×10^{-2} M
1560 ppm 6×10^{-2} M
Cyanide Content, CNF

Figure 16. Plot of fraction of ozone reacted with cyanide vs CN for ferricyanide at pH 7 and 12, 100% UV and for free CN^- at pH 12, flow rates of 0.4944 and 0.765 ml/s.

6.3 Proposed Mechanism for the Ferricyanide/O_3/UV Reaction

The influence of UV and cyanide content upon the oxidation rate constant can be explained by a plausible mechanism involving the formation of an ozonide intermediate. It has been known in organic chemistry that ozone can react with alkene to give an ozonide. The reaction of ferricyanide with ozone may also involve the following ozonide as an intermediate.

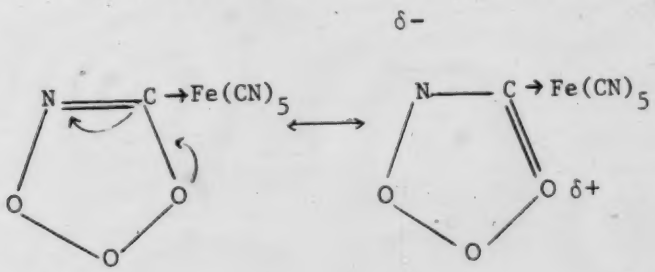

I II

Only a single form of ozonide would exist in that rearrangement by breaking the C = N bond is not feasible due to the double bond character. Furthermore, the C-O bond in the ozonide is strengthened by the resonance form II shown above, because of the δ+ charge developed at the carbon atom as a result of the stable bond between C and Fe and the electron withdrawing properties of Fe. The stability of this ozonide would account for the slow oxidation rate of ferricyanide. However, the decomposition of the ozonide could be catalyzed by another CN group, as it would provide a positive center to facilitate the electrophilic reaction

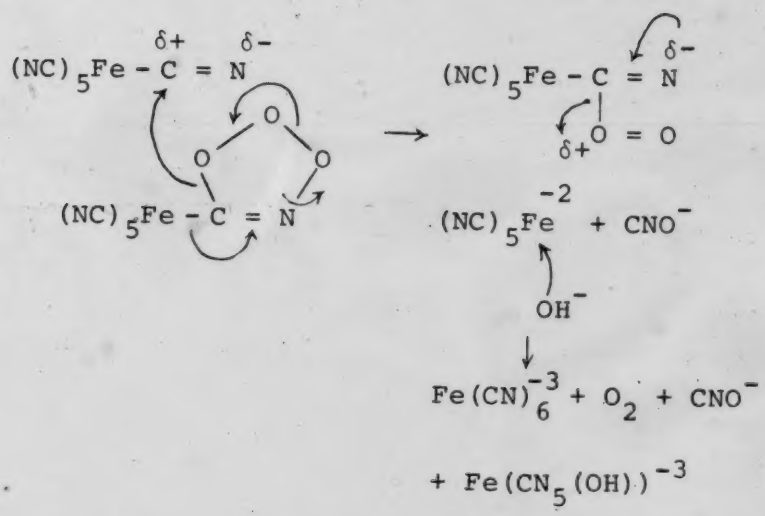

Schematically, the reactions can be written as

$$A + B \underset{k_{-1}}{\overset{k_1}{\rightleftharpoons}} B^*$$

$$B^* + B \xrightarrow{k_2} C + B$$

where A denotes ozone, B cyanide and C cyanate.

Rates can be expressed as

$$r_B = - k_1 C_A C_B + k_{-1} C_B^* \qquad (115)$$

$$r_{B^*} = k_1 C_A C_B - k_{-1} C_B^* - k_2 C_B C_B^* \quad . \qquad (116)$$

Using steady state hypothesis, the term r_{B^*} can be assumed to be zero, then

$$C_B^* = \frac{k_1 C_A C_B}{k_{-1} + k_2 C_B} \qquad (117)$$

$$\therefore \quad r_B = - \frac{k_1 k_2 C_A C_B^2}{k_{-1} + k_2 C_B} \qquad (118)$$

Several cases can be discussed:

i) As cyanide concentration is high, $k_2 C_B >> k_{-1}$,

$$r_B = - k_1 C_A C_B \qquad (119)$$

which is in agreement with the constant values of K determined at [CN] > 1.5×10^{-3} M (40 ppm) by the horizontal line in Figures 8, 9.

ii) As cyanide concentration is low, $k_2 C_B << k_{-1}$ and

$$r_B = - \frac{k_1 k_2}{k_{-1}} C_A C_B^2 \qquad (120)$$

iii) If UV stabilizes the ozonide intermediate and thus reduces k_{-1} or promotes the bimolecular ozonide reaction (k_2), then $k_2 C_B >> k_{-1}$ at 100% UV even at low cyanide level. The rate expression would have the same form as that in i), and the rate is first order to both ozone and cyanide concentrations. If the UV intensity is less than 100%, k_{-1} is suppressed but still larger than $k_2 C_B$, then

$$r_B \doteq - \frac{k_1 k_2}{k_{-1}} C_A C_B^2 = - K C_A C_B \qquad (121)$$

$$\therefore \quad K \doteq \frac{k_1 k_2}{k_{-1}} C_B \quad . \qquad (122)$$

From this expression, K is expected to depend on C_B in a linear fashion, and to increase with UV intensity. Indeed, it is what has been observed in Figures 8 and 9. The slopes of the curves on a log-log scale at cyanide concentrations less than 1.5×10^{-3} M (40 ppm) are

0% UV	1.3
15.5% UV	1.1
40.4% UV	0.95

which are close to the value of 1 indicated by Equation (122).

The reaction mechanism proposed gives a satisfactory explanation of the K values obtained, however, it should be noted that this is not the only mechanism which can account for the experimental K values. At this time, it is somewhat naive to claim that this mechanism is realistic, unless the actual experimental work is carried out to positively identify the intermediates. Further work has to be done to clarify the mechanism.

6.4 Other Possible Mechanisms

6.4.1 Free Radical Mechanism

It has been reported that ozone dissociates upon the absorption of UV[27].

$$O_3 + I \underset{k_2}{\overset{k_1}{\rightleftharpoons}} O + O_2$$

The atomic oxygen produced in the dissociation process is an active species and can react with ferricyanide as represented by the following reaction

$$O + CN_6^{-3} \xrightarrow{k_3} CNO^- + CN_5^{-2}$$

where CN_6^{-3} and CN_5^{-2} denote ferricyanide and its product after one cyano group has been oxidized, and I, the UV intensity. Using steady state hypothesis

$$r_0 = -k_1 I[O_3] - k_2[O][O_2] - k_3[O][CN_6^{-3}] = 0 \qquad (123)$$

$$r_{CN_6^{-3}} = -k_3[O][CN_6^{-3}] \qquad (124)$$

By solving these two equations, the rate of oxidation of ferricyanide can be expressed as

$$r_{CN_6^{-3}} = -\frac{k_1 k_2 [O_3][CN_6^{-3}] I}{k_2[O_2] + k_3[CN_6^{-3}]} = -K'[O_3][CN_6^{-3}] \qquad (125)$$

$$K' = \frac{k_1 k_3 I}{k_2[O_2] + k_3[CN_6^{-3}]} \qquad (126)$$

$$\lim_{[CN_6^{-3}]\to\infty} K' = \frac{k_1 I}{[CN_6^{-3}]} \qquad (127)$$

$$\lim_{[CN_6^{-3}]\to 0} K' = \frac{k_1 k_3 I}{k_2[O_3]} \qquad (128)$$

where K' is the lumped pseudo rate constant for the reaction assumed to be first order to O_3 and CN_6^{-3}. The effective intensity of UV in the reactor depends on the ferricyanide concentration because ferricyanide solution absorbs UV. The dependence of K' on $[CN_6^{-3}]$ and I can be shown schematically by the following diagram.

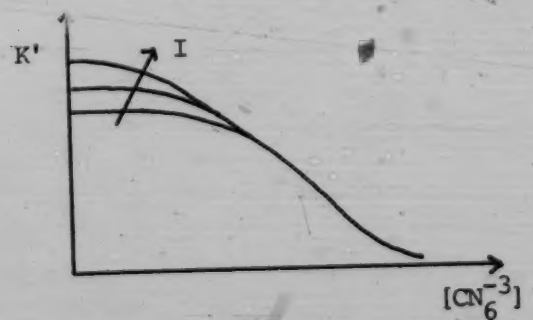

6.4.2 Mechanism Involving Ferricyanide Dissociation

Ohno[39] indicates that ferricyanide will dissociate into a free cyanide ion and an intermediate containing 5 cyano groups.

$$H_2O + Fe(CN)_6^{-3} + I \underset{k_2}{\overset{k_1}{\rightleftharpoons}} Fe(CN)_5(H_2O)^{-2} + CN^- \quad .$$

The CN^- produced is responsible for the oxidation reaction

$$CN^- + O_3 \xrightarrow{k_3} CNO^- + O_2 \quad .$$

Similar to the approach in 6.4.1 Free Radical Mechanism, the rate expressions can be written as

$$r_{CN} = k_1 I[CN_6^{-3}] - k_2[CN^-][CN_5^{-2}] - k_3[CN^-][O_3] = 0 \tag{129}$$

$$r_{CN_6^{-3}} = -k_1 I[CN_6^{-3}] + k_2[CN_5^{-2}][CN^-] \tag{130}$$

$$\therefore \quad r_{CN_6^{-3}} = -k_1[CN_6^{-3}][O_3]\left\{\frac{k_3 I}{k_2\{Co-[CN_6^{-3}]\}+k_3[O_3]}\right\} \tag{131}$$

$$K' = \frac{k_3 I}{k_2\{Co - [CN_6^{-3}]\} + k_3[O_3]} \tag{132}$$

where Co is the initial ferricyanide concentration, and is equal to $[CN_6^{-3}] + [CN_5^{-2}]$.

$$\lim_{[CN_6^{-3}]\to 0} K' = \frac{k_3 I}{k_2 Co + k_3[O_3]} \doteq \frac{k_3 I}{k_3[O_3]} \tag{133}$$

$$\lim_{[CN_6^{-3}]\to\infty} K' \doteq \frac{k_3 I}{k_2[CN_5^{-2}] + k_3[O_3]} \qquad (134)$$

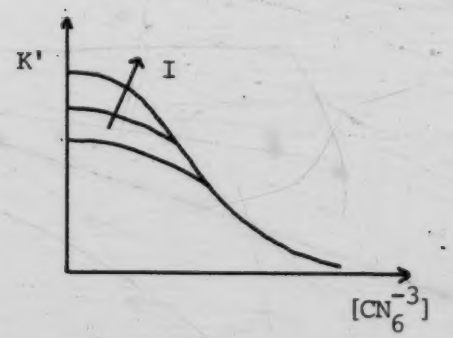

The shape of the K' vs $[CN_6^{-3}]$ curve for the mechanism involving ferricyanide dissociation is similar to that of the free radical mechanism. The only difference is that K' in the former case decreases with increasing ozone concentration; in other words, the reaction order of ozone in the ozonation of ferricyanide is less than 1.

6.5 Conclusions

Comparing the experimental K vs $[Fe(CN)_6^{-3}]$ plot with that from different possible mechanisms, the molecular reaction one through the formation of ozonide seems to fit the data best. However, the other two mechanisms cannot be excluded. The dip in the experimental K vs $[Fe(CN)_6^{-3}]$ plot (Figures 8, 9) remains unexplained by the ozonide mechanism. Since both the free radical and ferricyanide mechanisms predict a downward trend for K at high ferricyanide concentrations, this dip may be due to the presence of these two

mechanisms together with the ozonide one. The free radical and ferricyanide dissociation mechanisms will not be dominant at high cyanide concentrations, otherwise K would depend on the UV intensity and decreases with increasing ferricyanide concentration.

CHAPTER 7

FUTURE WORK

UV/ozone reaction systems have received wide attention this year (1977) as revealed by the number of papers presented in the International Ozone Institute Symposium held in Toronto[86]. The present trend shows clearly that ozone is a potential chemical which can replace the conventional chlorine in the foreseeable future in the municipal and industrial water treatment. The main barrier to bar the further usage of ozone in water treatment is the cost which can be overcome gradually with the advent of technology. However, in order to utilize ozone more effectively, the ozone reaction mechanism should be studied more rigorously. The ozone generating technology and ozone reaction mechanism are the two important areas that should be worked on.

As for the continuation of this piece of work, the following studies are recommended:

a) Most of the difficulties in the experiment arise from the uncertainty in the gas phase ozone balance due to the limitation of the surface area in the reactor. The transfer of ozone can be enhanced and thus the difference in ozone concentrations in the inlet and outlet streams be detected easily by a reactor of larger interfacial area. A bubble reactor capable of providing reproducible bubble size would be a

good choice. The interfacial area can be obtained by correlation or by carrying out a well-documented simple reaction, and the same surface area can be used for the ferricyanide/O_3/UV reaction should the experiment be carried out under the same conditions used in the surface area calibration. RT, the ozone consumption can be measured directly with good accuracy which allows the solution of K and K_B simultaneously.

b) In the treatment of data, ozone decomposition is assumed to be in parallel with ferricyanide oxidation, therefore ozone decomposition will decrease the effective ozone concentration in the solution and thus decrease the ferricyanide oxidation rate. According to the free radical mechanism, ozone decomposition would be in series with the ferricyanide oxidation reaction and thus increase the oxidation rate. The free radical mechanism can be tested by using the same computer program THES except that K is given by

$$K = \frac{k_1 k_3 I_0 \exp(-\varepsilon'[CN_6^{-3}])}{k_2[O_2] + k_3(CN_6^{-3}]} \qquad (135)$$

where I_0 is the incident UV intensity, ε' is the molar absorptivity multiplied by the distance from the bottom quartz plate of the reactor to the interface. $[O_2]$ can be assumed to be equal to the saturated concentration at the partial pressure of oxygen in air.

A sophisticated program can be written to include the free radical mechanism by assuming the following reaction scheme:

$$O_3 + CN_6^- \longrightarrow CNO^- \qquad \text{molecular mechanism}$$

$$O_3 \longrightarrow O_2 + O \xrightarrow{CN_6^-} CNO^- \qquad \text{free radical mechanism}$$

$$\longrightarrow O_2 \qquad \text{ozone decomposition}$$

The contribution of the ferricyanide dissociation mechanism to the ferricyanide/O_3/UV reaction can also be tested by running the reaction at different ozone partial pressures. If the rate constants calculated by the program THES decrease with increasing ozone partial pressure, the ferricyanide dissociation mechanism would be present (cf. Equation (132)).

c) The rate constant and the stoichiometry of CNO^-/O_3 reaction should be elucidated. This can be done using the same set-up as mentioned previously except that KCNO solution is passed through the reactor instead of $K_3Fe(CN)_6$.

d) The molecular mechanism proposed in Section 6.3.1 has to be tested by identifying the ozonide.

e) The rate constant obtained in this work can be cross-checked with the stop-flow technique developed in chemistry.

f) The same technique can be applied to other cyano complexes such as nickel, cobalt, silver, cadmium cyanide complexes. The rate constant might be able to be correlated with the instability constant of the complex. Then the rate constant of a cyanide complex can be predicted by the known instability constant.

Recently, the arsenic and cyanide problem in the gold mines operated at Yellowknife became a hot issue and received criticism from the public. Ozone finds its immediate application to this problem. Arsenic can be oxidized by ozone to the $As(V)$ state, which will form a calcium arsenate precipitate at high $_pH$. The treatability as well as the rate constant should be explored.

NOMENCLATURE

C	Concentration
CAO	Bulk concentration of A
C_A'	Effective ozone concentration in solution
CNF	Bulk concentration of cyanide
CNI	Feed concentration of cyanide
CNO	Concentration of cyanate in solution
CS	Interfacial concentration of ozone
D	Diffusivity
DT	Diffusivity of ozone in solution
E	UV intensity, W
EN, E_n	Enhancement factor
F	Flow rate
FRC	Fraction of ozone reacted with cyanate
FRCN	Fraction of cyanide destroyed
FRD	Fraction of ozone decomposed
H	Henry's law constant
I_o	UV intensity, quanta per second
J	Molar flux crossing a unit surface without chemical reaction
J'	Molar flux crossing a unit surface with chemical reaction
K	Rate constant for the O_3/ferricyanide reaction using the film model with a flat CNO profile

KP	Rate constant for the O_3/ferricyanide reaction using the penetration model with a flat CNO profile
KQ	Rate constant for the O_3/ferricyanide reaction using the film model with a quadratic CNO profile
K_{AB}	Rate constant for the reaction between A and B
K_B, XKB	Rate constant for the O_3/CNO^- reaction
K_D, XKD	Rate constant for the ozone decomposition reaction
K_f	Rate constant for the O_3/CN^- reaction
K_g	Gas phase mass transfer coefficient
K_L	Liquid mass transfer coefficient
K_0	Physical mass transfer coefficient
K_{0L}	Overall liquid mass transfer coefficient
ℓ	Optical path length
η_B	Fe^{2+} formed upon UV irradiation
$\dot{n}$	Ozone flow rate
P	Partial pressure
q	Stoichiometric ratio
r	Amount of A or B reacted per unit time and unit volume
R	Amount of cyanide reacted per second
RO, O3	Amount of ozone consumed obtained by direct gas phase ozone mass balance
RT	Amount of ozone consumed by calculation
S, ARA	Surface area

S_0, SO	Measured ozone consumption ratio
S_1, S1	Calculated ozone consumption ratio
ST	Moles of ozone required to react with one mole of cyanate
T	Temperature
t_L	Time delay
t_R, TR	Reaction time
$\bar{t}_R$	Residence time
t_D, TD	Diffusion time
t_{RD}, TRD	Ratio of reaction time to diffusion time
V	Reactor volume
x	Distance from the surface

Greek Letters

δ	Thickness of the film
θ	Contact time
ε	Molar absorptivity
ν	UV frequency

Subscripts

A	Gas component, i.e. ozone
B	Liquid reactant, i.e. cyanide or ferricyanide
C	Product of the reaction between A and B, i.e. cyanate
f	Exit stream
g	Gas phase

Subscripts (cont'd)

g	Gas phase
i	Feed
L	Liquid phase
o	Bulk phase
s	Surface

REFERENCES

(1) Wuhrmann K.; Woker H., Proc. of The International Association of Theoretical and Applied Liminology, 12, 795 (1955).

(2) Doudoraff P., Sewage and Industrial Wastes, 28, Aug. (1956).

(3) McKee J.E.; Wolf W.A., Water Quality Criteria, the Resources Agency of California, State Water Quality Control Board Publication No. 3-A (1963).

(4) Deichmann W.B., "Toxicology of Drugs and Chemicals" N.Y., Academic Press, 4th Ed., 722 (1969).

(5) Rowley W.J., "The Toxicity of Cyanide to Aquatic Organisms, A Literature Review", Environment Canada, Private Communication (1975).

(6) Sitting M., 'Pollutant Removal Handbook' Noyes Data Corporation, N.J., 155 (1973).

(7) Zievers J.F.; Crain R.W.; Barclay F.G., Plating, 55, 1171-79 (1968).

(8) Yatsimirskii K.B.; Vasil'ev V.P., 'Instability Constants of Complex Compounds', Consultants Bureau Enterprises, Inc., 139 (1959).

(9) Ford-Smith M.H., "The Chemistry of Complex Cyanides", A literature Survey, London, Her Majesty's Stationary Office, p. 15 (1964).

(10) Scott, L.F., U.S. Patent 3592586, July 13 (1971).

(11) Sloan, W.J., U.S. Patent 3656893, April 18 (1972).

(12) Lauria A.C.; Owens J.L., U.S. Patent 3697421, October 10 (1972).

(13) Ericson H.A.H.; Norstedt G.B., U.S. Patent 3645867, February (1972).

(14) "New Process Detoxifies Cyanide Waste", Envir. Sci. Tech. 5, 496-497 (1971).

(15) Hager D.G.; Rizzo J.L., U.S. Patent 3650949, March 21 (1972).

(16) Palla L.T.; Spicher R.G., Proc. 26th Purdue Industrial Waste Conf. (1971).

(17) Zievers J.F.; Riley C.W.; Crain R.W., U.S. Patent 3531405 Sept. 29 (1970).

(18) Besselievre E.B., 'The Treatment of Industrial Wastes', McGraw-Hill Book Co., N.Y. (1969).

(19) 'Ozone Counters Waste Cyanide's Lethal Punch', Chem. Engr. 63-64 (March 24, 1958).

(20) Mauk C.E.; Prengle H.W. Jr.; Legan R.W., Soc. of Min. Eng. AIME Transaction 260, 297 (1976).

(21) Eiring L.V., The Sov. J. of Nonferrous Metals, 81 (1969).

(22) Prengle H.W.; Mauk C.E.; Legan R.W.; Hewes III, C.G., Hydrocarbon Processing 82-87 (1975).

(23) Mauk C.E.; Prengle H.W.; Legan R.W., Soc. of Min. Eng. of AIME, Reprint no. 75-B-310, SME Fall meeting, Salt Lake City, Utah (1975).

(24) Garrison R.L.; Mauk C.E.; Prengle H.W. Jr., Proceedings of First International Symposium on Ozone for Water and Wastewater Treatment, International Ozone Institute, 551-576 (1973).

(25) Cotton F.A.; Wilkinson G., "Advanced Inorganic Chemistry", Interscience N.Y., 2nd Ed., p. 165 (1966).

(26) PCI Ozone Corp., 'Ozone Science and Technology', Communication (1975).

(27) Stephenson L.M.; McClure D.E., J.A.C.S. 95(9), 3074-3076 (1973).

(28) DeMore W.B.; O. Raper, J. of Chemistry 68(2), 412 (1962).

(29) Fieser L.F.; Fieser M., "Advanced Organic Chemistry" N.Y., Reinhold Publishing Corporation, p. 195 (1961).

(30) Murphy J.S.; Orr J.R., 'Ozone Chemistry and Technology, A Review of Literature 1961-1974', The Franklin Institute Press, Philadelphia, 190 (1975).

(31) Shambaugh R.L.; Melnyk P.B., "The Influence of Spontaneous Decomoposition and Mass Transfer upon Soluble Ozone Concentration", Pre-Publication Copy in Proceedings of The International Ozone Institute's Forum on Ozone Disinfection, Chicago, June (1976).

(32) Czapski G.; Samuni A.; Yelin R., Israel J. Chem. 6(6) 969 (1968).

(33) Heidt L.M.; Landi V.R., Chem. and Eng. News Jul 27, 38 (1964).

(34) Alder G.A.; Hill G.R., JACS 72, 1884 (1950).

(35) Netzer A.; Miyamoto H.K., 'Selected Bibliography on Ozone Disinfection; Research Report No. 27, Project No. 74-3-17, Environment Canada 1976'.

(36) International Ozone Institute, Inc., 'OZONEWS', Communication (1976).

(37) Weast R.C., "Handbook of Chemistry and Physics", CRC Press, D130 (1973).

(38) Devonshire R.; Weiss J.J., J. Phys. Chem. 72(11) 3815 (1968).

(39) Ohno S., Kagaku No Ryoiki 27(7), 562 (1973).

(40) Noggi L.; Bolletta F.; Balzani V.; Scandola F., J. Inorg. Nucl. Chem. 28, 2589 (1966).

(41) Perry R.H.; Chilton C.H., "Chemical Engineering Handbook", McGraw-Hill Book Co., 5th Ed., 3-98 (1973).

(42) Matrozov V.I.; Kashtanov S.A.; Stepanov A.M.; Tregubov B.A., Russ. J. Appl. Chem. 48, 1902 (1975).

(43) Matrozov V.I.; Kashtanov S.A.; Stepanov A.M.; Tregubov B.A., Russ. J. Appl. Chem. 49, 1111 (1976).

(44) Sondak N.E.; Dodge B., Plating 48(2) 777 (1961).

(45) ibid. 48(3) 280 (1961).

(46) Khandelwal K.K.; Barduhn A.J.; Grove Jr. C.S., 'Ozone Chemistry and Technology, Advances in Chemistry Series' 21, 78 (1959).

(47) Balyanskii G.V.; Selin M.E.; Kolychev V.B., Russ. J. Appl. Chem. 2261 (1972).

(48) Kandzas P.F.; Mokina A.A., Tr., Vses. Nauch. - Issled. Inst. Vodosnabzh. Kanaliz. Gidrotekh. Sooruzhenil. Inzh. Gidrogesl. 20, 40-45 (1967).

(49) Matsuda Y.; Fujisawa T.; Fujikawa S.; Takasu Y.; Tanaka Y.; Imagawa H., Nippon Kagaku Kaishi 4, 602 (1975).

(50) Heist J.A., Water AIChE Symposium Series 70, 456 (1973).

(51) Astarita G., 'Mass Transfer with Chemical Reaction' Elsevier Publishing Company (1967).

(52) Danckwerts, P.V., 'Gas-Liquid Reactions' McGraw-Hill Book Company (1970).

(53) Sherwood T.K.; Pigford R.L.; Wilke C.R., 'Mass Transfer' McGraw-Hill Inc., Chapter 8, 301 (1975).

(54) IBM Corporation, System/360 Scientific Subroutine Package (360A-CM-03X) Version III, Programmer's Manual, p. 217 (1969).

(55) Kristiansen G.K., "Zero of Arbitrary Function", BIT 3, 205 (1963).

(56) Brian P.L.T.; Beaverstock M.C., Chem. Engng. Sci. 20, 47 (1965).

(57) Sada E.; Kumazawa H.; Butt M.A., AIChE Journal 22(1), 196 (1976).

(58) Sada E.; Kumazawa H.; Butt M.A., Can. J. of Chem. Engng. 54, 421 (1976).

(59) Smith J.M., 'Chemical Engineering Kinetics', 2nd Ed., McGraw-Hill, 247 (1970).

(60) Levenspiel O., 'Chemical Reaction Engineering', 2nd Ed., John Wiley & Sons Inc., N.Y., 255 (1972).

(61) Sada E.; Kumazawa H.; Butt M.A.; Hayashi D., Chem. Eng. Sci. 31, 839-841 (1976).

(62) Danckwerts P.V.; Gillham A.J., Trans. Instr. Chem. Engrs. 44, T42 (1966).

(63) Reference (37), F45.

(64) Reference (41) 3-222.

(65) Reference (36), F68.

(66) Reference (41), 3-222.

(67) Blaedel W.J.; Meloche V.W., 'Elementary Quantitative Analysis, Theory and Practice', 2nd Ed., 795 (1963).

(68) Harris W.E.; Kratochvil B., 'Chemical Analysis', Barnes and Noble Inc., N.Y., 55 (1970).

(69) Reference (67), p. 358.

(70) Rowley J., Private communication.

(71) Treybal R.E., 'Mass Transfer Operation', 2nd Ed., McGraw-Hill, Chemical Engineering Series, 30 (1967).

(72) Shambaugh R.L.; Melnyk P.B., "Removal of Heavy Metals via Ozonation" Pre-Publication Copy in Proceedings of the International Ozone Institute's Forum on Ozone Disinfection, Chicago, June (1976).

(73) Calvert J.C.; Pitts J.N. Jr., 'Photochemistry', John Wiley and Sons Inc., 783 (1966).

(74) Parker C.A.; Hatchard C.G., Analyst 87, 664 (1962).

(75) Reference (73), p. 720.

(76) Reference (67), p. 120.

(77) Taras M.J.; Greenberg A.E.; Hoak R.D.; Rand M.C., 'Standard Methods for the Examination of Water and Wastewater', 13th Ed., American Public Health Association, American Water Works Association, 397 (1971).

(78) Kruse J.M.; Mellon M.G., Anal. Chemist 25(3) 446 (1953).

(79) Orion Research Inc., Cambridge, Mass. Bulletin 94-06.

(80) Drew, H.D., Anal Chem. 45(14) 2423 (1973).

(81) Shukla S.K., Chromatographia, 6(2) 84 (1973); 5(12) 310 (1973).

(82) Evans D.F., J. Chem. Soc. Dalton Trans. 23, 2587 (1973).

(83) Gould P.D.; Afghan B.K.; Brooksbank P., Anal. Chem. 44(11), 1845 (1972).

(84) Kruse J.M.; Thibault L.E., Anal. Chem. 45(13) 2260 (1973).

(85) Rowley J., M. Sc. Thesis, Department of Chemical Engineering, the University of Alberta (1978).

(86) Ozonews, International Ozone Institute, Inc., Communiation, Vol. 4, No. 8, September (1977).

(87) Candlin J.P.; Taylor K.A.; Thompson D.T., "Reactions of Transition - Metal Complexes" Elsevier Publishing Co. 52 (1968).

(88) Earnshaw A.; Harrington T.J., "The Chemistry of the Transition Elements", Clarendon Press, Oxford 70 (1973).

Appendix 1. Mueller's Method

This method[54,55] has been listed in IBM SSP scientific package bearing the names of RTMI and DRTMI (double precision). The whole subroutine is used in the computer program as MULR for free cyanide and ferricyanide with minor modifications and a change in the dummy arguments. RTMI or MULR are essentially the subroutines used to determine the root of the nonlinear equation $f(x) = 0$ in the range of x from x_{Li} up to x_{Ri} (by input) by means of Mueller's iteration scheme of successive bisection and inverse parabolic interpolation. The procedure assumes $f(x_{Li}) \cdot f(x_{Ri}) \leq 0$. Starting with $x_L = x_{Li}$ and $x_R = x_{Ri}$, the middle of the interval x_L, x_R is computed as shown in the following diagram.

$$x_m = \frac{1}{2}(x_L + x_R) \qquad (A1)$$

In case $f(x_m) \cdot f(x_R) < 0$, x_L and x_R are interchanged to ensure that $f(x_m) \cdot f(x_R) > 0$.

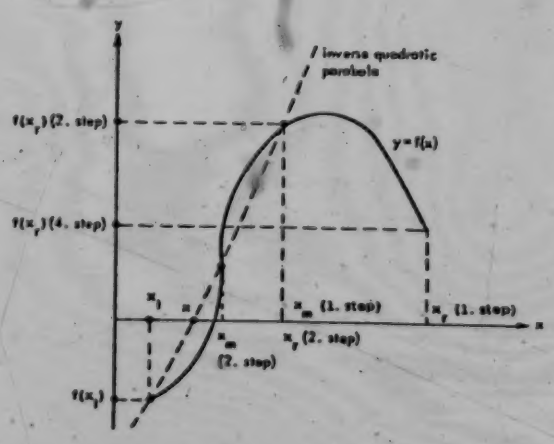

Mueller's iterative method

In case of rapid convergence, i.e. the root is neither too close to x_L nor x_R as described by the equation

$$2f(x_m)[f(x_m) - f(x_L)] - f(x_R)[f(x_R) - f(x_L)] \geq 0. \quad \text{(A2)}$$

x_R is replaced by x_m and the bisection step is repeated. If, after a specified number of successive bisections, the above inequality still persists, the error message is sent out. In case of slow convergence, i.e. the root is near to either x_L or x_R so that the above inequality is not satisfied, then the new point is generated by an inverse parabolic interpolation

$$\Delta x = f(x_L) \frac{x_m - x_L}{f(x_m) - f(x_L)} \left\{1 + f(x_m) \frac{f(x_R) - 2f(x_m) + f(x_L)}{[f(x_R) - f(x_m)][f(x_R) - f(x_L)]}\right\} \quad \text{(A3)}$$

and $x = x_L - \Delta x$. x is sure to be situated between x_L and x_m.

In the next iteration step, x becomes x_L and x_m becomes x_R if $f(x) \cdot f(x_L) > 0$ or x becomes x_R if $f(x) \cdot f(x_L) < 0$. The convergence is either linear or quadratic if the multiplicity of the root to be determined is equal to 1 or greater than 1 respectively, and if $f(x)$ can be differentiated continuously at least twice in the range x_{Li} and x_{Ri}. Each iteration step requires two evaluations of $f(x)$. This iterative procedure is terminated if either the two conditions below are satisfied:

i) $|x_R - x_L| \leq \varepsilon \cdot \max(1, |x_R|)$ and $|f(x_R) - f(x_L)| \leq 100 \cdot \varepsilon$ } check in bisection loop (A4)

ii) $|\Delta x| \leq \varepsilon \cdot \max(1, |x|)$ and $|f(x)| \leq 100 \cdot \varepsilon$ } check after inverse parabolic interpolation (A5)

Modified Mueller method

The modified Mueller method is an extension of Mueller method which is used to solve two nonlinear equations with 2 unknowns. Considering the following equations

$$y = f_1(x) \tag{A6}$$

$$y = f_2(x) \tag{A7}$$

with the solution of (x_s, y_s), then a function f(x) is defined as

$$f(x) = f_1(x) - f_2(x) \tag{A8}$$

if $x = x_s$, $f(x_s) = 0$

so Mueller method can be used to obtain x_s by solving the single equation f(x).

Appendix 2. Detailed Operating Procedure

General Operating Procedure

The procedure outlined here is general for all experiments pertained to the text with only minor variations for individual experiment.

1) Wet Test Meter Calibration: The wet test meter was calibrated by a device of known volume. Sufficient water was added into or drawn out from the meter until a cubic foot of displacement volume corresponded exactly to one revolution on the meter. A black adhesive tape was placed on the meter chamber to indicate the correct water level as it might fall gradually as a result of evaporation.

2) Leakage Checking: Distilled water was pumped through the reactor with stirrer on, bearing cooling water on and air regulator valve opened. The reactor was tested against leakage by pressurizing to 1.5 atm with air, and then the pump, and valves T3, T2 and T4 were shut down, with T1 turned to the position 'VENT'. The pressure should hold for an infinite period of time if the reactor was perfectly sealed. If so, the needle valve would be adjusted as the next step, otherwise the bolts holding the reactor had to be tightened until the leaking was stopped.

3) Needle Valve Adjustment: 350 ml and 125 ml of distilled water were added to the first and second bubblers (B1 and B2) respectively; the water level was also marked by the black tape. Both B1 and B2 should be appropriately

greased to avoid leakage before putting into place. The pumps were started again, T3 switched to the bubblers 'BUBB', T4 to 'EXIT' and the reactor pressure during sampling was recorded from M2. T3 was then turned back to the normal outlet position 'NEED', and the needle valve connected to T3 was properly adjusted to give a pressure reading in M2 the same as the value recorded previously. The reactor pressure would then stay unchanged in sampling, such that the steady state would not be upset.

4) Ozonator Settings: T1 and T2 were switched back to the normal position 'REAC' with ozonator on. The typical settings were:

Air Regulator Pressure		17.1 psi
Ozonator:	pressure dial	6 psig
	SCFH dial	7
	% ozone	100% or 75%

Under normal conditions the reading in the first manometer M1 would be around 27 cmHg. A reading far less than that indicated leakage.

5) Liquid Level Adjustment: The liquid level was brought to the mark on the reactor by controlling T4. T4 was closed had the level been low and turned to 'SAMP' position if it was too high. The inlet pump was delicately adjusted until the inlet and exit streams were exactly balanced; then the liquid level should remain unchanged for an appreciable length of time.

6) UV Intensity: The reactor could be operated at one of the four UV intensities listed below in an increasing order:

i) No UV: UV switch OFF

ii) Coarse filter:

iii) Fine filter:

iv) Full UV: UV switch ON without filter

The reactor was allowed to run for 45 minutes to reach the steady state, then the reactor pressure P_R and temperature T were measured.

7) Outlet Gas Sampling: The bubblers were filled with distilled water to the marks, 16 g and 6 g of KI were weighed into B1 and B2 respectively, which were then tightened into place. As soon as D1 was opened and the outlet gas sampling valve T3 was turned to 'BUBB' position in which the outlet ozone was sampled, the stop watch had to be started and the cap in B1 pressed down firmly by hand, otherwise the reactor pressure was just high enough to pop it up. After 1.5 minutes (±0.1 cubic foot) of sampling time, the watch was stopped, and T3 turned back to the normal 'REAC' position simultaneously. D1 was then closed and the volume of the gas sample collected was directly obtained from the wet test meter by taking the difference of the initial and final dial readings. Finally, the ozone trapped inside the bubblers was completely flushed out with air by opening D2.

8) Exit Stream Liquid Sampling: The liquid sampling had to be done in sequence right after the gas sampling because a fast drawing out of liquid would affect the liquid level and thus upset the steady state. In the sampling process, T4 was turned to 'SAMP' and a sufficient volume of liquid was collected in a flask depending on the concentration to be analyzed. The flask was weighed before and after the sampling step so that the amount of sample collected was known. The sample was then analyzed according to the procedure listed in individual experiments.

9) Inlet Gas Sampling: The procedure was essentially the same as that of 7) Outlet Gas Sampling except that the outlet gas sampling valve T2 was turned to the 'BUBB' position while T3 was still connected to the reactor 'REAC'. The inlet gas sampling had to be done after the liquid sampling.

10) Restart: The reactor was washed several times by fresh feeding solution with stirrer on. The same procedure was repeated from 4) on after changing the variables to be studied, for instance, stirring rate, inlet concentration, inlet partial pressure, pH and so on.

11) Shut-down: After the ozonator was switched off, air should still pass through the ozonator for another 10 minutes to flush out all the residual ozone which might cause extensive damage to the ozonator. The reactor should also be washed several times by distilled water. The solution containing electrolytes might stain the quartz plate at the bottom of the reactor which could hardly be rinsed off;

then the reactor had to be soaked with oxalic acid solution until all the stains were gone.

Gas Phase Data Treatment

The following terms are defined

F_G the total volumetric gas flow rate at T and P atm, L/min.

F_W the volumetric gas flow rate registered by the wet test meter after ozone stripping, L/min.

F_R the volumetric gas flow rate from the reactor gas outlet, i.e. at T and Pr, L/min.

$\dot{n}$ total gas molar flow rate, m mole/min.

$\dot{n}_{Af}$ the outlet molar flow rate of ozone, m mole/min.

$\dot{n}_{Ai}$ the inlet molar flow rate of ozone, m mole/min.

P_A the partial pressure of ozone in the reactor, atm.

P_R the total reactor pressure, atm.

P_{atm} the atmospheric pressure, atm.

t the gas sampling time, min.

V_b the blank for thiosulfate titration, ml.

V_1, V_2 the volume of thiosulfate solution required to titrate ozone in the outlet/inlet samples, ml.

x the mole fraction of ozone in the exit stream before stripping.

ρ the density of water at T, g/cc.

Flow Rate Registered by Wet Test Meter, F_W

$$F_W = \frac{\text{volume of gas registered in wet test meter, ft}^3 \times 28.316 \text{ L/ft}^3}{t, \text{min}} \quad \text{(A9)}$$

Inlet/Outlet Ozone Molar Flow Rate $\dot{n}_{Ai}$, $\dot{n}_{Af}$

$$\dot{n}_{Af} = \frac{(V_1 - 2V_b) \times [Na_2S_2O_3]}{2 \times t} \quad \text{(A10)}$$

$$\dot{n}_{Ai} = \frac{(V_2 - 2V_b) \times [Na_2S_2O_3]}{2 \times t} \quad \text{(A11)}$$

Since V_b is equal to 0.05 ml,

$$\dot{n}_{Af} = \frac{(V_1 - 0.1) \times [Na_2S_2O_3]}{2 \times t} \quad \text{(A12)}$$

$$\dot{n}_{Ai} = \frac{(V_2 - 0.1) \times [Na_2S_2O_2]}{2 \times t} \quad \text{(A13)}$$

Since two bubblers were used to sample ozone, the blank would be $2V_b$.

Partial Pressure of Ozone, P_A

The ideal gas law is assumed. In the wet test meter,

$$F_G = F_W(1 + x) = F_W + \frac{\dot{n}_A RT}{P_{atm}} \quad \text{(A14)}$$

$$P_{atm} F_G = \dot{n} RT \quad \text{(A15)}$$

In the reactor:

$$P_A F_R = \dot{n}_A RT \quad \text{(A16)}$$

$$P_R F_R = \dot{n} RT \quad \text{(A17)}$$

$$\dot{n} = \dot{n}_A + \dot{n}_{H_2O} + \dot{n}_{inert} \quad . \tag{A18}$$

Solving the above equations simultaneously, P_A can be expressed by the measurable quantities on the right side of the equation

$$P_A = \frac{P_R}{P_{atm}} \left[F_W + \frac{\dot{n}_A RT}{P_{atm}}\right]^{-1} RT\, \dot{n}_A \quad . \tag{A19}$$

Appendix 3. Mixing Pattern

Procedure

The following instruments were used:

Fisher Accumet, Model 520, Digital pH/ion meter

Fisher Scientific Co., Micro probe combination electrode

13-639-92

Sargent recorder.

A 10^{-3}M (pH 3) HCl solution was prepared and stored in a 20 liter plastic bottle. The end of the exit tubing was clamped in an upright position, so that air bubbles would not be trapped inside. The glass electrode was first standardized against a buffer solution of pH 4.00 (Coleman Certified Buffer) and then slipped into the exit tubing through the end opening until the tip of the probe was completely immersed into the effluent. A vessel was placed underneath the exit opening to receive the effluent. The reactor was cleaned thoroughly by pumping through distilled water with the stirrer and the cooling water on. The rpm was measured by counting the number of turns per unit time . The flow rate was set to around 70 ml/min by adjusting the displacement pumps. The inlet pump was then adjusted carefully to maintain the liquid surface sharply at the marked level which was slightly below the middle stirring blades.

An accurate measurement of flow rate was made by a graduate cylinder and a stop watch. The pumps were stopped and the inlet end of the tubing was dipped into the 20 liter

bottle containing 10^{-3} M HCl solution. As soon as the pumps were started again, the pH meter, the recorder and the stop watch were turned on. The pH values were read from the pH meter at the time intervals shown below:

Interval for taking reading	time
30 sec	0-2.2 min
10 sec	2.2-4 min
15 sec	4-6 min
20 sec	6-8 min
30 sec	8-11 min
1 min	11 min and on

The experiment was terminated at 30 minutes, and the pH of the 10^{-3} M HCl solution was taken down. The same procedure was repeated at the stirring rates of 0, 59.5, 85, 102 rpm.

The volume of the reactor was obtained from the weight of distilled water required to fill an acetone dried reactor to the marked level correcting for the total dead volume $V_{Di} + V_{Do}$. The inlet dead volume was determined by taking off the inlet line at the reactor, displacing the water trapped in the inlet system by pumping air and weighing the water pumped out. The outlet dead volume V_{Do} was determined in a similar fashion.

Data Treatment

Residence time can be defined mathematically as

$$\bar{t}_R = \int_0^\infty t_R dF(t_R) = \int_0^\infty t_R F(t_R) dt_R \qquad \text{(A20)}$$

where $F(t_R)$ is the residence time distribution function. Physically, it can be viewed as the fraction of the effluent stream that has a residence time less than t_R; and $dF(t_R)$ or $F'(t_R)dt_R$ is the volume fraction of the effluent stream that has a residence time between t_R and $t_R + dt_R$.

In the case of a CSTR, the following equation can be established:

$$V \frac{dC}{dt} = F_L(C_f - C) \quad . \tag{A21}$$

Initial condition

$$0 \leq t \leq t_L \qquad C = C_o$$

where

$$t_L = \frac{V_{Di} + V_{Do}}{F_L} \tag{A22}$$

C the outlet acid concentration

C_f the inlet acid concentration (step size)

C_o the background acid concentration in distilled water

F_L the liquid volumetric flow rate

V the reactor volume

t_L the time delay due to the finite volume of the tubing

V_{Di} the inlet dead volume

V_{Do} the outlet dead volume

$$\bar{t}_R = \frac{V}{F_L} \tag{A23}$$

The solution of the differential equation with the given initial condition is:

$$\frac{C - C_o}{C_f - C_o} = F(t_R) = 1 - \exp-(\frac{t - t_L}{\bar{t}_R}) \qquad (A24)$$

and

$$\ln \frac{C_f - C}{C_f - C_o} = - \frac{t - t_L}{\bar{t}_R} \quad .$$

In the experiment, the outlet pH was monitored at certain time intervals. A typical pH vs t curve at the stirring speed of 85 rpm is shown in Figure A1. If the reactor is an ideal CSTR, the response should obey Equation (A24) and the $\ln(\frac{C_f - C}{C_f - C_o})$ vs t plot (Figures A2, A3, A4, A5) should be a straight line with slope equal to $-1/\bar{t}_R$, or $-F_L/V$ and a value of zero at $t \leq t_L$.

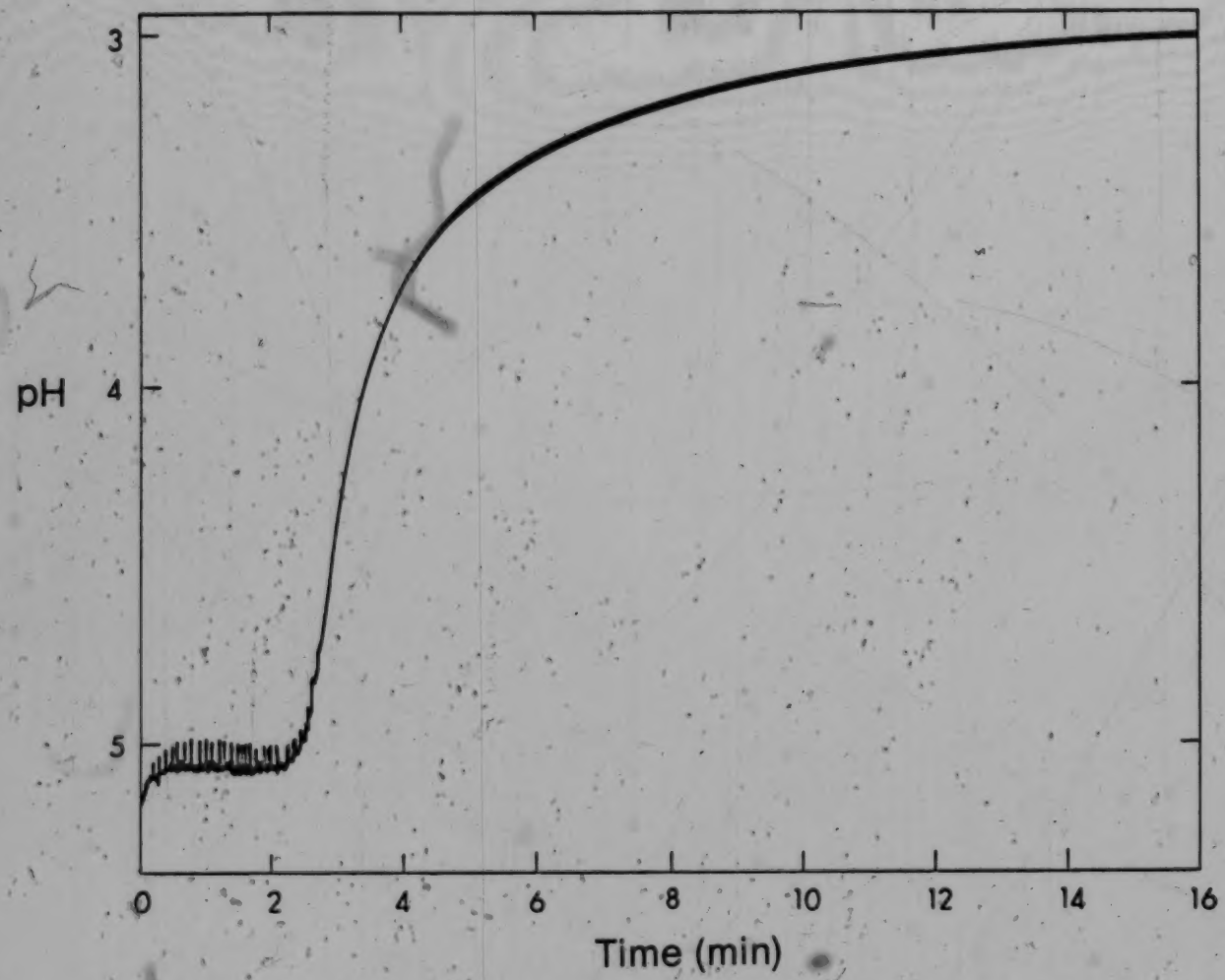

Figure A1. Typical recorder output; pH vs time at 85 rpm

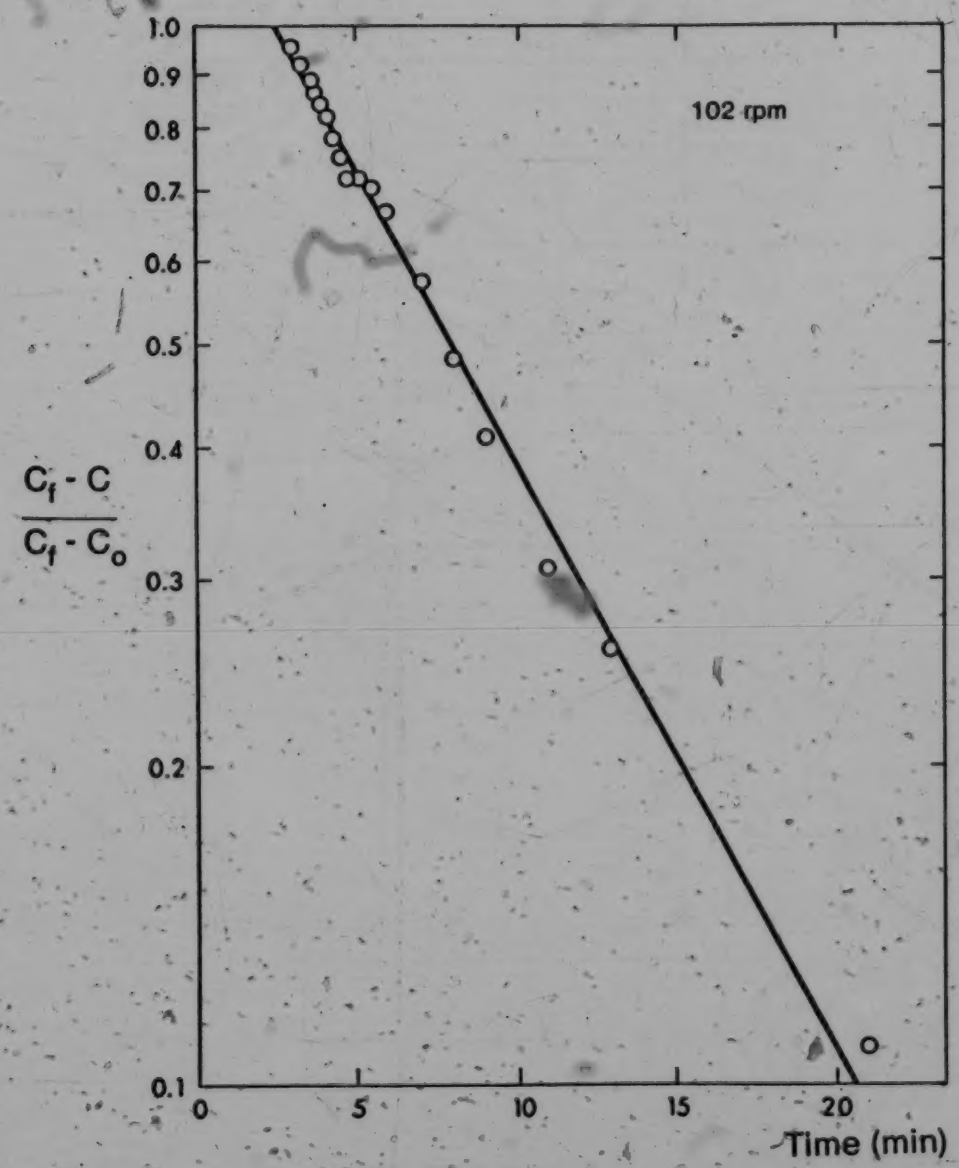

Figure A2. Plot of $\log(C_f - C)/(C_f - C_o)$ vs time at the stirring rate of 102 rpm.

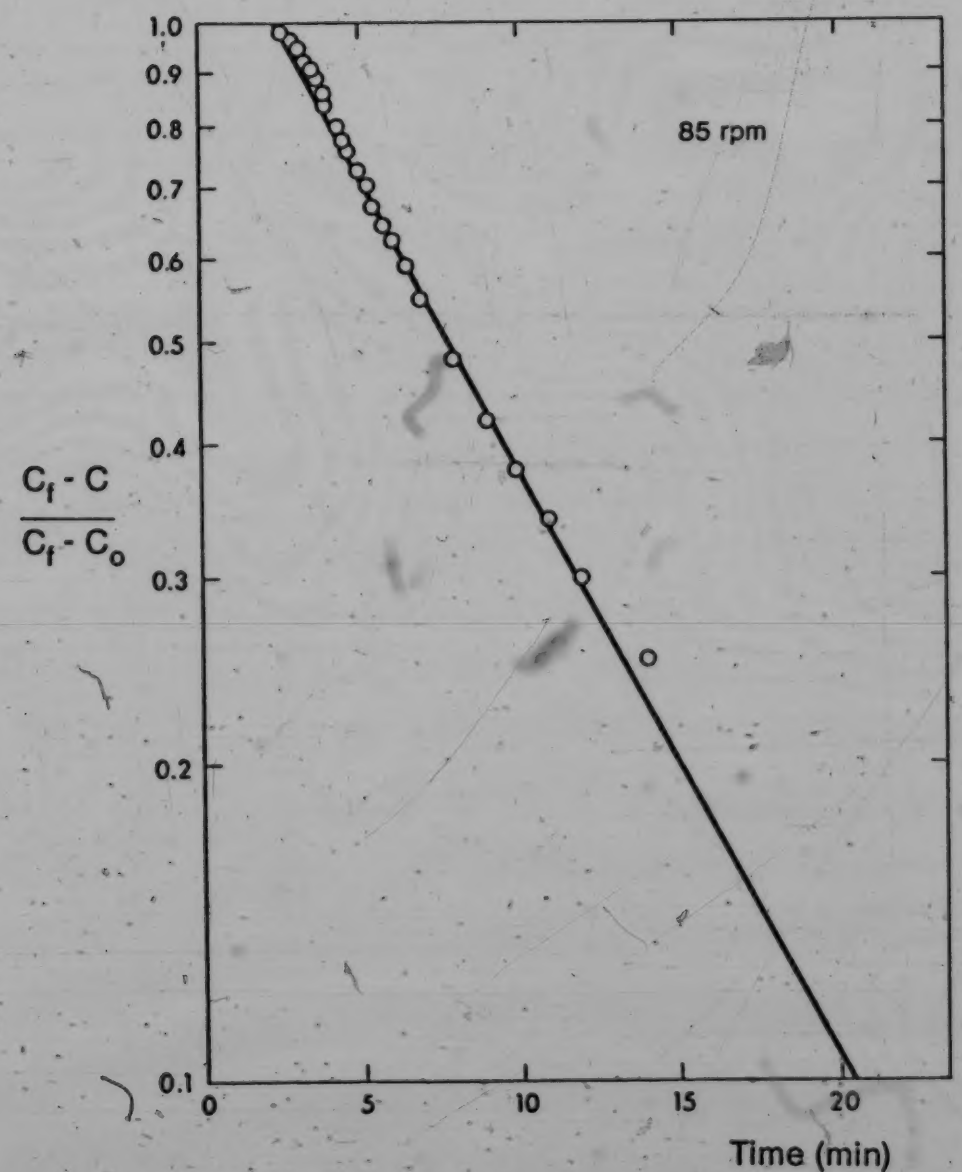

Figure A3. Plot of $\log(C_f - C)/(C_f - C_o)$ vs time at the stirring rate of 85 rpm.

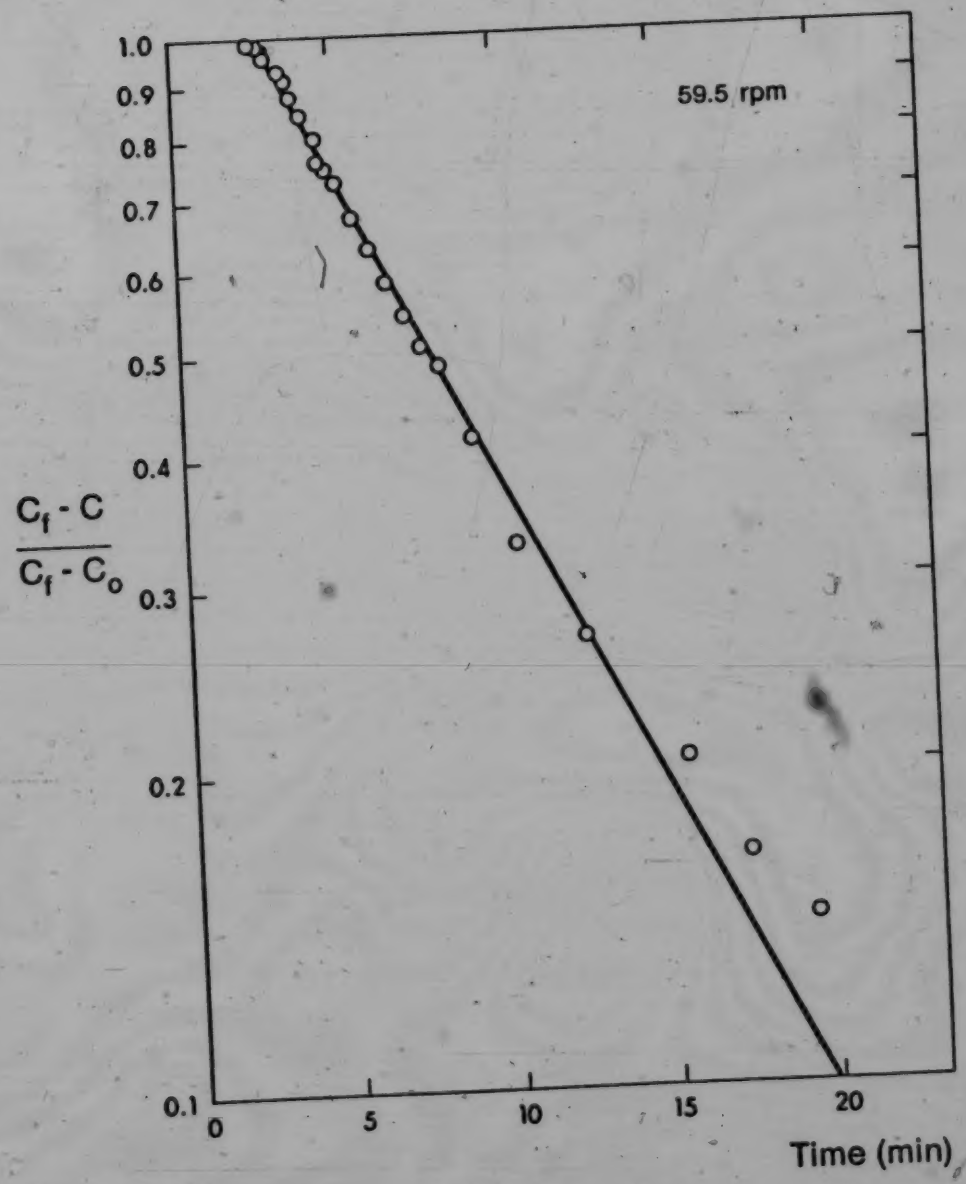

Figure A4. Plot of $\log(C_f-C)/(C_f-C_o)$ vs time at the stirring rate of 59.5 rpm.

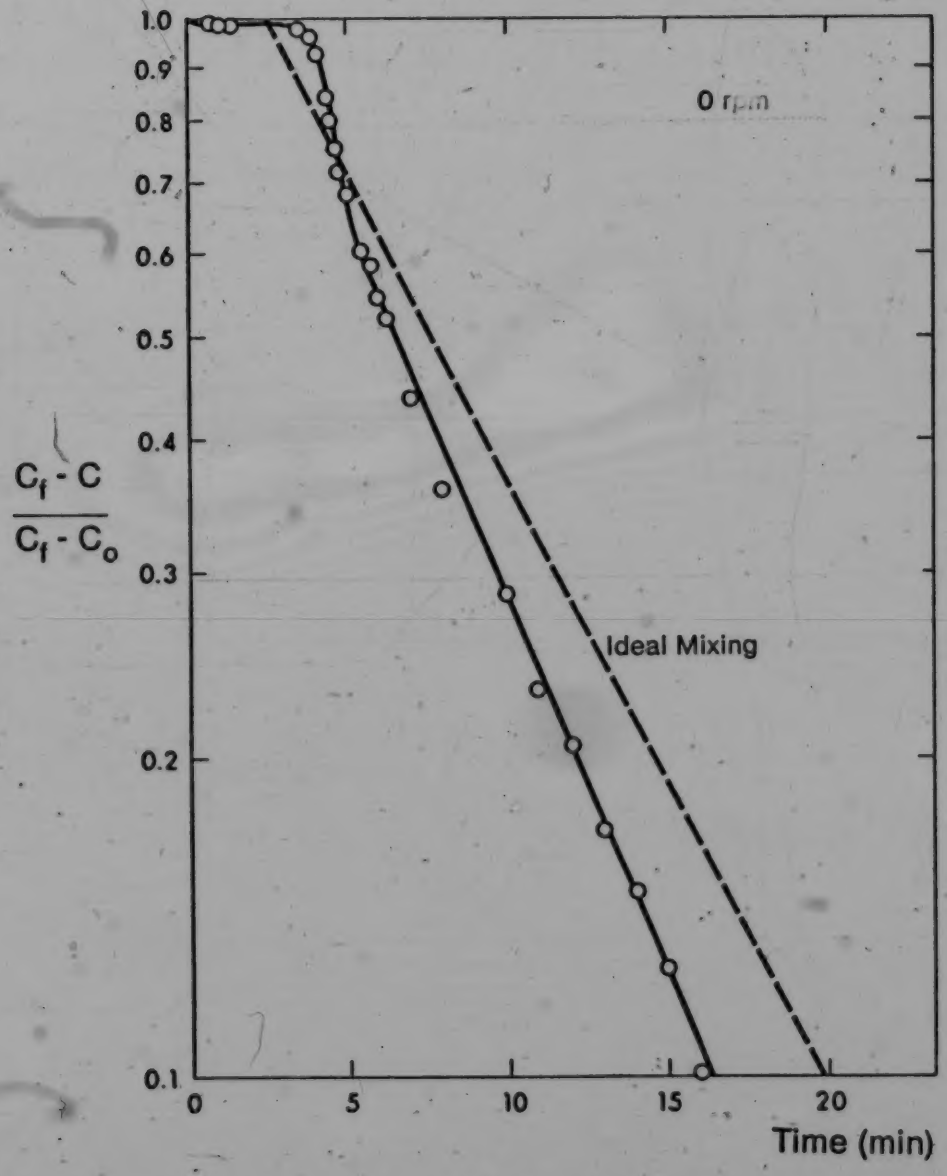

Figure A5. Plot of $\log(C_f-C)/(C_f-C_o)$ vs time at the stirring rate of 0 rpm.

Appendix 4. Detailed Physical Mass Transfer Measurement

Theory

Direct Measurement - O_3/H_2O System

Assuming a zero gas resistance, the material balance on A leads to

$$SK_0 = (C_{As} - C_A) = F_L C_A$$

$$\therefore \quad K_0 = \frac{F_L C_A}{S(\frac{P_A}{H_A} - C_A)} = K_{0L} \tag{A25}$$

Indirect Measurement - CO_2/H_2O System

According to the penetration model, $K_0(CO_2)$ can be related to $K_0(O_3)$ by Equation (A26)

$$\frac{K_0(CO_2)}{K_0(O_3)} = 2\sqrt{\frac{D_{CO_2}}{\pi\theta_{CO_2}}} \Bigg/ 2\sqrt{\frac{D_A}{\pi\theta_A}} \tag{A26}$$

where the subscript A stands for O_3. If the contact time depends only on the hydrodynamic conditions of the reactor and not the nature of the species, then θ_A should be equal to θ_{CO_2} and the above equation can be reduced to

$$\frac{K_0(CO_2)}{K_0(O_3)} = \sqrt{\frac{D_{CO_2}}{D_A}} \quad . \tag{A27}$$

The value of D can be predicted by Wilke and Chang correlation[71]

$$\frac{Dj(T_2)\mu(T_2)}{T_2} = 7.4 \times 10^{-8} \frac{(XM)^{0.5}}{V_{bj}^{0.6}} \quad . \tag{A28}$$

The effect of temperature on diffusivity is expressed as

$$\frac{Dj(T_2)\mu(T_2)}{T_2} = \frac{Dj(T_1)\mu(T_1)}{T_1} = \text{constant} .$$

The temperature effect on viscosity is given by Swindell's correlation[63]

$$\log \frac{\mu(T)}{\mu(20°C)} = \frac{1.3772(20-T) - 0.001053(T-20)^2}{T + 105} \qquad (A29)$$

$$20 \sim 100°C$$

where T is in degrees centigrade.

From the above equations, $K_0(O_3)$ at T_2 can be related to $K_0(CO_2)$ at T_1 by

$$\frac{K_0(O_3,T_2)}{K_0(CO_2,T_1)} = \left[\left(\frac{\mu(T_1)}{T_1}\right) \left(\frac{T_2}{\mu(T_2)}\right) \left(\frac{V_{b,CO_2}}{V_{bA}}\right)^{0.6} \right]^{\frac{1}{2}} \qquad (A30)$$

As O_3 is concerned, Equation (30) is reduced to

$$\frac{K_0(O_3,T_2)}{K_0(O_3,T_1)} = \left[\left(\frac{\mu(T_1)}{T_1}\right) \left(\frac{T_2}{\mu(T_2)}\right) \right]^{\frac{1}{2}} \qquad (A31)$$

Data from the Literature

V_b

CO_2 : V_{bCO_2} = 34 ml/mole[64]

O_3 : Boiling point of O_3 -112°C[65]

The density of O_3 liquid at normal boiling point 1.358 g/cc

Molecular weight of O_3 48

$\therefore \quad V_{ba} = 48/1.358 = 35.4$ ml/mole.

D

The values of D can be obtained from Wilke and Chang correlation or from experimental work. The values from various sources are tabulated.

Compounds	T°C	D, $10^{-5} \times cm^2/sec$ Wilke and Chang	D, $10^{-5} \times cm^2/sec$ experiment
CO_2	25	1.96	
	20	1.76	1.76 (66)
	18	1.71	1.71
O_3	25	1.984	1.47
	20	1.805	1.26 (43)

Wilke and Chang correlation works very well for CO_2, however it is higher than the experimental value by 30% when it is applied to O_3. Since O_3 and CO_2 are of comparable size and polarity, such a large discrepancy is unexpected. In Matrozov's work[43], the pH of the solution was not mentioned, and the author claimed that there would be no ozone decomposition due to short contact time. Such a conclusion is obviously premature. There is no doubt that brevity of contact means an enhanced K_0, and thus an increased t_R/t_D ratio; however, several important aspects have been overlooked. First of all, the slow reaction assumption owing to brief contact time is not justified unless the criterion $t_D << t_R$ is satisfied, and the knowledge of pH or the ozone decomposition rate K_d

is required to calculate t_R. Secondly even the surface reaction is minimized, yet the bulk reaction still goes on as the ozonated water travels from the absorption chamber to the ozone monitor. The decomposition tends to lower the ozone content in the solution, and thus accounts for the low D_A experimental value. As a matter of fact, the D_A from Wilke and Chang correlation is used to calculate $K_0(O_3)$ by the indirect method (H_2O-CO_2 system).

$\underline{H}$

O_3:

$$H_A(T) = H_A(T_1) + 2870(T - T_1) = 67680 + 2870(T - 20) \quad \text{(A32)}$$

the choice is supported by Shambaugh et al. in their recent work[31,72] in which the solubility of ozone was calculated based on the value of H_A quoted from Perry's Handbook, i.e. 67680 atm/mole/cc. The temperature coefficient of 2870 atm/mole/cc per°C is from Metrozov's work (cf 2.2.1 Solubility of Ozone in Aqueous Media).

CO_2:

The value of $H_{CO_2}(T)$ is obtained from Perry's Handbook by interpolation

$$H_{CO_2}(T) = 1420 + 44(T-20) \quad \text{atm/mole fraction} \quad \text{(A33)}$$

Procedure for Direct Measurement

The ozone partial pressure and the ozone concentration in the liquid phase were measured (cf. Appendix 2 for detailed operating procedure). The stirring rates of 61, 75, 94, 112, 131 rpm were tried in the absence of UV. In step 8) of Appendix 2 Exit Liquid Sampling, the flask to receive the liquid sample contained 100 ml of 5% KI solution, so that O_3 in the liquid sample was fixed immediately by reduction. The liberated I_2 was analyzed by iodometric method as illustrated in 4.3.1 Ozone Analysis, except that a microburette and a 0.005 N $Na_2S_2O_3$ solution were used to titrate the sample. The blank should consist of 100 ml of 5% KI solution with the addition of the same amount of 1:10 H_2SO_4.

Data Treatment - Direct Measurement

$$C_A = \frac{\text{volume of } 0.005\,\text{N } Na_2S_2O_3 \times [Na_2S_2O_3] \times \text{density}}{2 \times \text{weight of sample collected}}$$

$$K_0 = \frac{F_L C_A}{S\left(\frac{P_A}{H_A} - C_A\right)} \quad \text{(A25) assuming zero gas phase resistance}$$

$$S = 84\ cm^2$$

$$H_A = 67680 + 2870(T-20) \qquad \text{(A32)}$$

$$F_L = 66\ ml/min$$

K_0 can be solved. The assumption of zero gas phase resistance

is valid as indicated by J. Rowley's[85] work that the gas phase mass transfer coefficient is 1.53 cm/sec at 22°C.

Procedure for Indirect Measurement

The experimental procedure was essentially the same as that used for O_3-H_2O except that no gas sampling was required, because the partial pressure of CO_2 was directly given by the total reactor pressure corrected for the saturated water pressure at the reactor temperature. The detailed procedure in Appendix 2 could be followed starting from 6) without UV; 7), 9), 11) were skipped. In step 8), exit liquid sampling, the flask used to collect the liquid sample should contain 20 ml of standard 0.02 N NaOH solution delivered by burette, so that the CO_2 in the sample was fixed immediately by neutralization once it was out of the reactor. The flask was weighed before and after sampling to give the weight of sample collected. Only 20 ml of sample was required, and then the solution was titrated for CO_2. The stirring rates of 112, 102, 92.7, 86, 60.2 rpm and the blade positions of slightly above (normal), touching and 1 mm below the surface were tried.

CO_2 Analytical Procedure[67,68]

The following symbols are used:

$[OH^-]$ Concentration of NaOH solution as standardized by HCl solution with phenolphthalein as indicator, M.

$[HCO_3^-]_b$ Background HCO_3^- concentration in NaOH solution due to CO_2 absorption, M.

V_1, V_2 Volume of HCl required to titrate the sample to the first (phenolphthalein) end point and the second (bromocresol green) end point respectively, ml.

V_a Volume of NaOH added to the sample, ml.

V_b Volume of HCl required to titrate 125 ml distilled water to the phenolphthalein end point, ml.

C_1, C_2 Concentration of CO_2 in the sample as calculated by V_1 and V_2 respectively, M.

C_{avg} Average of C_1 and C_2, M.

ρ Density of water at temperature T, g/cc.

wt Weight of sample collected, g.

$[CO_2]_i$ Background CO_2 concentration in distilled water, M.

It has been known that NaOH absorbs CO_2 in the air[69], so the standard 0.02 N NaOH solution should contain a small amount of HCO_3^- besides OH^-. The addition of NaOH solution to the sample to fix the CO_2 would cause a background HCO_3^- error which has to be corrected for. In order to determine the amount of the background HCO_3^-, an indicator, such as bromocresol green which may change color at higher pH is added after all the OH^- has been neutralized to the phenolphthalein end point, and the solution is further titrated to the bromocresol green end point. The volume of acid used for the latter end point corresponds to the HCO_3^- in the standard NaOH solution.

Phenolphthalein $OH^- + H^+ \rightarrow H_2O$

Bromocresol green $HCO_3^- + H^+ \rightarrow H_2CO_3$

$$[OH^-] = \frac{\text{Volume of HCl used for phenolphthalein end point} \times [HCl]}{\text{Volume of NaOH solution}}$$

$$[HCO_3^-]_b = \frac{\text{Volume of HCl used for bromocresol green end point} \times [HCl]}{\text{Volume of NaOH used}}$$

A back titration method is used for the determination of CO_2 in the sample, because the CO_2 dissolved in water at 1 atm of CO_2 pressure may escape into air once the pressure is removed in the sampling step. NaOH can neutralize CO_2 and thus stabilize it in the solution in an ionic form HCO_3^-. Before titration, the sample solution contains background HCO_3^-, and the HCO_3^- formed by the reaction

$$CO_2 + OH^- \rightarrow HCO_3^-$$

and the excess OH^-. Similarly, the phenolphthalein end point gives the amount of excess OH^- in the solution while the bromocresol green gives the total HCO_3^-.

$$C_1 = \frac{(V_a[OH^-] - V_1[HCl])\rho}{wt}, \quad M \tag{A34}$$

$$C_2 = \frac{(V_2[HCl] - V_a[HCO_3^-]_b)\rho}{wt}, \quad M \tag{A35}$$

$$C_{avg} = \frac{C_1 + C_2}{2} \tag{A36}$$

Finally, the CO_2 background in distilled water is

$$[CO_2]_i = \frac{V_b[OH^-]}{125} \tag{A37}$$

where 125 ml is the volume of distilled water to be titrated.

Data Treatment CO_2-H_2O System

The Partial Pressure of CO_2, P_{CO_2}

Assuming the gas phase in the reactor is saturated with water vapor at the reactor temperature T, then it can be shown that

$$P_{CO_2} = P_R - P_{H_2O} \quad (A38)$$

P_R was found to be higher than P_{atm} by a pressure equivalent to 1.1 inch H_2O [70] so

$$P_R = P_{atm} + 1.1 \text{ inch } H_2O = P_{atm} + 2.703 \times 10^{-3}$$

$$P_{H_2O} = 0.0241 \quad \text{at} \quad 20°C$$

$$\therefore \quad P_{CO_2} = P_{atm} - 0.0241 + 2.703 \times 10^{-3} = P_{atm} - 0.0214 \text{ (atm)}.$$

The Interfacial CO_2 Concentration $[CO_2]_s$

$$X_s^{-1} = \frac{H_{CO_2}}{P_{CO_2}} \quad (A39)$$

where X_s is the interfacial CO_2 concentration expressed in mole fraction, H_{CO_2} is the Henry's law constant for CO_2 at temperature T, atm/mole fraction.

$$H_{CO_2} = 1420 + 44(T-20) \quad \text{atm/mole fraction} \quad (A33)$$

$$[CO_2]_s = \frac{1000\,\rho}{\frac{18}{X_s} + 26} = \frac{1000\,\rho}{\frac{18 \times H_{CO_2}}{P_{CO_2}} + 26} \quad . \quad (A40)$$

The Physical Mass Transfer Coefficient of CO_2, $K_0(CO_2)$

$$K_0(CO_2) = \frac{(C_{avg} - [CO_2]_i) F_L}{([CO_2]_s - C_{avg}) S}$$

$$= \frac{(C_{avg} - [CO_2]_i) F_L}{\frac{1000\rho}{18H_{CO_2}} - C_{avg}\, S} \qquad \text{(A41)}$$

$$\frac{}{P_{CO_2}} + 26$$

The Physical Mass Transfer Coefficient of CO_3, $K_0(O_3)$

$$K_0(O_3) = 0.988\ K_0(CO_2) \qquad \text{from Equation (A30)}$$

$$T_1 = T_2 = 21°C\ .$$

Appendix 5. Detailed UV Characterization Procedure

Through the years photochemists have determined the quantum yield, ϕ, of products of many photochemical systems as well as the intensity of the light beam by using the thermopile galvanometer combination[73]. Complex and tedious procedures are required in the calibration and application of the thermopile-galvanometer system, thus the trend among photochemists in recent years toward the use of chemical actinometers for light intensity determination is understandable. Besides convenience, results obtained with a well chosen, sensitive chemical actinometer are more reproducible and reliable than those obtained with the thermopile method.

The intensity of a light beam passing through the reactor can be measured chemically by a suitable reactant A, which absorbs light of the wavelength of interest and for which the quantum yield, ϕ_B, of some product B is known accurately for specific experimental conditions. Considering the following photochemical reaction:

$$A \xrightarrow{h\nu} B$$

the quantum yield of B, ϕ_B, is defined as the number of moles of B produced upon the absorption of a single photon at a specific wavelength. Then reactant A can be placed in the photochemical reactor to be studied with the exact optical train etc. which is to be used in the photochemical reaction i.e. O_3/ferricyanide/UV reaction. The temperature,

pressure and the concentration of the reactant A are adjusted to the appropriate range, and an exposure of A to the light beam is made for t sec. The following symbols are used for subsequent derivations.

I the intensity of the light transmitted

I_o the intensity of the light beam incident on the reactor

n_B the amount of product B after exposure time t sec

ϕ_B the quantum yield of B

t the exposure time, sec

$[A]$ the concentration of A

ε the molar absorptivity of A

ℓ the light path cm.

According to Beer's law, the fraction of the incident light absorbed by A is

$$1 - \frac{I}{I_o} = 1 - 10^{-\varepsilon[A]\ell} \tag{A42}$$

$$I_o = \frac{n_B}{\phi_B t(1 - 10^{-\varepsilon[A]\ell})} \quad \text{quanta/sec} \quad . \tag{A43}$$

For a reactant A with high molar absorptivity, where practically all the incident light is absorbed, the equation can be reduced to

$$I_o = \frac{n_B}{\phi_B t} \quad \text{quanta/sec} \quad . \tag{A44}$$

Since all terms on the right hand side are known, I_o can be calculated readily.

Potassium Ferrioxalate

By far the best solution-phase chemical actinometer for photochemical reasearch today is the potassium ferrioxalate system developed by Parker and Hatchard[74]. It is very sensitive over a wide range of wavelengths and yet simple to use. When sulfuric acid solutions of $K_3Fe(C_2O_4)_3$ are irradiated in the range from 2500 to 5770 A, simultaneous oxidation of oxalate and reduction of ferric to ferrous state occur. The quantum yields of Fe^{2+} formation and the fraction of light absorption by ferrioxalate have been accurately measured by Parker[74] and are shown in Table A1. In the UV region at wavelengths up to 3660 A, almost 100% of the incident light is absorbed with an average Fe^{2+} quantum yield of 1.24. The ferrous ion thus formed is made to be highly absorbing and easily analyzable by the formation of the red-colored 1,10-phenanthroline - Fe^{2+} complex.

The concentration of Fe^{2+} in the sample is read from the calibration by the net absorbance after correcting for the background i.e. the absorbance of the sample without UV irradiation. The number of Fe^{2+} produced in the reactor can be calculated by

$$n_B = \frac{\text{concentration of } Fe^{2+} \times 100 \times V}{20} \quad M \qquad \text{(A45)}$$

$$V = 0.499 \ \ell \quad .$$

According to Equation (A44), the number of quanta per sec is

Table A1. Quantum Yields of Fe^{2+} in the $K_3Fe(C_2O_4)_3$ Chemical Actinometer at 22°

Wavelength, A	$[K_3Fe(C_2O_4)_3]$, M	Fraction of Light Absorbed (l = 15 mm)	$\Phi_{Fe^{2+}}$
5770	0.15	0.118	0.013
5790			
5460	0.15	0.061	0.15
5090	0.15	0.132	0.86
4800	0.15	0.578	0.94
4680	0.15	0.850	0.93
4360	0.15	0.997	1.01
	0.006	0.615	1.11
4050	0.006	0.962	1.14
3660	0.006	1.00	1.21
	0.15	1.00	1.26
			1.15
3340	0.006	1.00	1.20
3130	0.006	1.00	1.23
2970	0.006	1.00	1.24
3020			
2537	0.006	1.00	1.24
			1.25

Table A2. Energy Distribution in Low- and Medium-Pressure Mercury Arcs

Wavelength, A	Relative Energy	
	Low-Pressure Mercury Arc[a]	Medium-Pressure Mercury Arc[b]
13,673	...	15.3
11,287	...	12.6
10,140	...	40.6
5770–5790	10.14	76.5
5461	0.88	93.0
4358	1.00	77.5
4045–4078	0.39	42.2
3650–3663	0.54	100.0
3341	0.03	9.3
3126–3132	0.60	49.9
3022–3028	0.06	23.9
2967	0.20	16.6
2894	0.04	6.0
2804	0.02	9.3
2753	0.03	2.7
2700	...	4.0
2652–2655	0.05	15.3
2571	...	6.0
2537	100.00	16.6[c]
2482	0.01	8.6
2400	...	7.3
2380	...	8.6
2360	...	6.0
2320	...	8.0
2224	...	14.0

[a] Hanovia Lamp Division, Engelhard Industries, Newark, N.J., SC-2537 lamp.
[b] Hanovia's Type A, 673 A, 550 w lamp.
[c] Reversed radiation.

$$I_o = \frac{n_B \times 6.023 \times 10^{23}}{\bar{\phi}_B t}$$

$\bar{\phi}_B = 1.24$ up to 3660 A .

The energy associated with the quanta flux I_o is

$$E = \frac{I_o \times h \times \bar{\nu} \times 6.023 \times 10^{23}}{10^7} \text{ watt} \qquad \text{(A46)}$$

where h is the Planck constant, and equal to 6.6256×10^{-27} erg sec and $\bar{\nu}$ is the weighed average frequency of the medium pressure mercury lamp. Being a continuous light source, the medium pressure mercury lamp emits a spectrum covering a broad range of wavelengths. The average light frequency can be obtained only if the energy distribution function is known.

$$\bar{\nu} = \frac{\sum_i \nu_i g_i}{\sum_i g_i} \qquad \text{(A47)}$$

where g_i is the relative energy at the frequency ν_i ($g = 100$ at $\lambda_i = 3650 \sim 3663$). Only the wavelengths up to 5461 A needs to be considered; beyond this the quantum field is so low that it can be ignored. The average frequency is found to be 3310 A from the energy distribution function published by Hanovia Company[75], Table A2. The power of the UV light incident on the reactor can then be written as

$$E = \frac{n_B \times 6.6256 \times 10^{-27} \times 6.023 \times 10^{23} \times 3 \times 10^{10}}{t \times 10^{7} \times 3310 \times 10^{-8} \times 1.24} \text{ watt} \quad \text{(A48)}$$

$$= \frac{2.9168 \times 10^{-5} \times n_B}{t} \text{ watt.}$$

Procedure

Synthesis of $K_3Fe(C_2O_4)_3 \cdot 3H_3O$

Reagents Ferric chloride, Fisher Scientific Co.,
Potassium oxalate monohydrate, Baker Analyzed
Reagent, J.T. Baker Chemical Co.

The procedure was carried out under reduced light condition. 600 ml of 1.5 M $K_2C_2O_4$ and 200 ml of 1.5 M $FeCl_3$ were mixed with rigorous stirring at 80°C, and the remaining undissolved solids were filtered while the solution was hot. The filtrate was seated in the ice bath to be crystallized. The green crude crystals of ferrioxalate had to be recrystallized once by dissolving in 200 ml of water and repeating the same procedure above. The crystals were dried in a current of warm air (45°C) by an air blower. The solid could be stored in the dark for long periods of time without change; however, a noticeable color change of the pure green crystals to a yellowish brown occurred rapidly, accompanied by crystal decomposition, when the crystals were exposed to direct UV light.

Preparation of Standard Solutions

Reagents: Ferrous ammonium sulfate, ACS Reagent,
The Nichols Chemical Co., Ltd.
1,10-phenanthroline monohydrate, Certified ACS
Fisher Scientific Company
Sodium acetate, Certified ACS, Fisher Scientific Co.
Sulfuric acid, Baker.

The following solutions were prepared:

0.015 M Ferrioxalate solution: 29.5 g of $K_3Fe(C_2O_4)_3 \cdot 3H_2O$ in a 4 liter brown bottle filled with 0.1 N H_2SO_4 solution.

0.2% 1,10-phenanthroline solution: 0.4 g in 200 ml distilled water.

10^{-3} M Fe^{2+} standard solution: 0.426 g of ferrous ammonium sulfate in a 1 liter volumetric flask containing 0.1 N H_2SO_4 solution.

Buffer solution: 600 gm of NaO_2CCH_3 and 360 ml 1 N H_2SO_4 diluted to 1 liter.

Standard Fe^{2+} solution for calibration: A burette was used to deliver 0, 2, 3, 4, 5 ml of standard 10^{-3} M Fe^{2+} solution to five 100 ml volumetric flasks. Then 5, 3, 2, 1, 0 ml of 0.1 N H_2SO_4 solution were added to the above flasks respectively to make up the volumes to 5 ml. After introducing 2 ml of phenanthroline solution and 5 ml of buffer solution to each flask, the solutions were

diluted to volume by distilled water and allowed to stand for 60 minutes before measurement.

UV Irradiation

The reactor was sheltered by black paper and the inlet tubing wrapped by black tape. The reactor was first rinsed by distilled water, then filled up to the mark by 0.015 M ferrioxalate solution with T4 closed (referring figure 2) and all the fluorescent lights in the room except the one in the hood off. The stirrer and the cooling water were turned on and the exposure time was recorded as soon as the UV lamp was on. The exposure time would be 90 sec for 100% UV, 100 sec for 'fine filter', 150 sec for 'coarse filter' and 150 sec for no UV. Then, the UV lamp and the hood light were both switched off and the solution in the reactor was collected in a beaker from which 20 ml of solution was pipetted into a 100 ml volumetric flask containing 2 ml of 0.2% phenanthroline and 5 ml of buffer solutions. The flask was then stored in a dark place after filling up with 0.1 N H_2SO_4 solution.

Spectrophotometric Measurement

The absorbance was measured by a Bausch and Lomb Spectrometer Spectronic 20. The procedure had been described in reference 76. A blank solution containing no ferrous ion was used to adjust the 100% transmittance. The

samples had to be measured as fast as possible once they were taken out from the dark storage place, under a reduced fluorescence light condition to avoid further photo-decomposition of ferrioxalate. The calibration curve is shown in Figure A6, and the absorbances of the standard solutions are tabulated in Table A3.

Intensity Determined by UV Intensity Meter

Intensity can also be measured by a Blak-Ray Ultra-violet Intensity Meter, J-225 (for wavelengths from 2300 A to 2700 A), Ultra-Violet Products, Inc., San Gabriel, Calif., U.S.A. The UV assembly was removed from the mount-ing pole, the UV intensities were taken by the meter at the center and the edge of the opening under various conditions i.e. 0 ~ 100% UV. The dimension of the opening was required in the calculation.

Run	Fe^{2+} added ml	$[Fe^{2+}]$ 10^{-5}M	Transmittance %	Absorbance
1	5	5.435	11.0	0.9586
2	4	4.348	23.0	0.6383
3	3	3.261	27.8	0.5560
4	2	2.174	42.0	0.3768
5	0	0	100.0	0

Stock Fe^{2+} solution concentration 1.087×10^{-3}M

Table A3. Absorbances of standard Fe^{2+} solutions for the calibration of Spectronic 20 spectrometer at 22°C.

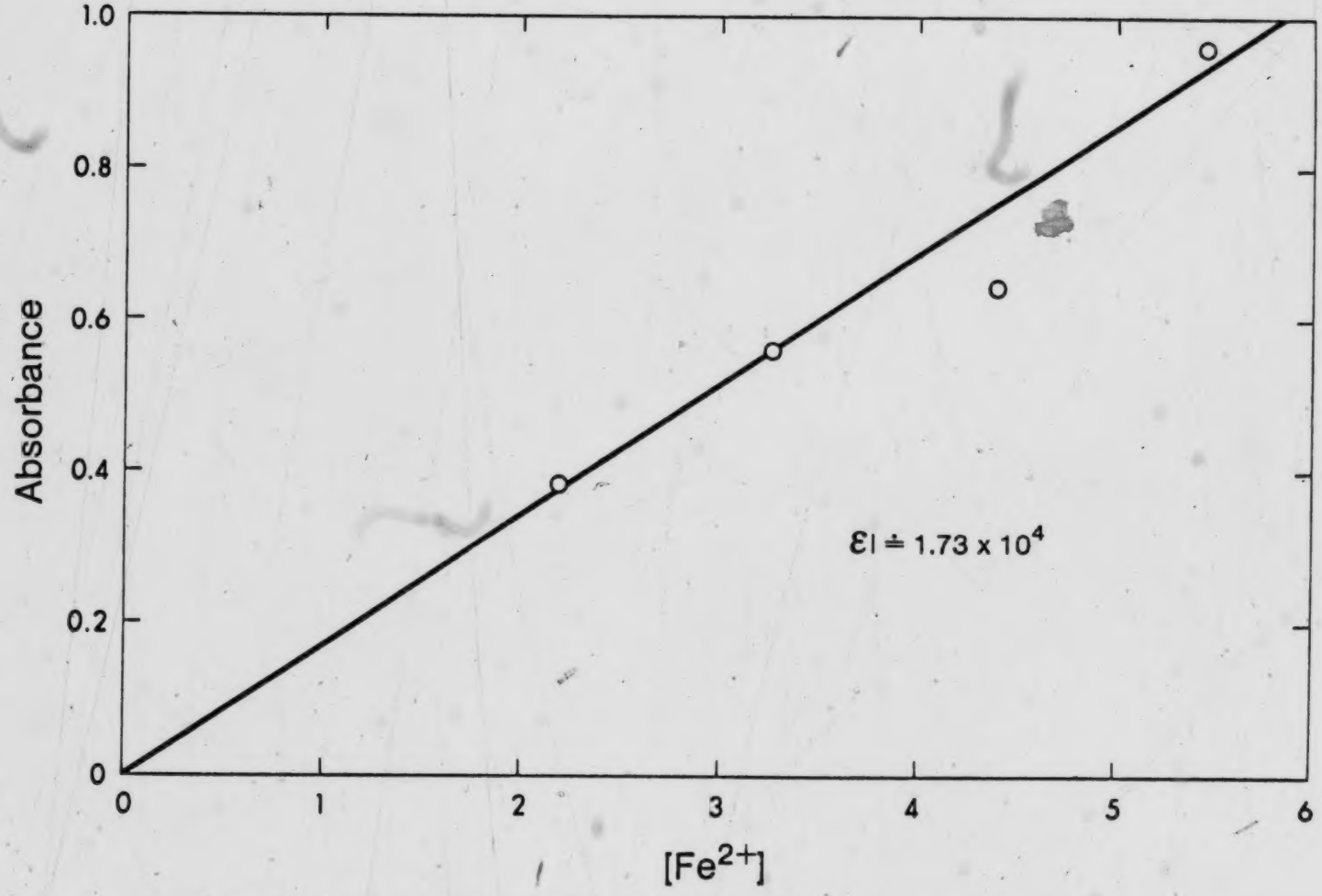

Figure A6. Calibration curve by plotting absorbance against the ferrous ion concentration at 22°C.

APPENDIX 6

Detailed Analyses of the Ozonation Reactions

The symbols used in Tables A4-A8:

KO	Physical mass transfer coefficient, $cm(s^{-1})$
KB	Rate constant for the cyanate oxidation reaction, $M^{-1}s^{-1}$
CS	Interfacial ozone concentration, M
CNO	Calculated cyanate concentration, M
SO	Measured ozone consumption ratio
S1	Calculated ozone consumption ratio
TR	Reaction time, s
TD	Diffusion time, s
TRD	Ratio of reaction time to diffusion time
R	Cyanide reacted per unit time, $mole(s^{-1})$
RT	Calculated ozone consumption per unit time, $mole(s^{-1})$
RO,O3	Measured ozone consumption per unit time, $mole(s^{-1})$
FRD	Fraction of ozone decomposed
FRC	Fraction of ozone reacted with cyanate
FRCN	Fraction of cyanide destroyed

RUN NO.	1	2	3	4	5
KO	0.2277E-02	0.2277E-02	0.2277E-02	0.2272E-02	0.2272E-02
CS	0.2401E-03	0.2420E-03	0.2373E-03	0.2360E-03	0.2377E-03
CNO	0.3629E-03	0.3573E-03	0.3560E-03	0.4625E-03	0.4650E-03
TR	0.2170E-01	0.2240E-01	0.2209E-01	0.1829E-01	0.1828E-01
TO	0.3832E 01	0.3832E 01	0.3832E 01	0.3832E 01	0.3832E 01
TRO	0.5662E-02	0.5845E-02	0.5764E-02	0.4772E-02	0.4770E-02
O3	0.6019E-06	0.5973E-06	0.5896E-06	0.6424E-06	0.6471E-06
SO	0.6516E 00	0.9953E 00	0.2610E 01	0.1800E 01	0.2008E 01
S1	0.1961E 01	0.1981E 01	0.1964E 01	0.1693E 01	0.1695E 01
R	0.3069E-06	0.3014E-06	0.3001E-06	0.3794E-06	0.3817E-06
FRO	0.3320E 00	0.3427E 00	0.3380E 00	0.2798E 00	0.2797E 00
FRC	0.1581E 00	0.1526E 00	0.1530E 00	0.1295E 00	0.1303E 00

RUN NO.	6	7	8	9	10
KO	0.2272E-02	0.2272E-02	0.2243E-02	0.2243E-02	0.2243E-02
CS	0.2407E-03	0.2341E-03	0.2571E-03	0.2551E-03	0.2551E-03
CNO	0.4642E-03	0.4642E-03	0.7376E-03	0.6603E-03	0.7000E-03
TR	0.1859E-01	0.1801E-01	0.1212E-01	0.1439E-01	0.1310E-01
TO	0.3832E 01	0.3832E 01	0.3832E 01	0.3832E 01	0.3832E 01
TRO	0.4851E-02	0.4701E-02	0.3163E-02	0.3755E-02	0.3419E-02
O3	0.6497E-06	0.6419E-06	0.8459E-06	0.7715E-06	0.8079E-06
SO	0.2756E 01	0.1049E 01	0.8422E-01	0.3788E 01	0.1513E 01
S1	0.1705E 01	0.1684E 01	0.1425E 01	0.1461E 01	0.1438E 01
R	0.3809E-06	0.3809E-06	0.5936E-06	0.5278E-06	0.5615E-06
FRO	0.2844E 00	0.2756E 00	0.1855E 00	0.2202E 00	0.2005E 00
FRC	0.1292E 00	0.1308E 00	0.1127E 00	0.9561E-01	0.1044E 00

Table A4. Detailed analysis of the $CN^-/O_3/UV$ reaction for the cyanide concentrations and experimental conditions listed in Table 6.

RUN NO.	11	12	13	14	15
KO	0.2243E-02	0.2243E-02	0.2243E-02	0.2243E-02	0.2243E-02
CS	0.2540E-03	0.2558E-03	0.2371E-03	0.2369E-03	0.2484E-03
CNO	0.6621E-03	0.7018E-03	0.9326E-03	0.9326E-03	0.9427E-03
TR	0.1425E-01	0.1309E-01	0.8217E-02	0.8209E-02	0.8668E-02
TD	0.3832E 01	0.3832E 01	0.3832E 01	0.3832E 01	0.3832E 01
TRD	0.3719E-02	0.3417E-02	0.2144E-02	0.2142E-02	0.2261E-02
O3	0.7719E-06	0.8103E-06	0.9438E-06	0.9437E-06	0.9634E-06
SO	0.2046E 01	0.9472E 00	0.2027E 00	0.9237E 00	0.3764E 01
S1	0.1458E 01	0.1439E 01	0.1275E 01	0.1275E 01	0.1287E 01
R	0.5293E-06	0.5630E-06	0.7397E-06	0.7397E-06	0.7481E-06
FRD	0.2180E 00	0.2003E 00	0.1257E 00	0.1256E 00	0.1326E 00
FRC	0.9616E-01	0.1048E 00	0.9051E-01	0.9053E-01	0.9085E-01

RUN NO.	16	17	18	19	20
KO	0.2243E-02	0.2243E-02	0.2253E-02	0.2253E-02	0.2253E-02
CS	0.2431E-03	0.2484E-03	0.2036E-03	0.2456E-03	0.2480E-03
CNO	0.9261E-03	0.9280E-03	0.1000E-02	0.9987E-03	0.9987E-03
TR	0.8655E-02	0.8920E-02	0.5976E-02	0.8159E-02	0.8284E-02
TD	0.3832E 01	0.3832E 01	0.3832E 01	0.3832E 01	0.3832E 01
TRD	0.2258E-02	0.2327E-02	0.1559E-02	0.2129E-02	0.2161E-02
O3	0.9434E-06	0.9500E-06	0.9511E-06	0.9853E-06	0.9875E-06
SO	0.7716E 00	0.3600E 01	0.1373E 01	0.1397E 01	0.1566E 01
S1	0.1284E 01	0.1291E 01	0.1205E 01	0.1251E 01	0.1254E 01
R	0.7343E-06	0.7359E-06	0.7887E-06	0.7871E-06	0.7871E-06
FRD	0.1324E 00	0.1364E 00	0.9143E-01	0.1248E 00	0.1267E 00
FRC	0.8915E-01	0.8892E-01	0.7935E-01	0.7628E-01	0.7612E-01

Table A4. (cont'd)

RUN NO.	21	22	23	24	25
KO	0.2253E-02	0.0000E 00	0.0000E 00	0.0000E 00	0.0000E 00
CS	0.2468E-03	0.0000E 00	0.0000E 00	0.0000E 00	0.0000E 00
CNO	0.9659E-03	0.0000E 00	0.0000E 00	0.0000E 00	0.0000E 00
TR	0.8725E-02	0.0000E 00	0.0000E 00	0.0000E 00	0.0000E 00
TD	0.3832E 01	0.0000E 00	0.0000E 00	0.0000E 00	0.0000E 00
TRD	0.2276E-02	0.0000E 00	0.0000E 00	0.0000E 00	0.0000E 00
O3	0.9581E-06	0.0000E 00	0.0000E 00	0.0000E 00	0.0000E 00
SO	0.1336E 01	0.0000E 00	0.0000E 00	0.0000E 00	0.0000E 00
S1	0.1260E 01	0.0000E 00	0.0000E 00	0.0000E 00	0.0000E 00
R	0.7604E-06	0.0000E 00	0.0000E 00	0.0000E 00	0.0000E 00
FRD	0.1335E 00	0.0000E 00	0.0000E 00	0.0000E 00	0.0000E 00
FRC	0.7290E-01	0.0000E 00	0.0000E 00	0.0000E 00	0.0000E 00

RUN NO.	26	27	28	29	30
KO	0.0000E 00	0.0000E 00	0.0000E 00	0.0000E 00	0.0000E 00
CS	0.0000E 00	0.0000E 00	0.0000E 00	0.0000E 00	0.0000E 00
CNO	0.0000E 00	0.0000E 00	0.0000E 00	0.0000E 00	0.0000E 00
TR	0.0000E 00	0.0000E 00	0.0000E 00	0.0000E 00	0.0000E 00
TD	0.0000E 00	0.0000E 00	0.0000E 00	0.0000E 00	0.0000E 00
TRD	0.0000E 00	0.0000E 00	0.0000E 00	0.0000E 00	0.0000E 00
O3	0.0000E 00	0.0000E 00	0.0000E 00	0.0000E 00	0.0000E 00
SO	0.0000E 00	0.0000E 00	0.0000E 00	0.0000E 00	0.0000E 00
S1	0.0000E 00	0.0000E 00	0.0000E 00	0.0000E 00	0.0000E 00
R	0.0000E 00	0.0000E 00	0.0000E 00	0.0000E 00	0.0000E 00
FRD	0.0000E 00	0.0000E 00	0.0000E 00	0.0000E 00	0.0000E 00
FRC	0.0000E 00	0.0000E 00	0.0000E 00	0.0000E 00	0.0000E 00

Table A4. (cont'd)

RUN NO.	1	2	3	4	5
KO	0.2236E-02	0.2236E-02	0.2236E-02	0.2236E-02	0.2236E-02
CS	0.2231E-03	0.2356E-03	0.2045E-03	0.2392E-03	0.2019E-03
CNO	0.2083E-03	0.2128E-03	0.3228E-03	0.2767E-03	0.5270E-03
TR	0.2833E-01	0.2898E-01	0.1729E-01	0.2457E-01	0.9218E-02
TO	0.3832E 01	0.3832E 01	0.3832E 01	0.3832E 01	0.3832E 01
TRO	0.7394E-02	0.7561E-02	0.4513E-02	0.6412E-02	0.2405E-02
O3	0.4816E-06	0.5031E-06	0.5632E-06	0.5542E-06	0.7576E-06
SO	0.9713E 01	0.5875E 01	0.6742E 01	0.7068E 01	0.3478E 01
S1	0.2019E 01	0.2062E 01	0.1532E 01	0.1771E 01	0.1275E 01
R	0.2384E-06	0.2439E-06	0.3675E-06	0.3128E-06	0.5940E-06
FRO	0.4336E 00	0.4434E 00	0.2646E 00	0.3760E 00	0.1410E 00
FRC	0.7129E-01	0.7172E-01	0.8273E-01	0.5950E-01	0.7495E-01

RUN NO.	6	7	8	9
KO	0.2201E-02	0.2201E-02	0.2252E-02	0.2252E-02
CS	0.2312E-03	0.2256E-03	0.2141E-03	0.2141E-03
CNO	0.6818E-03	0.6305E-03	0.1354E-02	0.1228E-02
TR	0.7659E-02	0.8451E-02	0.1765E-02	0.2213E-02
TO	0.3832E 01	0.3832E 01	0.3832E 01	0.3832E 01
TRO	0.1998E-02	0.2205E-02	0.4606E-03	0.5776E-03
O3	0.9353E-06	0.8696E-06	0.1799E-05	0.1614E-05
SO	0.1591E 01	0.2314E 01	0.1559E 01	0.1726E 01
S1	0.1223E 01	0.1232E 01	0.1164E 01	0.1157E 01
R	0.7647E-06	0.7056E-06	0.1544E-05	0.1394E-05
FRO	0.1171E 00	0.1293E 00	0.2701E-01	0.3387E-01
FRC	0.6520E-01	0.5925E-01	0.1145E 00	0.1023E 00

Table A5. Detailed analysis of the $CN^-/O_3/UV$ reaction for the cyanide concentrations and experimental conditions listed in Table 7.

RUN NO.	1	2	3	4	5
KL	0.2460E-02	0.2358E-02	0.2616E-02	0.2517E-02	0.2738E-02
KO	0.2297E-02	0.2297E-02	0.2236E-02	0.2236E-02	0.2236E-02
EN	0.1071E 01	0.1026E 01	0.1169E 01	0.1125E 01	0.1224E 01
DT	0.2022E-04	0.2022E-04	0.1917E-04	0.1917E-04	0.1917E-04
CS	0.2397E-03	0.2417E-03	0.2593E-03	0.2656E-03	0.2588E-03
CNO	0.3626E-05	0.1345E-05	0.8557E-05	0.6388E-05	0.1123E-04
TR	0.1773E 02	0.4766E 02	0.7286E 01	0.9928E 01	0.5443E 01
TO	0.3832E 01	0.3832E 01	0.3832E 01	0.3832E 01	0.3832E 01
TRO	0.4628E 01	0.1243E 02	0.1901E 01	0.2590E 01	0.1420E 01
R	0.1285E-07	0.1132E-07	0.1656E-07	0.1552E-07	0.1819E-07
RT	0.4955E-07	0.4789E-07	0.5699E-07	0.5618E-07	0.5954E-07
FRO	0.1507E-01	0.4051E-01	0.6193E-02	0.8438E-02	0.4626E-02
FRC	0.7255E 00	0.7231E 00	0.7031E 00	0.7152E 00	0.6898E 00
FRCN	0.1410E 00	0.1242E 00	0.1817E 00	0.1703E 00	0.1996E 00

RUN NO.	6	7	8	9	10
KL	0.2808E-02	0.2337E-02	0.2893E-02	0.2858E-02	0.2826E-02
KO	0.2236E-02	0.2297E-02	0.2297E-02	0.2285E-02	0.2285E-02
EN	0.1255E 01	0.1452E 01	0.1259E 01	0.1250E 01	0.1236E 01
DT	0.1917E-04	0.2022E-04	0.2022E-04	0.2002E-04	0.2002E-04
CS	0.2588E-03	0.2283E-03	0.2283E-03	0.2465E-03	0.2494E-03
CNO	0.1275E-04	0.2183E-04	0.1279E-04	0.1247E-04	0.1181E-04
TR	0.4745E 01	0.2575E 01	0.4672E 01	0.4846E 01	0.5149E 01
TO	0.3832E 01	0.3832E 01	0.3832E 01	0.3832E 01	0.3832E 01
TRO	0.1238E 01	0.6720E 00	0.1219E 01	0.1264E 01	0.1343E 01
R	0.1913E-07	0.2328E-07	0.1784E-07	0.1858E-07	0.1834E-07
RT	0.6106E-07	0.6402E-07	0.5550E-07	0.5920E-07	0.5923E-07
FRO	0.4033E-02	0.2189E-02	0.3971E-02	0.4119E-02	0.4376E-02
FRC	0.6826E 00	0.6341E 00	0.6744E 00	0.6818E 00	0.6859E 00
FRCN	0.2099E 00	0.2555E 00	0.1958E 00	0.1129E 00	0.1114E 00

Table A6. Detailed analysis of the ferricyanide/O_3/UV reaction for the ferricyanide concentrations and experimental conditions listed in Table 11.

RUN NO.	11	12	13	14	15
KL	0.3316E-02	0.3189E-02	0.3689E-02	0.3648E-02	0.4211E-02
KO	0.2270E-02	0.2270E-02	0.2270E-02	0.2270E-02	0.2285E-02
EN	0.1460E 01	0.1404E 01	0.1625E 01	0.1607E 01	0.1842E 01
DT	0.1975E-04	0.1975E-04	0.1975E-04	0.1975E-04	0.2002E-04
CS	0.2579E-03	0.2538E-03	0.2537E-03	0.2591E-03	0.2507E-03
CNO	0.2258E-04	0.1988E-04	0.3037E-04	0.2963E-04	0.4084E-04
TR	0.2528E 01	0.2908E 01	0.1802E 01	0.1862E 01	0.1280E 01
TD	0.3832E 01	0.3832E 01	0.3832E 01	0.3832E 01	0.3832E 01
TRD	0.6598E 00	0.7588E 00	0.4702E 00	0.4860E 00	0.3340E 00
R	0.2541E-07	0.2348E-07	0.2996E-07	0.2986E-07	0.3628E-07
RT	0.7186E-07	0.6802E-07	0.7863E-07	0.7942E-07	0.8869E-07
FRD	0.2149E-02	0.2472E-02	0.1531E-02	0.1583E-02	0.1088E-02
FRC	0.6442E 00	0.6522E 00	0.6174E 00	0.6224E 00	0.5897E 00
FRCN	0.1544E 00	0.1426E 00	0.1820E 00	0.1814E 00	0.2204E 00

RUN NO.	16	17	18	19	20
KL	0.4226E-02	0.3397E-02	0.2556E-02	0.3239E-02	0.3014E-02
KO	0.2285E-02	0.2236E-02	0.2236E-02	0.2277E-02	0.2277E-02
EN	0.1849E 01	0.1518E 01	0.1142E 01	0.1422E 01	0.1323E 01
DT	0.2002E-04	0.1917E-04	0.1917E-04	0.1987E-04	0.1987E-04
CS	0.2416E-03	0.2483E-03	0.2483E-03	0.2542E-03	0.2543E-03
CNO	0.4082E-04	0.2515E-04	0.7212E-05	0.2073E-04	0.1601E-04
TR	0.1268E 01	0.2217E 01	0.8703E 01	0.2777E 01	0.3699E 01
TD	0.3832E 01	0.3832E 01	0.3832E 01	0.3832E 01	0.3832E 01
TRD	0.3309E 00	0.5786E 00	0.2270E 01	0.7248E 00	0.9653E 00
R	0.3559E-07	0.2615E-07	0.1517E-07	0.2407E-07	0.2116E-07
RT	0.8578E-07	0.7087E-07	0.5331E-07	0.6917E-07	0.6439E-07
FRD	0.1078E-02	0.1885E-02	0.7397E-02	0.2361E-02	0.3144E-02
FRC	0.5839E 00	0.6290E 00	0.7079E 00	0.6495E 00	0.6682E 00
FRCN	0.2162E 00	0.1178E 00	0.6838E-01	0.1084E 00	0.9534E-01

Table A6. (cont'd)

RUN NO.	21	22	23	24	25
KL	0.3552E-02	0.4252E-02	0.4397E-02	0.5587E-02	0.5712E-02
KO	0.2277E-02	0.2236E-02	0.2236E-02	0.2322E-02	0.2322E-02
EN	0.1559E 01	0.1900E 01	0.1965E 01	0.2405E 01	0.2459E 01
DT	0.1987E-04	0.1917E-04	0.1917E-04	0.2067E-04	0.2067E-04
CS	0.2433E-03	0.2456E-03	0.2629E-03	0.2295E-03	0.2292E-03
CNO	0.2707E-04	0.4327E-04	0.4722E-04	0.6795E-04	0.7070E-04
TR	0.2038E 01	0.1183E 01	0.1089E 01	0.6861E 00	0.6538E 00
TD	0.3832E 01	0.3832E 01	0.3832E 01	0.3832E 01	0.3832E 01
TRD	0.5319E 00	0.3087E 00	0.2842E 00	0.1790E 00	0.1706E 00
R	0.2729E-07	0.3698E-07	0.4068E-07	0.5102E-07	0.5260E-07
RT	0.7261E-07	0.8772E-07	0.9714E-07	0.1077E-06	0.1100E-06
FRD	0.1732E-02	0.1005E-02	0.9260E-03	0.5832E-03	0.5557E-03
FRC	0.6224E 00	0.5774E 00	0.5802E 00	0.5257E 00	0.5213E 00
FRCN	0.1229E 00	0.1666E 00	0.1833E 00	0.1073E 00	0.1107E 00

RUN NO.	26	27	28	29	30
KL	0.6283E-02	0.5857E-02	0.6445E-02	0.6141E-02	0.6294E-02
KO	0.2342E-02	0.2342E-02	0.2342E-02	0.2342E-02	0.2322E-02
EN	0.2682E 01	0.2500E 01	0.2750E 01	0.2621E 01	0.2709E 01
DT	0.2103E-04	0.2103E-04	0.2103E-04	0.2103E-04	0.2067E-04
CS	0.2147E-03	0.2197E-03	0.2204E-03	0.2204E-03	0.2388E-03
CNO	0.8077E-04	0.7200E-04	0.8514E-04	0.7832E-04	0.8502E-04
TR	0.5434E 00	0.6311E 00	0.5151E 00	0.5705E 00	0.5316E 00
TD	0.3832E 01	0.3832E 01	0.3832E 01	0.3832E 01	0.3832E 01
TRD	0.1417E 00	0.1646E 00	0.1344E 00	0.1488E 00	0.1387E 00
R	0.5720E-07	0.5265E-07	0.6026E-07	0.5636E-07	0.6184E-07
RT	0.1133E-06	0.1081E-06	0.1193E-06	0.1137E-06	0.1262E-06
FRD	0.4619E-03	0.5365E-03	0.4378E-03	0.4849E-03	0.4519E-03
FRC	0.4950E 00	0.5125E 00	0.4946E 00	0.5039E 00	0.5098E 00
FRCN	0.1204E 00	0.1108E 00	0.1268E 00	0.1186E 00	0.1301E 00

Table A6. (cont'd)

RUN NO.	31	32	33	34	35
KL	0.6280E-02	0.7104E-02	0.7317E-02	0.9276E-02	0.6775E-02
KO	0.2322E-02	0.2319E-02	0.2319E-02	0.2277E-02	0.2277E-02
EN	0.2704E 01	0.3063E 01	0.3154E 01	0.4073E 01	0.2975E 01
DT	0.2067E-04	0.2061E-04	0.2061E-04	0.1987E-04	0.1987E-04
CS	0.2341E-03	0.2540E-03	0.2389E-03	0.2512E-03	0.2482E-03
CNO	0.8413E-04	0.1070E-03	0.1100E-03	0.1684E-03	0.1004E-03
TR	0.5341E 00	0.4120E 00	0.3879E 00	0.2312E 00	0.4376E 00
TO	0.3832E 01	0.3832E 01	0.3832E 01	0.3832E 01	0.3832E 01
TRO	0.1393E 00	0.1075E 00	0.1012E 00	0.6032E-01	0.1141E 00
R	0.6086E-07	0.7613E-07	0.7613E-07	0.1097E-06	0.7119E-07
RT	0.1235E-06	0.1516E-06	0.1468E-06	0.1958E-06	0.1412E-06
FRO	0.4540E-03	0.3502E-03	0.3297E-03	0.1965E-03	0.3719E-03
FRC	0.5068E 00	0.4975E 00	0.4812E 00	0.4392E 00	0.4956E 00
FRCN	0.1281E 00	0.1104E 00	0.1104E 00	0.1592E 00	0.1032E 00

RUN NO.	36	37	38	39	40
KL	0.6585E-02	0.6951E-02	0.7244E-02	0.7626E-02	0.9484E-02
KO	0.2277E-02	0.2277E-02	0.2319E-02	0.2319E-02	0.2272E-02
EN	0.2891E 01	0.3052E 01	0.3123E 01	0.3288E 01	0.4174E 01
DT	0.1987E-04	0.1987E-04	0.2061E-04	0.2061E-04	0.1978E-04
CS	0.2496E-03	0.2478E-03	0.2367E-03	0.2324E-03	0.2496E-03
CNO	0.9587E-04	0.1048E-03	0.1078E-03	0.1165E-03	0.1744E-03
TR	0.4641E 00	0.4150E 00	0.3959E 00	0.3564E 00	0.2201E 00
TO	0.3832E 01	0.3832E 01	0.3832E 01	0.3832E 01	0.3832E 01
TRO	0.1211E 00	0.1082E 00	0.1033E 00	0.9300E-01	0.5744E-01
R	0.6872E-07	0.7366E-07	0.7465E-07	0.7910E-07	0.1127E-06
RT	0.1380E-06	0.1447E-06	0.1440E-06	0.1489E-06	0.1988E-06
FRO	0.3945E-03	0.3527E-03	0.3365E-03	0.3029E-03	0.1871E-03
FRC	0.5018E 00	0.4905E 00	0.4814E 00	0.4685E 00	0.4330E 00
FRCN	0.9971E-01	0.1068E 00	0.1083E 00	0.1147E 00	0.1003E 00

Table A6. (cont'd)

RUN NO.	41	42	43	44	45
KL	0.9616E-02	0.8484E-02	0.8470E-02	0.1123E-01	0.7187E-02
KO	0.2272E-02	0.2272E-02	0.2272E-02	0.2272E-02	0.2272E-02
EN	0.4232E 01	0.3734E 01	0.3728E 01	0.4946E 01	0.3163E 01
DT	0.1978E-04	0.1978E-04	0.1978E-04	0.1978E-04	0.1978E-04
CS	0.2460E-03	0.2507E-03	0.2420E-03	0.2375E-03	0.2425E-03
CNO	0.1771E-03	0.1464E-03	0.1439E-03	0.2214E-03	0.1102E-03
TR	0.2141E 00	0.2754E 00	0.2763E 00	0.1566E 00	0.3857E 00
TD	0.3832E 01	0.3832E 01	0.3832E 01	0.3832E 01	0.3832E 01
TRD	0.5586E-01	0.7188E-01	0.7211E-01	0.4088E-01	0.1006E 00
R	0.1137E-06	0.9739E-07	0.9492E-07	0.1364E-06	0.7613E-07
RT	0.1987E-06	0.1787E-06	0.1722E-06	0.2242E-06	0.1464E-06
FRD	0.1819E-03	0.2341E-03	0.2349E-03	0.1331E-03	0.3278E-03
FRC	0.4276E 00	0.4548E 00	0.4485E 00	0.3912E 00	0.4797E 00
FRCN	0.1012E 00	0.8670E-01	0.8450E-01	0.1214E 00	0.6778E-01

RUN NO.	46	47	48	49	50
KL	0.8330E-02	0.8115E-02	0.1380E-01	0.1305E-01	0.1252E-01
KO	0.2272E-02	0.2272E-02	0.2299E-02	0.2299E-02	0.2299E-02
EN	0.3666E 01	0.3571E 01	0.6006E 01	0.5678E 01	0.5449E 01
DT	0.1978E-04	0.1978E-04	0.2025E-04	0.2025E-04	0.2025E-04
CS	0.2425E-03	0.2375E-03	0.2464E-03	0.2401E-03	0.2408E-03
CNO	0.1402E-03	0.1333E-03	0.3033E-03	0.2754E-03	0.2594E-03
TR	0.2858E 00	0.3013E 00	0.1062E 00	0.1188E 00	0.1290E 00
TD	0.3832E 01	0.3832E 01	0.3832E 01	0.3832E 01	0.3832E 01
TRD	0.7458E-01	0.7863E-01	0.2771E-01	0.3101E-01	0.3367E-01
R	0.9294E-07	0.8849E-07	0.1819E-06	0.1661E-06	0.1577E-06
RT	0.1697E-06	0.1619E-06	0.2858E-06	0.2633E-06	0.2534E-06
FRD	0.2429E-03	0.2561E-03	0.9029E-04	0.1010E-03	0.1096E-03
FRC	0.4521E 00	0.4531E 00	0.3634E 00	0.3692E 00	0.3775E 00
FRCN	0.8274E-01	0.7878E-01	0.6706E-01	0.6123E-01	0.5813E-01

Table A6. (cont'd)

RUN NO.	51	52	53	54	55
KL	0.1256E-01	0.1363E-01	0.1529E-01	0.1478E-01	0.1424E-01
KO	0.2299E-02	0.2332E-02	0.2282E-02	0.2282E-02	0.2282E-02
EN	0.5463E 01	0.5847E 01	0.6702E 01	0.6478E 01	0.6241E 01
DT	0.2025E-04	0.2085E-04	0.1996E-04	0.1996E-04	0.1996E-04
CS	0.2418E-03	0.2233E-03	0.2506E-03	0.2474E-03	0.2539E-03
CNO	0.2609E-03	0.2788E-03	0.3579E-03	0.3383E-03	0.3248E-03
TR	0.1283E 00	0.1121E 00	0.8530E-01	0.9130E-01	0.9838E-01
TD	0.3832E 01	0.3832E 01	0.3832E 01	0.3832E 01	0.3832E 01
TRD	0.3349E-01	0.2925E-01	0.2225E-01	0.2382E-01	0.2567E-01
R	0.1587E-06	0.1656E-06	0.2111E-06	0.2002E-06	0.1942E-06
RT	0.2551E-06	0.2558E-06	0.3220E-06	0.3073E-06	0.3038E-06
FRD	0.1091E-03	0.9528E-04	0.7251E-04	0.7760E-04	0.8362E-04
FRC	0.3778E 00	0.3525E 00	0.3443E 00	0.3484E 00	0.3604E 00
FRCN	0.5850E-01	0.3585E-01	0.4182E-01	0.3966E-01	0.3849E-01

RUN NO.	56	57	58	59	60
KL	0.2139E-01	0.1698E-01	0.1918E-01	0.1893E-01	0.3417E-01
KO	0.2351E-02	0.2351E-02	0.2351E-02	0.2319E-02	0.2289E-02
EN	0.9098E 01	0.7221E 01	0.8158E 01	0.8163E 01	0.1492E 02
DT	0.2119E-04	0.2119E-04	0.2119E-04	0.2061E-04	0.2008E-04
CS	0.2181E-03	0.2221E-03	0.2202E-03	0.2349E-03	0.2439E-03
CNO	0.5144E-03	0.3781E-03	0.4460E-03	0.4605E-03	0.1041E-02
TR	0.4629E-01	0.7349E-01	0.5758E-01	0.5750E-01	0.1719E-01
TD	0.3832E 01	0.3832E 01	0.3832E 01	0.3832E 01	0.3832E 01
TRD	0.1207E-01	0.1917E-01	0.1502E-01	0.1500E-01	0.4487E-02
R	0.2867E-06	0.2175E-06	0.2521E-06	0.2620E-06	0.5586E-06
RT	0.3920E-06	0.3168E-06	0.3549E-06	0.3736E-06	0.7001E-06
FRD	0.3935E-04	0.6247E-04	0.4894E-04	0.4887E-04	0.1461E-04
FRC	0.2686E 00	0.3134E 00	0.2896E 00	0.2986E 00	0.2020E 00
FRCN	0.3240E-01	0.2458E-01	0.2849E-01	0.2896E-01	0.3075E-01

Table A6. (cont'd)

RUN NO.	61	62	63	64	65
KL	0.2185E-01	0.3138E-01	0.2983E-01	0.3182E-01	0.0000E 00
KO	0.2289E-02	0.2289E-02	0.2339E-02	0.2339E-02	0.0000E 00
EN	0.9546E 01	0.1371E 02	0.1275E 02	0.1360E 02	0.0000E 00
DT	0.2008E-04	0.2008E-04	0.2097E-04	0.2097E-04	0.0000E 00
CS	0.2358E-03	0.2406E-03	0.2272E-03	0.2382E-03	0.0000E 00
CNO	0.5674E-03	0.9259E-03	0.8224E-03	0.9244E-03	0.0000E 00
TR	0.4204E-01	0.2038E-01	0.2357E-01	0.2071E-01	0.0000E 00
TD	0.3832E 01	0.3832E 01	0.3832E 01	0.3832E 01	0.0000E 00
TRD	0.1097E-01	0.5319E-02	0.6151E-02	0.5404E-02	0.0000E 00
R	0.3164E-06	0.4993E-06	0.4449E-06	0.4993E-06	0.0000E 00
RT	0.4329E-06	0.6344E-06	0.5695E-06	0.6368E-06	0.0000E 00
FRD	0.3574E-04	0.1732E-04	0.2003E-04	0.1760E-04	0.0000E 00
FRC	0.2691E 00	0.2128E 00	0.2186E 00	0.2159E 00	0.0000E 00
FRCN	0.1741E-01	0.2749E-01	0.2444E-01	0.2743E-01	0.0000E 00

RUN NO.	66	67	68	69	70
KL	0.0000E 00	0.0000E 00	0.0000E 00	0.0000E 00	0.0000E 00
KO	0.0000E 00	0.0000E 00	0.0000E 00	0.0000E 00	0.0000E 00
EN	0.0000E 00	0.0000E 00	0.0000E 00	0.0000E 00	0.0000E 00
DT	0.0000E 00	0.0000E 00	0.0000E 00	0.0000E 00	0.0000E 00
CS	0.0000E 00	0.0000E 00	0.0000E 00	0.0000E 00	0.0000E 00
CNO	0.0000E 00	0.0000E 00	0.0000E 00	0.0000E 00	0.0000E 00
TR	0.0000E 00	0.0000E 00	0.0000E 00	0.0000E 00	0.0000E 00
TD	0.0000E 00	0.0000E 00	0.0000E 00	0.0000E 00	0.0000E 00
TRD	0.0000E 00	0.0000E 00	0.0000E 00	0.0000E 00	0.0000E 00
R	0.0000E 00	0.0000E 00	0.0000E 00	0.0000E 00	0.0000E 00
RT	0.0000E 00	0.0000E 00	0.0000E 00	0.0000E 00	0.0000E 00
FRD	0.0000E 00	0.0000E 00	0.0000E 00	0.0000E 00	0.0000E 00
FRC	0.0000E 00	0.0000E 00	0.0000E 00	0.0000E 00	0.0000E 00
FRCN	0.0000E 00	0.0000E 00	0.0000E 00	0.0000E 00	0.0000E 00

// END 10 SEP 77 16.58.22

Table A6. (cont'd)

RUN NO.	1	2	3	4	5
KL	0.1691E-01	0.1802E-01	0.1759E-01	0.1970E-01	0.2522E-01
KO	0.2226E-02	0.2210E-02	0.2210E-02	0.2253E-02	0.2236E-02
EN	0.7597E 01	0.8155E 01	0.7961E 01	0.8743E 01	0.1127E 02
KO	0.1377E 02	0.1377E 02	0.1377E 02	0.1459E 02	0.1496E 02
OT	0.1900E-04	0.1871E-04	0.1871E-04	0.1946E-04	0.1917E-04
CS	0.2517E-03	0.2549E-03	0.2591E-03	0.2493E-03	0.2734E-03
CNO	0.3385E-04	0.9037E-04	0.7158E-04	0.1292E-03	0.3929E-03
TR	0.6639E-01	0.5762E-01	0.6046E-01	0.5013E-01	0.3012E-01
TO	0.3832E 01	0.3832E 01	0.3832E 01	0.3832E 01	0.3832E 01
TRO	0.1732E-01	0.1503E-01	0.1577E-01	0.1308E-01	0.7861E-02
R	0.2149E-07	0.5690E-07	0.4530E-07	0.8066E-07	0.2408E-06
RT	0.3577E-06	0.3859E-06	0.3829E-06	0.4126E-06	0.5796E-06
FRO	0.9145E 00	0.7938E 00	0.8328E 00	0.7314E 00	0.4508E 00
FRC	0.2534E-01	0.5873E-01	0.4881E-01	0.7305E-01	0.1335E 00
FRCN	0.4086E-01	0.5540E-01	0.4410E-01	0.3847E-01	0.7527E-01

RUN NO.	6	7	8	9	10
KL	0.2060E-01	0.2007E-01	0.0000E 00	0.0000E 00	0.0000E 00
KO	0.2236E-02	0.2277E-02	0.0000E 00	0.0000E 00	0.0000E 00
EN	0.9212E 01	0.8816E 01	0.0000E 00	0.0000E 00	0.0000E 00
KO	0.1496E 02	0.1114E 02	0.0000E 00	0.0000E 00	0.0000E 00
OT	0.1917E-04	0.1987E-04	0.0000E 00	0.0000E 00	0.0000E 00
CS	0.2581E-03	0.2319E-03	0.0000E 00	0.0000E 00	0.0000E 00
CNO	0.1704E-03	0.2105E-03	0.0000E 00	0.0000E 00	0.0000E 00
TR	0.4515E-01	0.4930E-01	0.0000E 00	0.0000E 00	0.0000E 00
TO	0.3832E 01	0.3832E 01	0.0000E 00	0.0000E 00	0.0000E 00
TRO	0.1178E-01	0.1286E-01	0.0000E 00	0.0000E 00	0.0000E 00
R	0.1060E-06	0.1303E-06	0.0000E 00	0.0000E 00	0.0000E 00
RT	0.4468E-06	0.3911E-06	0.0000E 00	0.0000E 00	0.0000E 00
FRO	0.6758E 00	0.5495E 00	0.0000E 00	0.0000E 00	0.0000E 00
FRC	0.8678E-01	0.1170E 00	0.0000E 00	0.0000E 00	0.0000E 00
FRCN	0.3314E-01	0.4840E-01	0.0000E 00	0.0000E 00	0.0000E 00

Table A7. Detailed analysis of the ferricyanide/O_3/UV reaction for the ferricyanide concentrations and experimental conditions listed in Table 12.

APPENDIX 7

Listing of Program THES

(i) CN^- Free Cyanide, Film Model, Flat CNO Profile, pH 7 and 12

```
// JOB    M    P    X                TANG    13 OCT 78 15.19.35
// FOR THES    13 OCT 78 15.19.37
*IOCS(CARD,1443 PRINTER)
      REAL KOAT,KO
      DIMENSION GP(60),GT(60),GCNI(60),GCNF(60),GCNO(60),GKB1(60)
      DIMENSION GKB2(60),GKB3(60),GEN(60),GK1(60),GK2(60),GK3(60)
      DIMENSION GTR(60),GTO(60),GTRO(60),GRO(60),GRC(60),GCS(60),GR(60)
      DIMENSION GRO(60),MM(60),GKO(60),GINT(60),GKL(60)
      DIMENSION GK4(60),GKB4(60)
      DIMENSION GKL2(60),GKL3(60),GKL4(60),GEN3(60),GEN4(60)
      DIMENSION GO3(60)
      DIMENSION SO(60),S1(60)
      DATA SO,S1/120*0./
      DATA GO3/60*0./
      DATA GKL2,GKL3,GKL4,GEN3,GEN4/300*0./
      DATA GK4,GKB4/120*0./
      DATA GK3,GTR,GTO,GTRO,GRO,GRC,GCS,GR,GRO,GKO,GINT,GKL/720*0./
      DATA GP,GT,GCNI,GCNF,GCNO,GKB1,GKB2,GKB3,GEN,GK1,GK2/660*0./
      DATA MM/60*0/
      KK=0
      IJK=1
      FL=.765
      GO TO 1
997   FL=1.094
      KK=0
      IJK=IJK+1
1     READ(5,2)M,P,XNI,XNO,T,CNI,CNF
2     FORMAT(I1,6F10.5)
      IF(M-5)3,9,9
3     KK=KK+1
      II=1
      XKO=15.3
      ST=3.25
      ARA=84.
      RO=(XNI-XNO)*.001/60.
      R=(CNI-CNF)*.001*FL
      S=2.302586*(1.3272*(20-T)-.001053*(T-20)*(T-20))/(T+105.)
      U=1.002*EXP(S)
      DT=(T+273.2)*1.805E-05/(293.2*U)
      KOAT=.184*SQRT(DT/1.8389E-05)
      KO=KOAT/ARA
      H=67680.+2870.*(T-20.)
      CS=P/H*1000.
      CALL MULR(X,XKB,CNF,DT,KO,CS,R,RO,CNI,XKO,II)
      GK1(KK)=X
      GKB1(KK)=XKB
      GKL(KK)=2.15*RO/(2.15*ARA*CS/1000.-RO)
      GEN(KK)=GKL(KK)/KO
      II=II+1
      CALL MULR(X,XKB,CNF,DT,KO,CS,R,RO,CNI,XKO,II)
      GK2(KK)=X
      GKB2(KK)=XKB
      GKL2(KK)=1.498*2.15*R/(2.15*ARA*CS/1000.-R*1.498)
      GINT(KK)=GKL2(KK)/KO
      II=II+1
      CALL MULR(X,XKB,CNF,DT,KO,CS,R,RO,CNI,XKO,II)
      GK3(KK)=X
      GKB3(KK)=XKB
      GKL3(KK)=1.200*2.15*R/(2.15*ARA*CS/1000.-R*1.200)
      GEN3(KK)=GKL3(KK)/KO
      II=II+1
```

```
      CALL MULR(X,XKB,CNF,DT,KD,CS,R,RD,CNI,XKD,II)
      GK4(KK)=X
      GKB4(KK)=XKB
      CND=1./(1./(CNI-CNF)+XKB/X/CNF)
      TR=1./(X*CNF+XKD+ST*CND*XKB)
      TD=DT/KD/KD
      TRD=TR/TD
      RC=CND*XKB*ST/(X*CNF+XKD+ST*CND*XKB)
      RD=XKD/(X*CNF+XKD+ST*CND*XKB)
      GKL4(KK)=SQRT(DT*(X*CNF+XKB*ST*CND+XKD))
      GEN4(KK)=GKL4(KK)/KD
      GD3(KK)=R*(X*CNF+XKD+ST*XKB*CND)/X/CNF
      GCNI(KK)=CNI
      GCNF(KK)=CNF
      GT(KK)=T
      GP(KK)=P
      GCND(KK)=CND
      GKD(KK)=KD
      GCS(KK)=CS
      GTR(KK)=TR
      GTD(KK)=TD
      GTRD(KK)=TRD
      GRD(KK)=RD
      GRC(KK)=RC
      GR(KK)=R
      GRD(KK)=RD
      SD(KK)=GRD(KK)/GR(KK)
      S1(KK)=(X*CNF+ST*XKB*CND+XKD)/X/CNF
      MM(KK)=M
      GO TO 1
9     ILINE=0
      DO 30 I=1,KK
      ILINE=ILINE+1
      IF(ILINE-1)10,11,10
10    IF(ILINE-42)12,11,12
11    WRITE(6,13)
13    FORMAT('1',/////,6X,'RUN',3X,'UV',5X,'CNI',9X,'CNF',9X,
     *'PA',9X,'T',5X,'RD')
      WRITE(6,111)
111   FORMAT(' ',18X,'M',11X,'M',11X,'ATM',8X,'DEG C',1X,'MOLE/S')
6     WRITE(6,20)
20    FORMAT(/)
      ILINE=ILINE+1
      IF(ILINE-42)7,11,7
12    IP=I-1
      IF(GCNI(IP)-GCNI(I))6,7,6
7     IF(MM(I)-1)14,14,15
14    WRITE(6,24)I,GCNI(I),GCNF(I),GP(I),GT(I),GRD(I)
24    FORMAT(' ',5X,I2,3X,'ND',5X,3(E11.4,1X),F5.2,E11.4)
      GO TO 30
15    WRITE(6,29)I,GCNI(I),GCNF(I),GP(I),GT(I),GRD(I)
29    FORMAT(' ',5X,I2,3X,'FULL',3X,3(E11.4,1X),F5.2,E11.4)
30    CONTINUE
      II0=0
      II=9
      ITEST=0
      DO 60 I=1,KK
```

```
      I10=I10+1
      IF(I-1)32,35,32
32    IF(I-8)33,48,33
33    IP=I-1
      IF(I10-II)37,35,35
37    IF(GCNI(IP)-GCNI(I))38,39,38
38    WRITE(6,34)
34    FORMAT(/)
      ITEST=ITEST+1
      GO TO 39
35    WRITE(6,36)
36    FORMAT('1',/////,7X,'RUN NO.',4X,'A',12X,'B',12X,'C',12X,'D')
      I10=0
39    WRITE(6,40)I,GK1(I),GK2(I),GK3(I),GK4(I)
40    FORMAT(' ',5X,I2,5X,'K',3X,3(E11.4,2X),E11.4)
      WRITE(6,41)GKB1(I),GKB2(I),GKB3(I),GKB4(I)
41    FORMAT(' ',12X,'KB',2X,3(E11.4,2X),E11.4)
      WRITE(6,45)GKL(I),GKL2(I),GKL3(I),GKL4(I)
45    FORMAT(' ',12X,'KL',2X,3(E11.4,2X),E11.4)
      WRITE(6,47)GEN(I),GINT(I),GEN3(I),GEN4(I)
47    FORMAT(' ',12X,'EN',2X,3(E11.4,2X),E11.4)
      IF(ITEST-3)51,52,52
52    IF(ITEST-7)53,54,54
51    II=9
      GO TO 60
53    II=8
      GO TO 60
54    II=7
      GO TO 60
48    WRITE(6,55)
55    FORMAT(' ',///,6X,'TABLE    THE COMPARISON OF RATE CONSTANTS AND M
     *ASS TRANSFER',/,10X,'COEFFICIENTS OBTAINED BY 4 DIFFERENT WAYS',
     */,10X,'A  RT FROM GAS PHASE MASS BALANCE',/10X,'B  RT=1.5*R',
     */,10X,'C  RT=1.2*R',/,10X,'D  KB=K/5.1, RT FROM R')
      GO TO 35
60    CONTINUE
      J2=-1
61    J2=J2+1
      I1=1+J2*5
      I2=2+J2*5
      I3=3+J2*5
      I4=4+J2*5
      I5=5+J2*5
      IF(J2-J2/2*2)65,62,65
62    WRITE(6,72)I1,I2,I3,I4,I5
72    FORMAT('1',/////,7X,'RUN NO.',2X,4(I2,12X),I2)
      GO TO 79
65    WRITE(6,75)I1,I2,I3,I4,I5
75    FORMAT(' ',/////,7X,'RUN NO.',2X,4(I2,12X),I2)
79    WRITE(6,81)GKO(I1),GKO(I2),GKO(I3),GKO(I4),GKO(I5)
81    FORMAT(' ',/,7X,'KO',7X,4(E11.4,3X),E11.4)
      WRITE(6,83)GCS(I1),GCS(I2),GCS(I3),GCS(I4),GCS(I5)
83    FORMAT(' ',6X,'CS',7X,4(E11.4,3X),E11.4)
      WRITE(6,84)GCNO(I1),GCNO(I2),GCNO(I3),GCNO(I4),GCNO(I5)
84    FORMAT(' ',6X,'CNO',6X,4(E11.4,3X),E11.4)
      WRITE(6,87)GTR(I1),GTR(I2),GTR(I3),GTR(I4),GTR(I5)
87    FORMAT(' ',6X,'TR',7X,4(E11.4,3X),E11.4)
```

```
      WRITE(6,88)GTD(I1),GTD(I2),GTD(I3),GTD(I4),GTD(I5)
 88   FORMAT(' ',6X,'TD',7X,4(E11.4,3X),E11.4)
      WRITE(6,89)GTRD(I1),GTRD(I2),GTRD(I3),GTRD(I4),GTRD(I5)
 89   FORMAT(' ',6X,'TRD',6X,4(E11.4,3X),E11.4)
      WRITE(6,91)G03(I1),G03(I2),G03(I3),G03(I4),G03(I5)
 91   FORMAT(' ',6X,'03 ',6X,4(E11.4,3X),E11.4)
      WRITE(6,995)S0(I1),S0(I2),S0(I3),S0(I4),S0(I5)
 995  FORMAT(' ',6X,'S0 ',6X,4(E11.4,3X),E11.4)
      WRITE(6,992)S1(I1),S1(I2),S1(I3),S1(I4),S1(I5)
 992  FORMAT(' ',6X,'S1 ',6X,4(E11.4,3X),E11.4)
      WRITE(6,90)GR(I1),GR(I2),GR(I3),GR(I4),GR(I5)
 90   FORMAT(' ',6X,'R',8X,4(E11.4,3X),E11.4)
      WRITE(6,92)GRD(I1),GRD(I2),GRD(I3),GRD(I4),GRD(I5)
 92   FORMAT(' ',6X,'RD',6X,4(E11.4,3X),E11.4)
      WRITE(6,93)GRC(I1),GRC(I2),GRC(I3),GRC(I4),GRC(I5)
 93   FORMAT(' ',6X,'RC',6X,4(E11.4,3X),E11.4)
      IF(J2-KK/5)61,61,999
 999  IF(IJK-1)997,997,998
 998  STOP
      END


FEATURES SUPPORTED
 ONE WORD INTEGERS
 IOCS

CORE REQUIREMENTS FOR THES
 COMMON       0  INSKEL COMMON       0
  VARIABLES   4100  PROGRAM   2018



END OF COMPILATION
THES
DMP FUNCTION COMPLETED
// FOR EMU   13 OCT 78 15.22.33
      SUBROUTINE EMU(TOL,XKB,CNF,DT,KD,CS,R,F,CNI,XKD,RO,II)
      REAL KD
      ST=3.25
      ARA=R4.
      IF(II-2)1,2,3
 1    RT=RO
      GO TO 10
 2    RT=1.498*R
      GO TO 10
 3    IF(II-3)5,5,6
 5    RT=1.2*R
 10   XKB=1.00/(ST/(TOL*CNF*(RT/R-1.)-XKD)-1./TOL/CNF)/(CNI-CNF)
      CNO=1./(1./(CNI-CNF)+XKB/TOL/CNF)
      GO TO 7
 6    XKB=TOL/5.1
      CNO=1./(1./(CNI-CNF)+XKB/TOL/CNF)
      RT=R*(TOL*CNF+ST*XKB*CNO+XKD)/TOL/CNF
 7    F=2.15*RT/(2.15*ARA/1000.*CS-RT)-SQRT(DT*(TOL*CNF+ST*XKB*CNO+XKD))
      RETURN
      END
```

```
FEATURES SUPPORTED
 ONE WORD INTEGERS

CORE REQUIREMENTS FOR EMU
 COMMON       0   INSKEL COMMON       0
  VARIABLES     16   PROGRAM     276



END OF COMPILATION
EMU
DMP FUNCTION COMPLETED
// FOR MULR    13 OCT 78 15.23.03
      SUBROUTINE MULR(X,XKB,CNE,DT,KD,CS,R,RD,CNI,XKD,II)
      REAL KD
      XLI=1000.
      XRI=1000000.
      EPS=.01
      IEND=32000
      IER=0
      XL=XLI
      XR=XRI
      X=XL
      TOL=X
      CALL EMU(TOL,XKB,CNE,DT,KD,CS,R,E,CNI,XKD,RD,II)
      IF(E-0.)1,16,1
1     EL=E
      X=XR
      TOL=X
      CALL EMU(TOL,XKB,CNE,DT,KD,CS,R,E,CNI,XKD,RD,II)
      IF(E-0)2,16,2
2     ER=E
      IF(SIGN(1.,EL)+SIGN(1.,ER))25,3,25
3     I=0
      TOLE=100.*EPS
4     I=I+1
      DO 13 K=1,IEND
      X=.5*(XL+XR)
      TOL=X
      CALL EMU(TOL,XKB,CNE,DT,KD,CS,R,E,CNI,XKD,RD,II)
      IF(E-0.)5,16,5
5     IF(SIGN(1.,E)+SIGN(1.,ER))7,6,7
6     TOL=XL
      XL=XR
      XR=TOL
      TOL=EL
      EL=ER
      ER=TOL
7     TOL=E-EL
      A=E*TOL
      A=A+A
      IF(A-ER*(ER-EL))8,9,9
8     IF(I-IEND)17,17,9
9     XR=X
```

```
      FR=F
      TOL=EPS
      A=ABS(XR)
      IF(A-1.)11,11,10
 10   TOL=TOL*A
 11   IF(ABS(XR-XL)-TOL)12,12,13
 12   IF(ABS(FR-FL)-TOLF)14,14,13
 13   CONTINUE
      IER=1
 14   IF(ABS(FR)-ABS(FL))16,16,15
 15   X=XL
      F=FL
 16   RETURN
 17   A=FR-F
      DX=(X-XL)*FL*(1.+F*(A-TOL)/(A*(FR-FL)))/TOL
      XM=X
      FM=F
      X=XL-DX
      TOL=X
      CALL FMU(TOL,XKB,CNF,DT,KD,CS,R,F,CNT,XKD,RD,IT)
      IF(F)18,16,18
 19   TOL=EPS
      A=ABS(X)
      IF(A-1.)20,20,19
 19   TOL=TOL*A
 20   IF(ABS(DX)-TOL)21,21,22
 21   IF(ABS(F)-TOLF)16,16,22
 22   IF(SIGN(1.,F)+SIGN(1.,FL))24,23,24
 23   XR=X
      FR=F
      GO TO 4
 24   XL=X
      FL=F
      XR=XM
      FR=FM
      GO TO 4
 25   IER=2
      RETURN
      END

FEATURES SUPPORTED
 ONE WORD INTEGERS

CORE REQUIREMENTS FOR MULR
 COMMON       0  INSKEL COMMON       0
  VARIABLES     36  PROGRAM     580



END OF COMPILATION
MULR
DMP FUNCTION COMPLETED
// XEQ THES   13 OCT 78 15.24.04
*CCEND
```

(ii) Ferricyanide, Penetration Model, Flat CNO Profile, pH 7.

```
*IOCS(CARD,1443 PRINTER)
      REAL KO,KOAT
      EXTERNAL FCT
      DIMENSION GCNI(80)
      DIMENSION GKP(80)
      DATA GCNI/80*0./
      DATA GKP/80*0./
      KK=0
1     READ(5,2)M,P,T,CNI,CNF,PH
2     FORMAT(I1,5F10.5)
      IF(M-5)3,9,9
3     KK=KK+1
      ARA=84.
      FL=.5525
      XKR=3470.
      OH=1.E-14/10.**(-PH)
      XKD=700.*OH
      R=(CNI-CNF)*.001*FL
      S=2.302585*(1.3272*(20-T)-.001053*(T-20)*(T-20))/(T+105)
      U=1.002*EXP(S)
      DT=(T+273.2)*1.805E-05/(293.2*U)
      KOAT=.184*SQRT(DT/1.8389E-05)
      KO=KOAT/ARA
      H=67680.+2870.*(T-20.)
      CS=P/H*1000.
      XRI=100000.
      XLI=1.
      EPS=.00001
      IEND=1000
      NEMU=2
      CALL HILR(X,F,XLI,XRI,EPS,IEND,IER,CNF,DT,KO,CS,R,CNI,XKD,NEMU)
      GKP(KK)=X
      GCNI(KK)=CNI
      GO TO 1
9     ILINE=0
      DO 40 I=1,KK
      ILINE=ILINE+1
      IF(ILINE-1)31,32,31
31    IF(ILINE-44)33,32,33
32    WRITE(6,35)
35    FORMAT('1',/////,10X,'RUN NO.',10X,'K')
37    WRITE(6,38)I,GKP(I)
38    FORMAT(' ',/,10X,I2,15X,F11.4)
      ILINE=ILINE+1
      IF(ILINE-44)40,34,40
34    ILINE=ILINE-1
      GO TO 40
33    IP=I-1
      IF(GCNI(IP)-GCNI(I))37,39,37
39    WRITE(6,36)I,GKP(I)
36    FORMAT(' ',9X,I2,15X,F11.4)
40    CONTINUE
      STOP
      END


FEATURES SUPPORTED
 ONE WORD INTEGERS
```

```
 IOCS

CORE REQUIREMENTS FOR PEN
 COMMON       0  INSKEL COMMON       0
  VARIABLES     384  PROGRAM     434



END OF COMPILATION
PEN
DMP FUNCTION COMPLETED
// FOR MULR    15 SEP 77 10.37.18
      SUBROUTINE MULR(X,F,XLI,XRI,EPS,IEND,IER,CNF,DT,KD,CS,R,CNI,XKD,N)
      REAL KD
      IER=0
      XL=XLI
      XR=XRI
      X=XL
      TOL=X
      CALL EMU(TOL,CNF,DT,KD,CS,R,F,CNI,XKD,N)
      IF(F-0.)1,16,1
1     FL=F
      X=XR
      TOL=X
      CALL EMU(TOL,CNF,DT,KD,CS,R,F,CNI,XKD,N)
      IF(F-0.)2,16,2
2     FR=F
      IF(SIGN(1.,FL)+SIGN(1.,FR))25,3,25
3     I=0
      TOLF=100.*EPS
4     I=I+1
      DO 13 K=1,IEND
      X=.5*(XL+XR)
      TOL=X
      CALL EMU(TOL,CNF,DT,KD,CS,R,F,CNI,XKD,N)
      IF(F-0.)5,16,5
5     IF(SIGN(1.,F)+SIGN(1.,FR))7,6,7
6     TOL=XL
      XL=XR
      XR=TOL
      TOL=FL
      FL=FR
      FR=TOL
7     TOL=F-FL
      A=F*TOL
      A=A+A
      IF(A-FR*(FR-FL))8,9,9
8     IF(I-IEND)17,17,9
9     XR=X
      FR=F
      TOL=EPS
      A=ABS(XR)
      IF(A-1.)11,11,10
10    TOL=TOL*A
11    IF(ABS(XR-XL)-TOL)12,12,13
12    IF(ABS(FR-FL)-TOLF)14,14,13
```

```
 13    CONTINUE
       IER=1
 14    IF(ABS(FR)-ABS(FL))16,16,15
 15    X=XL
       F=FL
 16    RETURN
 17    A=FR-F
       DX=(X-XL)*FL*(1.+F*(A-TOL)/(A*(FR-FL)))/TOL
       XM=X
       FM=F
       X=XL-DX
       TOL=X
       CALL FMU(TOL,CNF,DT,KD,CS,R,F,CNI,XKD,N)
       IF(F)18,16,18
 18    TOL=EPS
       A=ABS(X)
       IF(A-1.)20,20,19
 19    TOL=TOL*A
 20    IF(ABS(DX)-TOL)21,21,22
 21    IF(ABS(F)-TOLF)16,16,22
 22    IF(SIGN(1.,F)+SIGN(1.,FL))24,23,24
 23    XR=X
       FR=F
       GO TO 4
 24    XL=X
       FL=F
       XR=XM
       FR=FM
       GO TO 4
 25    IER=2
       RETURN
       END


FEATURES SUPPORTED
 ONE WORD INTEGERS

CORE REQUIREMENTS FOR MULR
 COMMON       0   INSKEL COMMON       0
  VARIABLES      26   PROGRAM     576



END OF COMPILATION
MULR
DMP FUNCTION COMPLETED
// FOR FMU   15 SEP 77 19.37.55
       SUBROUTINE FMU(TOL,CNF,DT,KD,CS,R,F,CNI,XKD,N)
       REAL KD
       EXTERNAL FCT
       ARA=84.
       XKB=3470
       CND=1./(1./(CNI-CNF)+XKB/TOL/CNF)
       RT=(1.+(XKD+3.25*CND*XKB)/TOL/CNF)*R
       W1=XKB*CND*3.25+TOL*CNF+XKD
       W2=W1*4.*DT/3.1416/KD/KD
```

```
      XU=SQRT(W2)
      IPS=1.0E-10
      NIM=100
      CALL INTG(0.,XU,IPS,NIM,FCT,FER)
      TE=ARA*CS*SQRT(W1*DT)*(FER*(1.+.5/W2)+EXP(-W2)/SQRT(3.1416*W2))
      TE=TE*.001
      F=TE-RT
      RETURN
      END


FEATURES SUPPORTED
 ONE WORD INTEGERS

CORE REQUIREMENTS FOR FMU
 COMMON       0  INSKEL COMMON       0
  VARIABLES     34  PROGRAM     222



END OF COMPILATION
FMU
DMP FUNCTION COMPLETED
// FOR INTG   15 SEP 77 19.38.14
      SUBROUTINE INTG(XL,XU,EPS,NDIM,FCT,Y)
      DIMENSION AUX(100)
      DATA AUX/100*0./
      AUX(1)=.5*(FCT(XL)+FCT(XU))
      H=XU-XL
      IF(NDIM-1)8,8,1
 1    IF(H)2,10,2
 2    HH=H
      E=EPS/ABS(H)
 8    DELT2=0.
      P=1.
      JJ=1
      DO 7 I=2,NDIM
      Y=AUX(1)
      DELT1=DELT2
      HD=HH
      HH=.5*HH
      P=.5*P
      X=XL+HH
      SM=0.
      DO 3 J=1,JJ
      SM=SM+FCT(X)
 3    X=X+HD
      AUX(I)=.5*AUX(I-1)+P*SM
      Q=1.
      JI=I-1
      DO 4 J=1,JI
      II=I-J
      Q=Q+Q
      Q=Q+Q
 4    AUX(II)=AUX(II+1)+(AUX(II+1)-AUX(II))/(Q-1.)
      DELT2=ABS(Y-AUX(1))
```

```
      IF(I-5)7,5,5
 5    IF(DELT2-E)10,10,6
 6    IF(DELT2-DELT1)7,11,11
 7    JJ=JJ+JJ
 8    IER=2
 9    Y=H*AUX(1)
      RETURN
 10   IER=0
      GO TO 9
 11   IER=1
      Y=H*Y
      RETURN
      END

FEATURES SUPPORTED
 ONE WORD INTEGERS

CORE REQUIREMENTS FOR INTG
 COMMON      0  INSKEL COMMON       0
  VARIABLES    230  PROGRAM      340



END OF COMPILATION
INTG
DMP FUNCTION COMPLETED
// FOR FCT    15 SEP 77 19.38.42
      FUNCTION FCT(XF)
      FCT=1.12838*EXP(-XF*XF)
      RETURN
      END

FEATURES SUPPORTED
 ONE WORD INTEGERS

CORE REQUIREMENTS FOR FCT
 COMMON      0  INSKEL COMMON       0
  VARIABLES      4  PROGRAM       26



END OF COMPILATION
FCT
DMP FUNCTION COMPLETED
// XEQ PEN    15 SEP 77 19.38.56
*CCEND
 MPX, BUILD PEN

 MPX, PEN   LD XQ
```

(iii) Ferricyanide, Film Model, Flat and Quadratic Profiles, pH 7.

```
// JOB    M    P    X                    TANG    10 SEP 77 16.50.23
// FOR THES - 10 SEP 77 16.50.24
*IOCS(CARD,1443 PRINTER)
      REAL KO,KL,KOAT
      DIMENSION GCNI(80),GCNF(80),GP(80),GT(80),GK(80),GKO(80),GDT(80)
      DIMENSION GKO(80),GKL(80),GEN(80),GCS(80),GCNO(80),GTR(80),GTD(80)
      DIMENSION GTRD(80),GR(80),GRT(80),GERD(80),GERC(80),GERCN(80)
      DIMENSION MM(80)
      DATA GCNI,GCNF,GP,GT,GK,GKO,GDT,GKO,GKL,GEN/800*0./
      DATA GCS,GCNO,GTR,GTD,GTRD,GR,GRT,GERD,GERC,GERCN/800*0./
      DATA MM/80*0/
      KK=0
 1    READ(5,2)M,P,T,CNI,CNF
 2    FORMAT(I1,4F10.5)
      IF(M-5)3,9,9
 3    KK=KK+1
      ARA=84.
      FL=.4944
      XKB=3470.
      XKO=8.5E-04
      R=(CNI-CNF)*.001*FL
      S=2.302585*(1.3272*(20-T)-.001053*(T-20)*(T-20))/(T+105)
      U=1.002*EXP(S)
      DT=(T+273.2)*1.805E-05/(293.2*U)
      KOAT=.184*SQRT(DT/1.8389E-05)
      KO=KOAT/ARA
      H=67680.+2870.*(T-20.)
      CS=P/H*1000.
      XRI=100000.
      XLI=1.
      EPS=.00001
      IEND=1000
      NEMU=1
      CALL MULR(X,F,XLI,XRI,EPS,IEND,IER,CNF,DT,KO,CS,R,CNI,XKO,NEMU)
      GKO(KK)=X
      NEMU=2
      CALL MULR(X,F,XLI,XRI,EPS,IEND,IER,CNF,DT,KO,CS,R,CNI,XKO,NEMU)
      CNO=1./(1./(CNI-CNF)+XKB/X/CNF)
      RT=(1.+(XKO+XKB*CNO*3.25)/X/CNF)*R
      KL=RT/ARA/CS*1000.
      EN=KL/KO
      GK(KK)=X
      RR=R*1000./CNI/FL
      TR=1./(X*CNF+XKO+3.25*CNO*XKB)
      TD=DT/KO/KO
      TRD=TR/TD
      RC=CNO*XKB*3.25/(X*CNF+XKO+3.25*CNO*XKB)
      RD=XKO/(X*CNF+XKO+3.25*CNO*XKB)
      GP(KK)=P
      GT(KK)=T
      GCNI(KK)=CNI
      GCNF(KK)=CNF
      MM(KK)=M
      GR(KK)=R
      GRT(KK)=RT
      GKL(KK)=KL
      GKO(KK)=KO
      GDT(KK)=DT
      GEN(KK)=EN
```

```
      GCS(KK)=CS
      GCNO(KK)=CNO
      GERCN(KK)=RR
      GTR(KK)=TR
      GTD(KK)=TD
      GTRD(KK)=TRD
      GERC(KK)=RC
      GERD(KK)=RD
      GO TO 1
    9 ILINE=0
      DO 30 I=1,KK
      ILINE=ILINE+1
      IF(ILINE-1)10,11,10
   10 IF(ILINE-42)12,11,12
   11 WRITE(6,13)
   13 FORMAT('1',/////,6X,'RUN NO.',4X,'UV',6X,'CNI',10X,'CNF',10X,
     *'P',10X,'T')
    6 WRITE(6,20)
   20 FORMAT(/)
      ILINE=ILINE+1
      IF(ILINE-42)7,11,7
   12 IP=I-1
      IF(GCNI(IP)-GCNI(I))6,7,6
    7 IF(MM(I)-1)14,14,15
   15 IF(MM(I)-2)16,16,17
   17 IF(MM(I)-3)18,18,19
   14 WRITE(6,24)I,GCNI(I),GCNF(I),GP(I),GT(I)
   24 FORMAT(' ',5X,I2,8X,'NO',6X,F11.4,2X,F11.4,2X,F11.4,2X,F5.2)
      GO TO 30
   16 WRITE(6,26)I,GCNI(I),GCNF(I),GP(I),GT(I)
   26 FORMAT(' ',5X,I2,8X,'COARSE',2X,F11.4,2X,F11.4,2X,F11.4,2X,F5.2)
      GO TO 30
   18 WRITE(6,28)I,GCNI(I),GCNF(I),GP(I),GT(I)
   28 FORMAT(' ',5X,I2,8X,'FINE',4X,F11.4,2X,F11.4,2X,F11.4,2X,F5.2)
      GO TO 30
   19 WRITE(6,29)I,GCNI(I),GCNF(I),GP(I),GT(I)
   29 FORMAT(' ',5X,I2,8X,'FULL',4X,F11.4,2X,F11.4,2X,F11.4,2X,F5.2)
   30 CONTINUE
      ILINE=0
      DO 40 I=1,KK
      ILINE=ILINE+1
      IF(ILINE-1)31,32,31
   31 IF(ILINE-44)33,32,33
   32 WRITE(6,35)
   35 FORMAT('1',/////,10X,'RUN NO.',10X,'K',20X,'KO')
   37 WRITE(6,38)I,GK(I),GKO(I)
   38 FORMAT(' ',/,10X,I2,15X,F11.4,9X,F11.4)
      ILINE=ILINE+1
      IF(ILINE-44)40,34,40
   34 ILINE=ILINE-1
      GO TO 40
   33 IP=I-1
      IF(GCNI(IP)-GCNI(I))37,39,37
   39 WRITE(6,36)I,GK(I),GKO(I)
   36 FORMAT(' ',9X,I2,15X,E11.4,9X,F11.4)
   40 CONTINUE
      J2=-1
```

```
   41    J2=J2+1
         I1=1+J2*5
         I2=2+J2*5
         I3=3+J2*5
         I4=4+J2*5
         I5=5+J2*5
         IF(J2-J2/2*2)45,42,45
   42    WRITE(6,52)I1,I2,I3,I4,I5
   52    FORMAT('1',/////,7X,'RUN NO.',2X,4(I2,12X),I2)
         GO TO 59
   45    WRITE(6,55)I1,I2,I3,I4,I5
   55    FORMAT(' ',/////,7X,'RUN NO.',2X,4(I2,12X),I2)
   59    WRITE(6,61)GKL(I1),GKL(I2),GKL(I3),GKL(I4),GKL(I5)
   61    FORMAT(' ',/,7X,'KL',7X,4(F11.4,3X),F11.4)
         WRITE(6,62)GKD(I1),GKD(I2),GKD(I3),GKD(I4),GKD(I5)
   62    FORMAT(' ',6X,'KD',7X,4(F11.4,3X),F11.4)
         WRITE(6,63)GEN(I1),GEN(I2),GEN(I3),GEN(I4),GEN(I5)
   63    FORMAT(' ',6X,'EN',7X,4(F11.4,3X),F11.4)
         WRITE(6,64)GDT(I1),GDT(I2),GDT(I3),GDT(I4),GDT(I5)
   64    FORMAT(' ',6X,'DT',7X,4(F11.4,3X),F11.4)
         WRITE(6,65)GCS(I1),GCS(I2),GCS(I3),GCS(I4),GCS(I5)
   65    FORMAT(' ',6X,'CS',7X,4(F11.4,3X),F11.4)
         WRITE(6,66)GCND(I1),GCND(I2),GCND(I3),GCND(I4),GCND(I5)
   66    FORMAT(' ',6X,'CND',6X,4(F11.4,3X),F11.4)
         WRITE(6,67)GTR(I1),GTR(I2),GTR(I3),GTR(I4),GTR(I5)
   67    FORMAT(' ',6X,'TR',7X,4(F11.4,3X),F11.4)
         WRITE(6,68)GTD(I1),GTD(I2),GTD(I3),GTD(I4),GTD(I5)
   68    FORMAT(' ',6X,'TD',7X,4(F11.4,3X),F11.4)
         WRITE(6,69)GTRD(I1),GTRD(I2),GTRD(I3),GTRD(I4),GTRD(I5)
   69    FORMAT(' ',6X,'TRD',6X,4(F11.4,3X),F11.4)
         WRITE(6,71)GR(I1),GR(I2),GR(I3),GR(I4),GR(I5)
   71    FORMAT(' ',6X,'R',8X,4(F11.4,3X),F11.4)
         WRITE(6,72)GRT(I1),GRT(I2),GRT(I3),GRT(I4),GRT(I5)
   72    FORMAT(' ',6X,'RT',7X,4(F11.4,3X),F11.4)
         WRITE(6,73)GERD(I1),GERD(I2),GERD(I3),GERD(I4),GERD(I5)
   73    FORMAT(' ',6X,'ERD',6X,4(F11.4,3X),F11.4)
         WRITE(6,74)GERC(I1),GERC(I2),GERC(I3),GERC(I4),GERC(I5)
   74    FORMAT(' ',6X,'ERC',6X,4(F11.4,3X),F11.4)
         WRITE(6,75)GERCN(I1),GERCN(I2),GERCN(I3),GERCN(I4),GERCN(I5)
   75    FORMAT(' ',6X,'ERCN',5X,4(F11.4,3X),F11.4)
         IF(J2-KK/5)41,41,999
  999    STOP
         END
```

```
FEATURES SUPPORTED
 ONE WORD INTEGERS
 IOCS

CORE REQUIREMENTS FOR THES
 COMMON       0  INSKEL COMMON       0
  VARIABLES   3368  PROGRAM   1604
```

```
DMP FUNCTION COMPLETED
// FOR MULR   10 SEP 77 16.51.53
      SUBROUTINE MULR(X,F,XLI,XRI,EPS,IEND,IER,CNF,DT,KD,CS,R,CNI,XKD,N)
      REAL KD
      IER=0
      XL=XLI
      XR=XRI
      X=XL
      TOL=X
      CALL FMU(TOL,CNF,DT,KD,CS,R,F,CNI,XKD,N)
      IF(F-0.)1,16,1
1     FL=F
      X=XR
      TOL=X
      CALL FMU(TOL,CNF,DT,KD,CS,R,F,CNI,XKD,N)
      IF(F-0.)2,16,2
2     FR=F
      IF(SIGN(1.,FL)+SIGN(1.,FR))25,3,25
3     I=0
      TOLF=100.*EPS
4     I=I+1
      DO 13 K=1,IEND
      X=.5*(XL+XR)
      TOL=X
      CALL FMU(TOL,CNF,DT,KD,CS,R,F,CNI,XKD,N)
      IF(F-0.)5,16,5
5     IF(SIGN(1.,F)+SIGN(1.,FR))7,6,7
6     TOL=XL
      XL=XR
      XR=TOL
      TOL=FL
      FL=FR
      FR=TOL
7     TOL=F-FL
      A=F*TOL
      A=A+A
      IF(A-FR*(FR-FL))8,9,9
8     IF(I-IEND)17,17,9
9     XR=X
      FR=F
      TOL=EPS
      A=ABS(XR)
      IF(A-1.)11,11,10
10    TOL=TOL*A
11    IF(ABS(XR-XL)-TOL)12,12,13
12    IF(ABS(FR-FL)-TOLF)14,14,13
13    CONTINUE
      IER=1
14    IF(ABS(FR)-ABS(FL))16,16,15
15    X=XL
      F=FL
16    RETURN
17    A=FR-F
      DX=(X-XL)*FL*(1.+F*(A-TOL)/(A*(FR-FL)))/TOL
      XM=X
      FM=F
      X=XL-DX
      TOL=X
      CALL FMU(TOL,CNF,DT,KD,CS,R,F,CNI,XKD,N)
```

```
      IF(F)18,16,18
18    TOL=EPS
      A=ABS(X)
      IF(A-1.)20,20,19
19    TOL=TOL*A
20    IF(ABS(DX)-TOL)21,21,22
21    IF(ABS(F)-TOLF)16,16,22
22    IF(SIGN(1.,F)+SIGN(1.,FL))24,23,24
23    XR=X
      FR=F
      GO TO 4
24    XL=X
      FL=F
      XR=XM
      FR=FM
      GO TO 4
25    IER=2
      RETURN
      END

FEATURES SUPPORTED
 ONE WORD INTEGERS

CORE REQUIREMENTS FOR MULR
 COMMON       0   INSKEL COMMON       0
  VARIABLES     26   PROGRAM     576


END OF COMPILATION
MULR
DMP FUNCTION COMPLETED
// FOR EMU   10 SEP 77 16.52.30
      SUBROUTINE EMU(TOL,CNF,DT,KO,CS,R,F,CNI,XKO,N)
      REAL KO
      REAL KL
      XKR=3470.
      ARA=84.
      FL=.4944
      CNO=1./(1./(CNI-CNF)+XKB/TOL/CNF)
      RT=(1.+(XKO+3.25*CNO*XKB)/TOL/CNF)*R
      KL=RT/ARA/CS*1000.
      IF(N-1)1,1,2
 1    UU1=3.25*FL*CNO*KO/ARA/DT/(4.25*TOL*CNF+XKO)
      UU2=SQRT((4.25*TOL*CNF+XKO)*DT)
      UU3=(EXP(UU2/KO)-EXP(-UU2/KO))/2.
      F=UU2*UU1/CS/UU3+(CS-UU1)*UU2/CS/TANH(UU2/KO)-KL
      GO TO 3
 2    U1=SQRT(DT*(TOL*CNF+XKO+3.25*CNO*XKB))
      F=U1/TANH(U1/KO)-KL
 3    RETURN
      END
```

```
FEATURES SUPPORTED
 ONE WORD INTEGERS

CORE REQUIREMENTS FOR FMU
 COMMON       0  INSKEL COMMON       0
  VARIABLES     26  PROGRAM     280


END OF COMPILATION
FMU
DMP FUNCTION COMPLETED
// XEQ THES   10 SEP 77 16.52.49
*CCEND
 MPX, BUILD THES

 MPX, THES  LD XQ
```